Alma Mater Studiorum · Università di Bologna

Scuola di Scienze
Corso di Laurea Magistrale in Fisica

Graph-based analysis of brain resting-state fMRI data in nocturnal frontal lobe epileptic patients

Relatore:
Prof. Gastone Castellani

Correlatore:
Dott.ssa Claudia Testa

Presentata da:
Lorenzo Rossi Magi

Sessione III
Anno Accademico 2014/2015

To me,
to my family
and to those who have never doubted me.

ABSTRACT

Il lavoro che ho sviluppato presso l'unità di RM funzionale del Policlinico S.Orsola-Malpighi, DIBINEM, è incentrato sull'analisi dati di resting state - functional Magnetic Resonance Imaging (rs-fMRI) mediante l'utilizzo della graph theory, con lo scopo di valutare eventuali differenze in termini di connettività cerebrale funzionale tra un campione di pazienti affetti da Nocturnal Frontal Lobe Epilepsy (NFLE) ed uno di controlli sani.

L'epilessia frontale notturna è una peculiare forma di epilessia caratterizzata da crisi che si verificano quasi esclusivamente durante il sonno notturno. Queste sono contraddistinte da comportamenti motori, prevalentemente distonici, spesso complessi, e talora a semiologia bizzarra.

L'fMRI è una metodica di neuroimaging avanzata che permette di misurare indirettamente l'attività neuronale. Tutti i soggetti sono stati studiati in condizioni di resting-state, ossia di veglia rilassata.

In particolare mi sono occupato di analizzare i dati fMRI con un approccio innovativo in campo clinico-neurologico, rappresentato dalla graph theory. I grafi sono definiti come strutture matematiche costituite da nodi e links, che trovano applicazione in molti campi di studio per la modellizzazione di strutture di diverso tipo.

La costruzione di un grafo cerebrale per ogni partecipante allo studio ha rappresentato la parte centrale di questo lavoro. L'obiettivo è stato quello di definire le connessioni funzionali tra le diverse aree del cervello mediante l'utilizzo di un network. Il processo di modellizzazione ha permesso di valutare i grafi neurali mediante il calcolo di parametri topologici che ne caratterizzano struttura ed organizzazione.

Le misure calcolate in questa analisi preliminare non hanno evidenziato differenze nelle proprietà globali tra i grafi dei pazienti e quelli dei controlli. Alterazioni locali sono state invece riscontrate nei pazienti, rispetto ai controlli, in aree della sostanza grigia profonda, del sistema limbico e delle regioni frontali, le quali rientrano tra quelle ipotizzate essere coinvolte nella fisiopatologia di questa peculiare forma di epilessia.

CONTENTS

INTRODUCTION

Nocturnal frontal lobe epilepsy (NFLE) is a peculiar form of focal epilepsy in which seizures, characterized predominantly by dystonic-dyskinetic postures, but often with complex motor behavioral semiology, appear almost exclusively during nocturnal sleep. To date, the pathophysiology of disease has not yet been fully characterized, and several studies performed over the last thirty years with different techiniques have allowed to make assumptions about multiple brain structures from which the typical seizures may originate, predominantly subcortical like the basal ganglia and limbic system.

The problem of differential diagnosis between NFLE and parasomnias is an important clinical challenge. In fact, the techniques, such as EEG and conventional brain neuroimaging, usually utilized to investigate both these paroxysmal nocturnal events often show no specific abnormalities. On the other hand, many studies showed the possibility and the advantages of investigating non invasively changes in functional brain connectivity of different forms of epilepsy. Therefore, a possible way to improve the clarification of pathophysiology of NFLE could be to analyze the possible variations of brain functional organization of NFLE patients compared to those of healthy controls.

Different techinques allow to explore the functional connectivity of the brain areas. We used one of these, called functional magnetic resonance imaging (fMRI). It is a neuroimaging technique that measures the brain activity indirectly, by detecting associated changes in blood flow related to energy used by neurons. This procedure relies on the fact that cerebral blood flow and neuronal activation are coupled: when a certain area of the brain is activated, blood flow to that region increases.

Also during rest condition the brain network is not inactivate, but it shows a spontaneous activity that is highly correlated between multiple brain regions. The main focus of the application of fMRI technique in rest condition, also called resting state functional magnetic resonance imaging (rs-fMRI), is to map functional associations between multiple brain regions at their basal state.

This study make use of rs-fMRI technique to analyze eventual differences of functional brain connectivity in rest condition between a group of NFLE patients and a group of healthy controls, using a relatively new methodological approach to investigate neuroimaging data, called graph-based analysis.

The graph theory is the study of graphs, which are mathematical structures, made by nodes and edges that connect them. The graph theory is used to model many types of relations and processes and it can be applied in different fields of study.

In the present work, we performed a graph theoretical analysis on rs-fMRI data to construct a brain network for each of the subjects in this study, with the aim of characterizing the functional pattern of these graphs. This objective may be achieved measuring different topological parameters from the resulting networks. This kind of analysis of rs-fMRI data of NFLE patients and healthy controls using the graph theoretical approach has never been done before.

This thesis is organized as follows: the first chapter describes the basic principles of fMRI technique, with a detailed explanation of the rs-fMRI and its main features. The second chapter goes into the graph theory, starting from the description of what a graph is and how a graph can be generated, and ending with a description of several possible measures that can be performed on these networks. The third chapter provides a brief description of nocturnal frontal lobe epilepsy, which summarizes the main diagnostic tools and describes the main pathophysiological hypothesis. The fourth chapter reports the methods and the materials that we used during the entire analysis and the fifth one shows the obtained results. The sixth chapter provides the discussion and the interpretation of the results, while the seventh chapter analyzes the possible future directions which might be explored.

1 FUNCTIONAL MAGNETIC RESONANCE IMAGING

Functional Magnetic Resonance Imaging (fMRI) is a neuroimaging technique that indirectly measures brain activity by detecting associated changes in blood flow related to energy use by brain cells [1]. This procedure relies on the fact that cerebral blood flow and neuronal activation are coupled: when a certain area of the brain is activated, blood flow to that region increases. Therefore neuronal activity is not measured in itself, but the metabolic consequences of such activity (haemodynamic response). The signal that allows us to measure the hemodynamic response is called Blood Oxygen Level Dependent (BOLD) effect: it is generated by the dilution of the deoxyhemoglobin of blood (see section 1.1).

Tipically, fMRI acquisitions are useful to find associations between different stimuli (visual, auditive, motor or cognitive) and a variation of BOLD signal in specific areas of the brain. However, it is also possible to evaluate regional functional interactions that occur when subjects are not engaged in a particular task. This method of brain imaging is called resting state fMRI. This approach is useful to explore the functional organization of the brain at rest, because the brain activity is present even in the absence of an external task. In fact, in the awake resting state, the brain receives 11% of the cardiac output and accounts for 20% of the total oxygen consumption of the body, despite the fact that it represents only 2% of body weight [4].

For the basic principles of nuclear magnetic resonance (NMR) and magnetic resonance imaging (MRI) we refer you to [2] and [3].

1.1 THE BASIC PRINCIPLES OF FMRI

There are two ways in which the information is transferred within the brain: through propagation of an altered membrane potential and through the release of chemical neurotransitters [1]. Both processes involve the ion transport across the neuronal cell membranes, using sodium-potassium (Na^+/K^+) pumps. The Na^+/K^+ pumps, located in the plasma membrane of cells, work through an active transport procedure. Therefore they use chemical energy (in the form of adenosine triphosphate, ATP). It is possible to affirm that if a particular area of the brain consumes a certain quantity of ATP in response to a stimulus, then this region can be considered activated.

The glycolysis is the metabolic pathway that converts glucose into pyruvate and the energy released is used to form the high energy compounds ATP (and also the nicotinamide adenine dinucleotide or NADH).

The brain requires glucose and oxygen to work properly but it does not store neither of them. The brain absorbs these two primary sources of energy from blood, in particular it takes O_2 from red blood cells (RBCs) and glucose from plasma.

The oxygen is carried by hemoglobin (Hb) in the RBCs. It is a protein composed of four sub-unities (2α and 2β). Each sub-unity is formed by one proteic group and one (heme) group with an atom of Fe^{2+} (which is the one that binds the oxygen) in the middle, as we see in Figure 1 . Each Hb molecule transports four O_2 molecules.

The hemoglobin can be saturated with oxygen molecules (oxyhemoglobin) or desatureted with oxygen molecules (deoxyhemoglobin):

- when O_2 is bound with Hb (HbO_2), the electrons of Fe^{2+} are paired up and they are located in the state of lower energy. Therefore HbO_2 is diamagnetic.
- When O_2 detaches from Hb, the electrons of Fe^{2+} are unpaired and they are located in the state of greater energy: Hb is paramagnetic.

The diamagnetic substances generate an insignificant quantity of inhomogeneities in the external magnetic field. Instead, the paramagnetic ones distort the sorrounding magnetic field induced by MR scanner, causing a phase displacement of nuclear spin. The transversal relaxation and the signal go to zero more rapidly than the situation without inhomogeneities. Consequently, the contrast in magnetic resonance images depends on different ratio between oxy/deoxy-hemoglobin concentration in the activated/inactivated regions of the brain.

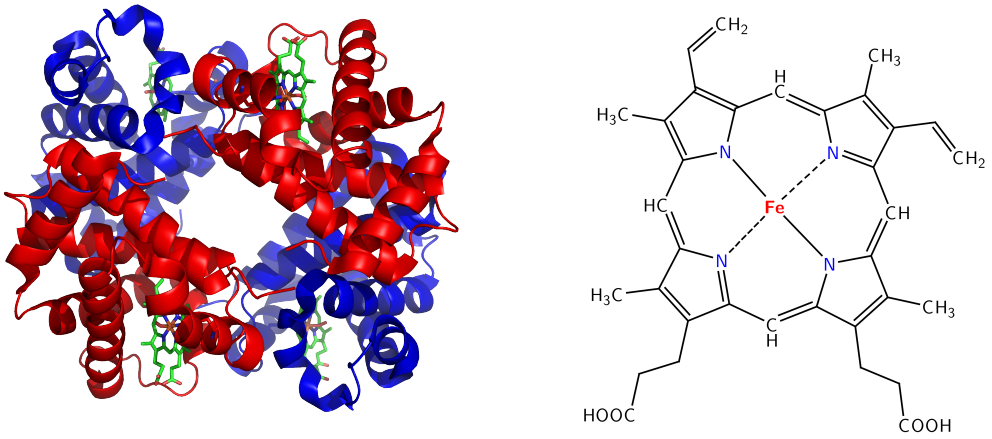

(a) (b)

Figure 1: **(a)** Structure of hemogoblin: the proteins' α and β sub-units are in red and in blue. The heme groups, that contain iron, are in green. *The image is taken from Protein Data Bank, www.rccsb.org.*
(b) Heme group in detail.
The image is taken from http://en.wikipedia.org/wiki/Hemoglobin

Hence, if the brain consumes the oxygen of the blood, a reduction of the signal in that region is expected. Indeed this effect does not occur and to an increase of metabolism corresponds the increase of the MR signal. It seems to be a nonsense. Actually, all the consequences of the metabolism were not considered. In fact, an increase of metabolism produces also a vasodilation and the consequent increase of the blood flow. Therefore, the oxygen quantity carried by the blood is higher than the quantity of oxygen consume, and the result is an increase of concentration of the oxyhemoglobin with a reduction of concentration of the deoxyhemoglobin. Consequently, an increase of MR signal respect to the baseline follows, and it can be measured by the BOLD effect. The BOLD signal is an indirect measure of neuronal activity, which is generated from the dilution of deoxyhemoglobin in the vessel blood, so it does not measures neuronal activity directly, but it measures the metabolic consequences of that activity (hemodynamic response).

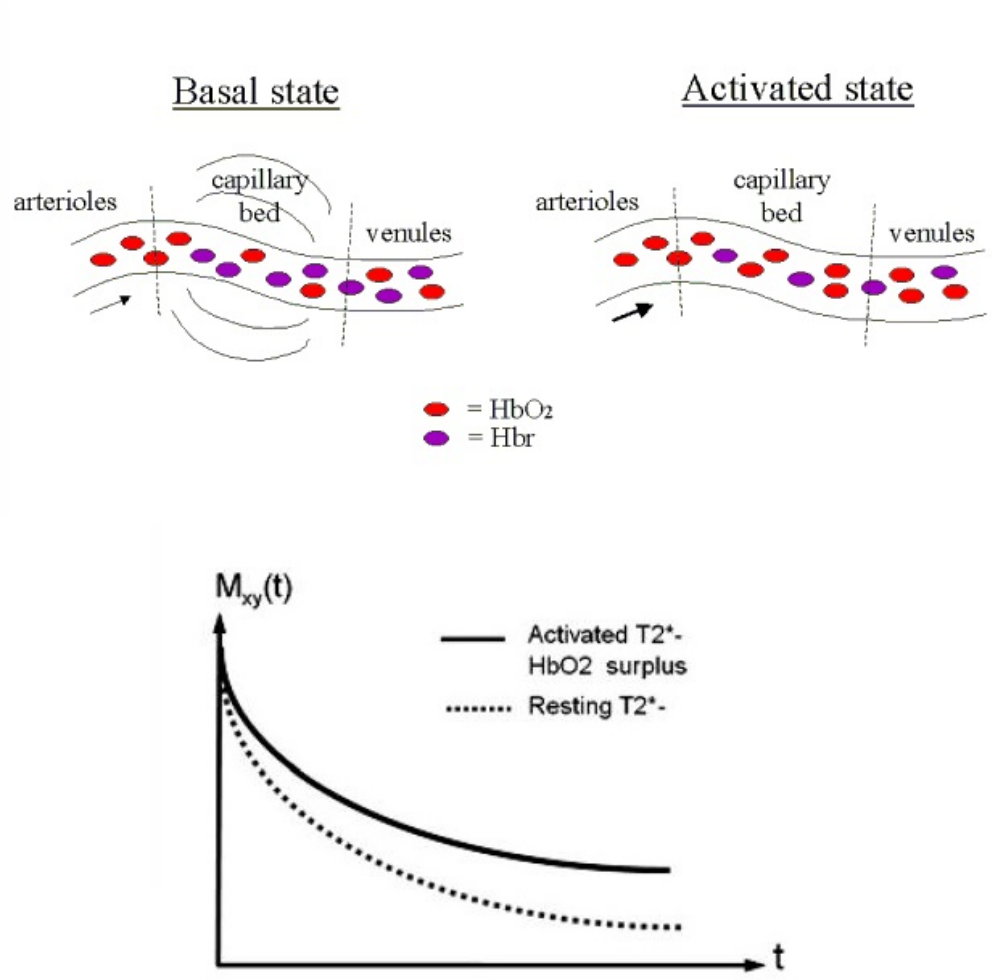

Figure 2: Hemoglobin as an MRI contrast agent. Blood oxygenation or deoxygenation in the brain can result from changes in metabolic-related oxygen uptake, and changes in blood flow. This is manifested as an increase or decrease in signal intensity in T_2^*-weighted images. As the oxygenation state of hemoglobin changes to deoxyhemoglobin, the iron molecule becomes paramagnetic and thus alters the local T_2^* by disturbing the local magnetic field. This causes decreases in T_2^* *(in the upper left of the image)*.
As more oxygenated blood is delivered to the area the T_2^* is then increased, causing an increase in signal *(in the upper right of the image)*. The T_2^* is higher in the activated state. The echo time with the optimal fMRI contrast is about equal to T_2^* *(in the lower of the image)*.

1.2 FMRI ACQUISITION

The sequence used during fMRI acquisition is the GE-EPI sequence (Gradient Echo - Echo Planar Imaging).

Gradient echo imaging

In the gradient echo (GE) imaging sequence initially a slice selective RF pulse is applied [3]. This RF pulse typically produces a rotation angle of the magnetization less than 90°. At the same time of the RF pulse, a slice selection gradient is applied (G_s). Subsequently, a phase encoding gradient is applied (G_ϕ). A dephasing frequency encoding gradient (G_f) is applied at the same time as the phase encoding gradient, so as to cause the spins to be in phase at the center of the acquisition period. This gradient is negative in sign from that of the frequency encoding gradient turned on during the acquisition of the signal. An echo is produced when the frequency encoding gradient is turned on because this gradient refocuses the dephasing which occurred from the dephasing gradient. This type of echo is called a gradient echo.

The period called echo time (TE) is defined as the time between the start of the RF pulse and the maximum in the signal. The repetition time (TR) instead is defined as the time between the RF pulse and the following one.

In a gradient echo sequence, a gradient is used instead of a 180° RF pulse to rephase the spins (unlike the spin echo sequence). Imaging with a gradient echo is intrinsically more sensitive to magnetic field inhomogeneities because of the use of the refocusing gradient. The use of a small flip angle and of a gradient for the refocusing of magnetization vectors allow this sequence to have a shorter duration.

In Figure 3 the temporal diagram of the gradient echo sequence is shown.

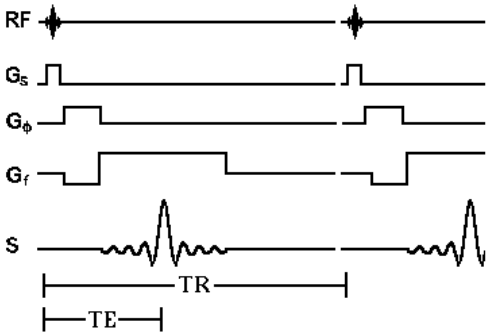

Figure 3: The temporal diagram of the gradient echo sequence.
The image is taken from [2]

Echo Planar imaging

Echo-planar imaging (EPI) is a rapid magnetic resonance imaging technique, by which it is possible to record an entire image in a few seconds. To reduce the acquisition time it is possible to derive multiple echoes from a single excitation pulse, using n echoes to encode n lines of k-space in a single image. This is done by reversing the polarity of the read gradient for alternate echoes, which leads to the formation of the train of gradient echoes, with each echo representing a point where the net applied read gradient refocused. This process can be repeated as long as there is appreciable transverse magnetization present. The EPI is the most widely used acquisition method in fMRI. In these cases the EPIs are usually acquired with a relative long TR (2-3 sec) that allows a large number of slices to be registred, even covering the whole brain volume.

If we are interested in acquisition of N volumes, the brain activity is monitored for a time of TRxN. Hence, this period TR represents the temporal resolution of the acquisition technique.

The main advantages of the GE-EPI sequence are that it is sensible to magnetic susceptivity variations and it is a ultra fast acquisition method. The disadvantages are the low contrast of the images, the low Signal to Noise Ratio (SNR) and the distorsions that are created in the images.

In Figure 4 the temporal diagram of the GE-EPI sequence is shown.

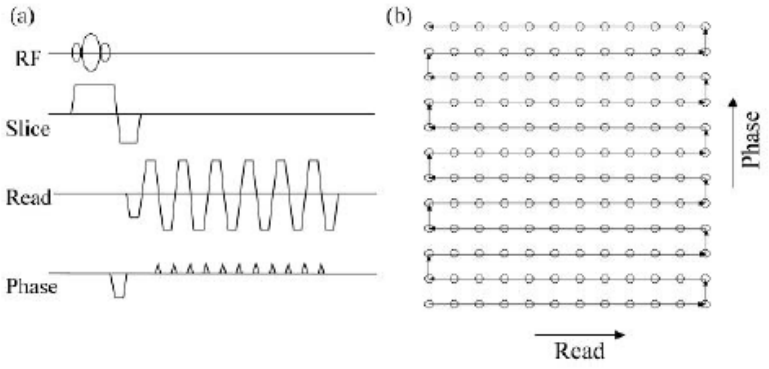

Figure 4: The temporal diagram of the GE-EPI sequence.

1.3 RESTING-STATE FUNCTIONAL MAGNETIC RESONANCE IMAGING

Biswal et al. [8] were the first who demonstrated that, during rest condition, the left and the right hemispheric regions of the primary motor cortex showed a high temporal correlation between their fMRI BOLD time series. This pioneering study, [8], with others subsequently performed (*e.g.* [9], [10]), demonstrated that during rest the brain network is not inactivate, but it shows a spontaneus activity that is highly correlated between multiple brain regions. The main focus of these analysis was to map functional association between these regions.

1.3.1 Rs-fMRI BOLD signal

In order to investigate the basal activity through fMRI technique, it is important to minimize any sensorial input or cognitive task. In fact, during fMRI acquisition, the subjects should lie down with eyes closed, they should not sleep and they should not focus on a single thought.

We described the spontaneus neuronal activity as an activity not referred to an input or an output, but it represented the basal neuronal activation of the brain. These fluctuations are carachterized by a frequency range of $0.01 - 0.1$Hz. The neuronal basis of these low frequency rs-fMRI oscillations is not yet fully understood. An important issue consists of taking into account that different sources of noise could be present, like termal noise, system noise, movement noise and physiological noise, such as respiratory and cardio-oscillatory ones. It is however important to consider that the observed spontanues BOLD signals are mainly dominated by lower frequency (< 0.01Hz) with only a minimal contribution of higher frequent cardiac and respiratory oscillations (> 0.3Hz), [11].

1.3.2 Definition of a baseline

In cognitive neuroscience, the physiological baseline of the brain is defined as the absence of activation, where the concept of activation represents an increase in blood flow (and glucose utilization) that is not accompanied by a commensurate increase in oxygen consumption, [4] and [21]. As a result of this process, the quantity of blood oxygen in the area of activations increases (which substantially represents the BOLD signal).

We can define the concept of baseline with the absence of these changes.

Instead, the deactivation process represents the opposite configuration of metabolic and circulatory changes, and Gusnard et al. in [4] and [21] hypothesized that the deactivation that is observed in an area with the functional imaging may reflect a decrease in the activity of the cells that are projecting to that area. The authors proposed also to consider the uniformity of Oxygen Extraction Fraction (OEF, which represents the percentage of the oxygen delivered to the brain that is utilyzed by the brain) at rest as the baseline level of neuronal activity.

This uniformity, in the awake (with eyes closed) resting state, represents an equilibrium reached by the metabolic requirement and blood flow in the region of interest. Those areas with less OEF than baseline are considered activated and those areas in which OEF is greater than level of baseline is defined inactivated.

In figure 5 the tipical parameters during activation and deactivation processes are shown.

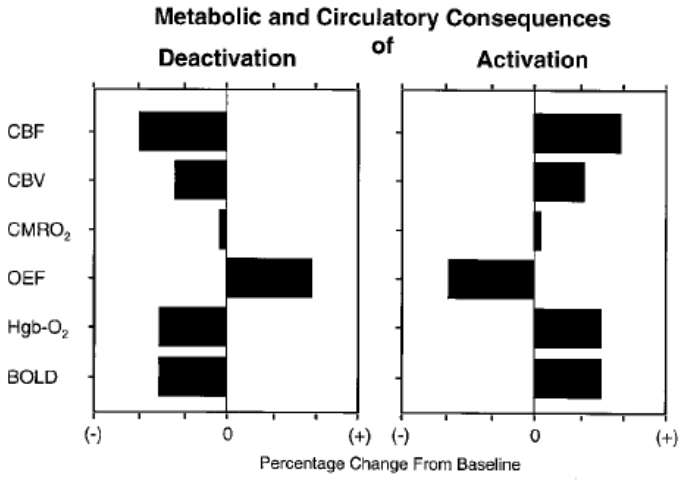

Figure 5: Schematic representation of changes of several metabolic and circulatory parameters during activation and deactivation processes: the cerebral blood flow (CBF), the cerebral blood volume (CBV), the cerebral metabolic rate for oxygen ($CMRO_2$), the oxygen extraction function (OEF), the amount of oxygen attached to hemoglobin (HbO_2) and the blood oxygen level dependent (BOLD). On the left side the deactivation is shown and on the right side the activation is displayed.
The image was taken from Reichle et al., A default mode of brain function, [21]

.

1.3.3 Resting-state networks

Several studies showed a high level of functional connectivity in rest condition between the left and right hemispheric motor cortex, but also between other brain areas. Many functional networks have been identify, like the primary visual cortex, the auditory cortex and the language system (*e.g.* [9], [10], [12]).

For functional connectivity we mean the temporal correlation between spatially remote neurophysiological events [13]. Particularly, resting state functional connectivity focuses on connectivity assessed across the BOLD time points during resting conditions [14].

It can be defined as the temporal correlation between spatially remote neurophysiological events, expressed as deviation from statistical independence across these events in distributed neuronal groups and areas.

As reported in [11], these resting-state networks (RSNs) consist of anatomically separated, but functionally linked brain regions that show a high level of ongoing functional connectivity during rest. To date, the most often reported RSNs are, [15]: *the Default Mode Network (DMN)*, that is the most studied RSN; *the somatomotor network*, which includes primary and higher order motor and sensory area; *the visual network*, which spans much of the occipital cortex; *the auditory network* consisting of Heschl's gyrus, superior temporal gyrus and posterior insula; *the language network*, that includes Broca's and Wernicke's areas and it is extended to prefrontal, parietal and subcortical regions; *the dorsal attention network*, which includes the intraparietal sulcus and frontal eye field; *the ventral attenction network*, which includes the tempoparietal junction and ventral frontal cortex; *the frontoparietal control network*, which includes the lateral prefrontal cortex and inferior parietal lobule; *the cingulo-opercular network*, which includes the medial superior frontal cortex, anterior insula and anterior prefrontal cortex. The most interesting thing is that these networks were obtained in different studies, performed with different MR scanners and data analysis. It demostrates the robust formation of resting state networks during rest. In Figure 6 these RSNs are showed.

Of particular interest is the so-called Default Mode Network. The functionally linked areas that make up the network are posterior cingulate cortex/precuneus, medial frontal and inferior parietal regions. The regions of DMN are known to show an elevated level of neuronal activity during rest, in comparison to when tasks are performed, in which these regions are consistently deactivated, [20]. This fact suggests that neuronal activity of this network reflects a *default state* of neuronal activity of the human brain, [11].

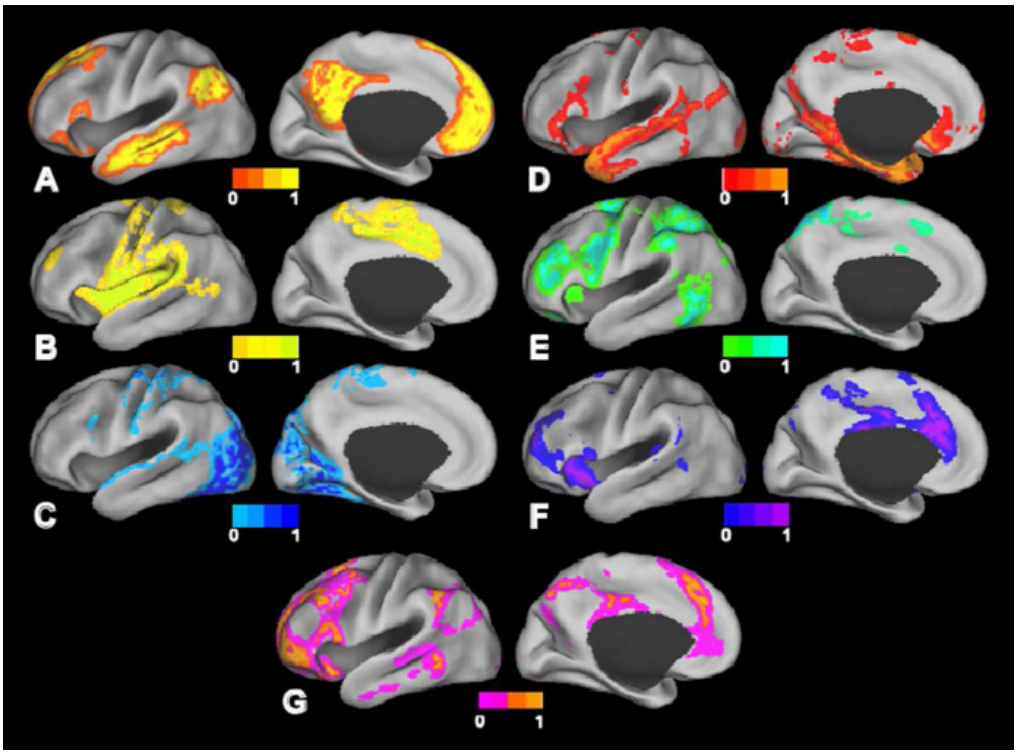

Figure 6: The most often reported RSNs in literature: **(A)** Default Mode Network, **(B)** Somatomotor network, **(C)** Visual network, **(D)** Language network, **(E)** Dorsal attention netwok, **(F)** Ventral attention network, **(G)** Frontoparietal control network.
The image was taken from [15].

1.3.4 Pre-processing of BOLD fMRI data

Pre-processing is necessary in fMRI analysis in order to take data from the scanner and prepare them for statistical analysis. The aim of the different steps of the pre-processing phase is to apply various image and signal processing techniques to reduce noise and artefacts. The aim of these steps is to improve the power of the subsequent analyses.

Generally, the usual method of pre-processing is to apply a sequence of individual steps in a particular order [1]:

- Reconstruction from k-space data: the raw signal is obtained by digitizing the RF signal detected by the receiver coil. This raw datum does not appear as an image, but it is represent by a k-space datum, that must be convert into image-space, so an inverse transformation is required. Generally a fast fourier transform is performed.

  The reconstruction stage often includes some form of artefact correction technique, like the *ghost correction*. It is a correction technique for the artefact known as the N/2 *ghost* (or Nyquist ghost). This artefact is represented by a lower intensity replication of the image, shifted by half the field of view in the phase-encode direction.

- Motion correction: if a subject moves his head during an fMRI acquisition, the position of the brain within the functional images will vary over time. This means that any voxel's temporal series does not refer to the same point in the brain. Therefore, motion correction is always recommendable in fMRI experiments. This step has the aim of find a common orientation for all images and resample the original data to this reference orientation. This objective is achieved by registering each volume of the series to a chosen reference one.

- Slice timing correction: functional volumes are tipically acquired one slice at a time with the timing of the slice acquisition equally spread over the repetition time (TR). Therefore it is not correct to assume that all slices were acquired at the same time or that the timing in all voxels is the same. Hence, the slice timing correction has the aim of adjust the voxel temporal series so that a common reference timing exists for all voxels. The reference time is often chosen as that corresponding to the first slice. The temporal adjustment is achieved by shifting the time series of values forward and backward in time.

- Spatial filtering: this step is usually applied because blurring can potentially increase signal to noise ratio (SNR) in the data - so we want to reduce the noise level while retaining the underlying signal - and also because certain later steps require the functional images to be spatially smooth. The most common method of carrying out spatial filtering is to convolve each volume with a Gaussian filter. The width of this filter will determine the extent of the blurring that take place.

- Intensity normalisation: this step attempts to rescale the mean intensity of the fMRI signal in order to compensate for variations of global signal within, and also between, sessions.

- Temporal filtering: it works on each voxel time series separately. The main point of this step is to remove unwanted components of a time series, without damaging the signal of interest. It can be used a high-pass filter to remove slowly varying unwanted signals, such as physiological effects like heartbeat and breathing, or a low-pass filter to reduce high frequency noise in each voxel time series (a simple convolution with a Gaussian filter is generally performed).

1.3.5 Rs-fMRI analysis methods

After preprocessing the BOLD signals, different methods can be used to analyze the data, each with its own advantages and disadvantages.

- The first used method, and also the most robust, is the *seed based analysis*. This method performs a correlation between the resting state time series of a particular region and the time series of all other regions. This region of interest (ROI) is called *seed*, and it can be selected from task dependent activation map acquired in another fMRI experiment or it can be "a priori" defined region. The main advantages of this method consist in relative simplicity of the analysis and in straight forwardness of the results. Besides, the disadvantages are that the information is limited to the functional connections of the selected region, and this makes difficult to investigate functional connections on a whole-brain scale, and the fact that this approach requires "a priori" selection of ROIs.

- Another approach is *Independent Component Analysis (ICA)*, a method that maximizes statistical independence between its components. Compared to seed-methods, ICA has the advantage of requiring few "a priori" assumptions, but to use this procedure the

users must select manually the most important components and distinguish noise from physiologic signal by themselves.

- Other kinds of methods are *clustering algorithms*, which attempt to group items that are based on relevant characteristics to the problem of interest. For example we may want to group some regions that have similarities in their BOLD temporal series, such as correlation metrics.
- We can use also *multivariate pattern classification* as a method to analyze fMRI data. This approach uses patterns in the data that were previously assumed important in a training dataset to classify new datasets.
- *Graph-based analysis*: this approach considers the Resting State Networks as a collection of nodes connected by edges. The ROIs are represented as nodes and the association between them as the connectivity of the edges. After definition of the model, topological parameters of these networks can be calculated.
- One of the methods which allow to investigate the directionality of the neural interactions is the *Granger Causality*. Matematically, this analysis is based on the concept of predictability: a signal y is said to causally influence a signal x if the future course of x is more accurately predicted based on the history of signals x and y compared to that based on the history of the signal x alone [25].

1.3.6 Clinical research applications

To date, many potential clinical applications of rs-fMRI are currently being investigated even though they are still experimental [15], [16]. For example, rs-fMRI has been applied to identify specific brain RSNs for presurgical planning in patients with brain tumor, like the study of Zhang et al. [17] in which they reported the successful localization of motor areas in patients with tumors distorting sensorimotors regions.

Moreover, rs-fMRI may also be used for presurgical planning in patients with epilepsy, mapping the epileptic foci or networks, as Liu et al. did [18].

Several studies have also demonstrated the potential utility of rs-fMRI in identifying patients with Alzheimer disease, using, for example, tipical topological parameters of graph-based analysis during a comparison between patients and healthy controls [19].

In conclusion, despite the use of resting state fMRI in clinical applications has not been fully developed, there are already application attempts that bode well for future improvements. Further work is needed

to compare the various analysis methods and their efficacy in detecting different disease states both in groups and especially in individual subjects.

2 GRAPH THEORY

The graph theory is the study of the mathematical structures called *graphs*, which are made by nodes (vertices) and links (edges) that connect them.

These theoretical instruments are very useful to model pairwise relations between different kinds of objects. In fact, the graph theory finds application in various fields: in computer science, graphs are used to represent networks of data organization or to represent the flow of the information; in linguistics, the analysis of semantic, phonology and morphology through the use of graphs is frequent; in chemistry and physics, graph theory is used to model molecules (where vertices represents the atoms and edges the bonds) or local connections between interacting parts of a physical system; in sociology, the graph theory is used to model the social networks; in biology and in neuroscience, the graph theory represents a very efficient technique of modelling biology structures, from the organization of human brain connectome or the protein dynamics to the migration process of particular species of animal.

In this study we analyzed rs-fMRI data with graph theory, in order to model the human brain connectome as a set of nodes, represented by anatomical regions, and edges, represented by the connections between them.

To have a better understanding of this new, relative simple, way of describing the complex systems, like neuronal connections pattern, it is summarized how a brain graph can be constructed. We analyzed the different types of graphs that can be constructed and the characteristic measures that can be calculated on these networks.

2.1 WHAT IS A GRAPH

A graph can be represented by G = G(N,E), with N denoting the number of the nodes and E the number of the edges.

Graphs can be divided in *directed* or *undirected*, based on whether egdes have directionality or not.

They also can be classified as *unweighted* (*binary*) or *weighted*, based on the value of the weights of the edges: if each edge has an equal weight of 1, the graph is called binary; if edges have different weights, the graph is called weighted.

In the specific case of unweighted and undirected graphs, the connectivity structure can be represented by NxN symmetric square matrix called *adjacency matrix*. If in the position *i,j* there is a 1, the node *i* and node *j* are linked, otherwise they are not.

In the case of weighted (and undirected) graphs, the connectivity pattern is described by a *correlation matrix* (see section 4.4.3), that is a symmetric and a square matrix and in each position *i,j* there is a value between 0 and 1, which represents the strenght of that particular association.

In Figure 7 different types of graphs are displayed.

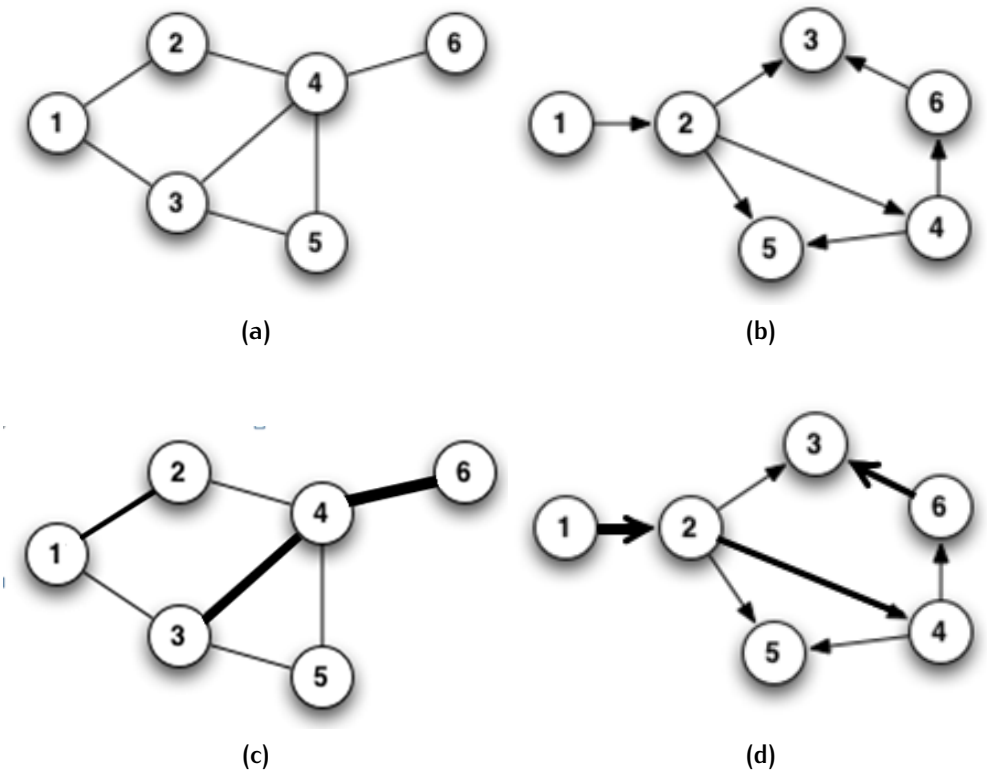

Figure 7: Different type of graphs: (a) directed and unweighted graph, (b) undirected and unweighted graph, (c) directed and weighted graph, (d) undirected and weighted graph.
The images are taken from http://think-like-a-git.net/sections/graph-theory/directed-versus-undirected-graphs.html. They were later partially modified.

2.2 CONSTRUCTION OF A BRAIN GRAPH

During the construction of a graph, an accurate method for defining nodes and edges is necessary. As reported by Sporns et al. [26], these foundamental network elements can be described at different spatial level: *microscale*, *mesoscale* and *macroscale*.

- attempting to construct the human brain connectome at *microscale* level means that each node corresponds to a neuron and each edge to a synapse. This is unrealistic because this choice implies the definition of 10^{11} neurons and 10^{15} connections. The excessive number, variability and dynamics of these elements, make this choice inappropriate.
- The description of connection pattern at *mesoscale* level involves the use of elementary processing units that correspond to local populations of neurons, such as *cortical minicolumns*. These structures generally containe about 100 neurons each and they may represent functional elements that are crucial for cortical information processing.
- To date, the most feasible organizational level for describing an accurate model of human connectome is the *macroscale* level, with the definition of anatomically distinct brain regions and inter-regional connections. Most current studies focus on macroscale networks, also because of technical limitations and computational demand.

After the choice of the description level, nodes and edges must be defined: the first ones generally correspond to Regions Of Interest (ROIs) derived from anatomical atlas or appropriate segmentation process, and the edges can be defined as functional or structural association between these ROIs.

2.2.1 Nodes decision

In the opinion of Bullmore and Bassett [27], a node is a portion of the system that is separable from the rest of the system. Nodes should be encapsulated informational components that have internal integrity and external independence, [74].

Generally, as we defined above, nodes should represent brain regions, which are labelled by a particular atlas. The choice of a template is a very important and delicate step because it determines different network structures and different topological characteristics, as reported by

Wang et al. [28]. They used resting state fMRI data to investigate the effects of different brain parcellation atlases on the topological organization of brain functional networks. They constructed two different networks starting from two different anatomical parcellation schemes. At the end of the graph theoretical analysis, they found that there were significant differences in multiple topological parameters (*e.g.* small-worldness and degree distribution) between the two structures. This study, but many others exist too, provides quantitative evidence on how the topological organization of brain networks is affected by the different parcellation strategies applied.

The main advantage of using an anatomically defined atlas is that results of different studies could be compared. The main disadvantage is the step of the registration from EPI image to a standard space, such as MNI 152. A secondary issue is that the size of the ROIs (defined as number of underlying voxels) can vary considerably, which means that nodal values obtained by averaging across voxels in larger regions will be less noisy than nodal values estimated by averaging across smaller regions. In order to avoid this bias, it could be possible to sample randomly the same number of voxels in estimation of each nodal value.

In order to minimize the registration problem a possible way is to introduce a subject-specific segmentation process, based on the volumetric high resolution images.

A *voxel-based* modality of choosing nodes also exists: these networks are constructed by assigning a node to each equally sized brain area, called *voxel*, which corresponds to the spatial resolution of the image. The fMRI series recorded from each voxel is then used to create the functional network. This method is greatly appreciated because it is not limited by *a priori* assumptions. Nevertheless, it has its advantages and its disadvantages, like all the other techniques. Represented equally sized nodes, for example, allows the voxel-based approach to escape the problem of averaging the signals across regions of different size. Instead, a common criticism is that connectivity between neighboring nodes is spurious and over-represented. Moreover, there are also serious problem concerning the Signal to Noise Ratio (SNR) and spurious connections due to the low signal in the small voxels [59].

2.2.2 Links decision

It is correct to affirm that a single method to define nodes does not exist. The same thing happens with the choice of edges.

Links between nodes are differentiated on the basis of the type of the connectivity, which could be *functional* or *structural*, but also on the fact that they could have weights and directionality.

We focused our attention on functional association between nodes, because we were interested in obtain the functional connectivity between brain regions, and not the structural one. The first thing to do is to choose the statistical association between time series. Many different measures of functional connectivity exist, each ones with specific characteristics. The most used in literature is the Pearson correlation coefficient: this is considered the most reliable measure of connectivity for rs-fMRI data. It measures the extent to which two processes behave similarly over time, but it evaluates only linear interactions. Instead other measures such as mutual information, phase synchronization or synchronization likelihood are sensitive to both linear and non linear associations [27]. Many others typologies of measures exist, like those that are sensitive to interactions relative to a particular frequency range (*e.g.* wavelet correlation) or those that are specific for building undirected graphs, like partial correlation or partial coherence, [29].

A similar approach can be considered for graph theoretical analysis of the structural networks derived from measures of anatomical connectivity between regions. This connectivity can be defined in different ways, based on different kinds of MRI data. For diffusion tensor imaging for example, it is possible to assign a probability of axonal connection between any pair of regions on the basis of tractographic analysis of a subject. The main disadvantage of DTI based networks is that tractography on data seems generally to underestimate the probability of the connections between regions that are a long distance apart in the brain, because long distance projections are more likely to intersect with other projections, and it is more difficult to trace the course of a single tract in this condition [27].

In addition to the type of the connectivity, we said that we can also distinguish links for the presence, or not, of the weights and directionality. The difference between binary and weighted links consists in the fact that the first ones contain simply information about presence or absence of connection, instead the second ones contain also information about the strenght of the association.

Regarding the presence of directionality into a brain network, a directed edge expresses causal relation between nodes whereas undirected ones is simply a representation of an association.

2.2.3 Definition of correlation and adjacency matrices

In the study of binary graphs, after the definition of the correlation matrix, which is immediatly subsequent to the choice of the correlation metric (each element a_{ij} of the correlation matrix is a value corresponding to the correlation coefficient between node i and j), an adjacency

matrix must be generated (in weighted graphs, the correlation matrix already represents the final network). Generally, this procedure involves an application of a threshold to all values of the correlation matrix: if $a_{ij} \geqslant \tau$ the corresponding element of the adjacency matrix is set to 1; 0 otherwise.

For the choice of the implementation process of a threshold to the adjacency matrix, there were two possibilities:

- to choose a single, optimal value of threshold to apply to the correlation matrix and describe the topological parameters of the network only at that threshold;
- to choose different values of threshold and describe the network properties as a function of threshold (or connection density);

The adjacency matrix so defined corresponds to the final network.

2.3 MEASURES ON GRAPHS

After constructing the brain networks, it possible to characterize them usiyng topological measures. These measures are numerous and grow in number year after year, thanks to the continuous expansion of the application of graph theory to neuroscience. In this work we proposed only a few of these measures.

There is not a specific way to classify topological parameters, so we decided to refer to the schematic representation made by Rubinov and Sporns in [74].

- An important category of topological measures is that related to the *functional segregation*. Segregation and integration are two important aspects of neural systems [30]. Segregation refers to the existence of specialized neurons and brain areas, organized into distinct neuronal populations and grouped together to form segregated cortical areas. Measures of segregation primarily quantify the presence of such groups, known as *clusters* or *modules*. One of these measures is *Clustering Coefficient*, which is equivalent to the fraction of the node's neighbors that are also neighbors of each other and is defined as

$$C = \frac{1}{n}\sum_{i\in\mathbb{N}} C_i = \frac{1}{n}\sum_{i\in\mathbb{N}} \frac{2t_i}{k_i(k_i-1)} \tag{1}$$

  where C_i is the Clustering Coefficient of node *i*, n is the number of nodes and t_i is the number of triangles around the node *i*.

  Instead the *Modularity* is a parameter that describes the exact size and composition of interconnected groups. This measure provides to define a modular structure of the networks, through a maximization of number of within-group links and a minimization of number of between-group links [31]. Modularity is defined as

$$Q = \sum_{u\in\mathbb{N}} \left[e_{uu} - \left(\sum_{v\in\mathbb{N}} e_{uv} \right)^2 \right] \tag{2}$$

  where the network is subdivided into a set of nonoverlapping modules N, and e_{uv} is the proportion of all links that connect nodes in module u with nodes in module v.

- Another foundamental category is represented by the measures of *functional integration*. This is the ability to combine specialized information from distribuited brain regions [74]. One important measure belonging to this group of parameters is the *Characteristic*

Path Length which is the average shortest path length between all pairs of nodes in the network. It is defined as

$$L = \frac{1}{n}\sum_{i\in\mathbb{N}} L_i = \frac{1}{n}\sum_{i\in\mathbb{N}} \frac{\sum_{j\in\mathbb{N} j\neq i} d_{ij}}{n-1} \tag{3}$$

where L_i is the average distance between node i and all other nodes and d_{ij} is the shortest path length (distance), between nodes i and j.

The average inverse shortest path length is related measure called *Global Efficiency*, which is defined as

$$E = \frac{1}{n}\sum_{i\in\mathbb{N}} E_i = \frac{1}{n}\sum_{i\in\mathbb{N}} \frac{\sum_{j\in\mathbb{N} j\neq i} d_{ij}^{-1}}{n-1} \tag{4}$$

where E_i is the efficiency of node i.

A great difference exists between these two parameters: the Global Efficiency may be calculated for disconnected networks, on the contrary the Characterist Path Length may be computed only for connected ones.

Another measure of efficiency is the *Local Efficiency*. Global Efficiency and Local Efficiency measure the ability of a network to transmit information at the global and local level, respectively. Local Efficiency is defined as

$$E_{loc} = \frac{1}{n}\sum_{i\in\mathbb{N}} E_{loc,i} = \frac{1}{n}\sum_{i\in\mathbb{N}} \frac{\sum_{j,h\in\mathbb{N} j\neq i} a_{ij}a_{ih}\left[d_{jh}(N_i)\right]^{-1}}{K_i(k_i-1)} \tag{5}$$

where $E_{loc,i}$ is the local efficiency of node i, and $d_{jh}(N_i)$ is the length of the shortest path between j and h, that contains only neighbors of i.

- A very useful measure that "combines" both segregation and integration ability of networks is the *Small-Worldness*. A network that is simultaneously segregated and integrated has small-world topology. It is defined as a network that has more clusters than random networks and has the same Characteristic Path Length as random ones, as follows

$$S = \frac{C/C_{rand}}{L/L_{rand}} \tag{6}$$

where C and C_{rand} are the Clustering Coefficients, and L and L_{rand} are the Characteristic Path Lengths of the respective tested network and a random network. Small-world networks often have $S \gg 1$.

- Measures of *centrality* assess the importance of the individual nodes. In fact they may play important role in network resilience for example, or they may are foundamental in functional integration.

  To date, many measures of centrality exist. One of these corresponds to measure that we discusses above, the Degree. In fact, in functional networks, a node that interacts with many others partecipates actively in many network's (functional) processes.

  A great number of centrality parameters is based on the idea that central nodes partecipate in many short paths within a network. The most common, and probably most used, is the *Degree* (or *Nodal Degree*). The Degree of a node is equal to the number of links connected to that node. This value reflects the importance of the individual node inside the entire network. It is a simply measure of centrality. The Degree of a node *i* is defined as

$$k_i = \sum_{j \in \mathbb{N}} a_{ij} \tag{7}$$

  where N is the set of all nodes in the network and a_{ij} is the connection status between *i* and *j*. $a_{ij} = 1$ when link *(i,j)* exists; $a_{ij} = 0$ otherwise ($a_{ii} = 0$ for all *i*). For the directed graphs, it should be considered that there is a difference between incoming connectivity (k_i^{in}) and outgoing connectivity (k_i^{out}), while for the weighted ones the weighs could be considered.

  The collection of the Node Degree of all nodes represents the so-called *Degree Distribution*, which is an important marker of network development and resilience to the removal of nodes.

  Closeness Centrality and *Betweenness Centrality* are other two measures that are part of this group of centrality measures. The first one is defined as the inverse of the average shortest path length from one node to all the others nodes. For the node *i*, the Closeness Centrality is defined as

$$L_i^{-1} = \frac{n-1}{\sum_{j \in \mathbb{N} j \neq i} d_{ij}} \tag{8}$$

  The second one is defined as the fraction of all shortest paths in the network that pass through a given node. Nodes with high

Betweenness Centrality are considered to be "hubs" that tend to link other, more segregated nodes in the network [35]. For the node *i*, the Betweenness Centrality is defined as

$$b_i = \frac{1}{(n-1)(n-2)} \sum_{\substack{h,j \in \mathbb{N} \\ h \neq j, h \neq i, j \neq i}} \frac{\rho_{hi}(i)}{\rho_{hi}\rho_{hi}} \tag{9}$$

where ρ_{hj} is the number of shortest paths between *h* and *j*, and $\rho_{hi}(i)$ is the number of shortest paths between *h* and *j* that pass through *i*.

Betweenness Centrality is extended also to links and it is used to detect important functional connections.

Spectral Centrality and *Salient Centrality* are other two measures of centality. k-Spectral Centrality of a subset B of a connected graph is defined as a measurement of the relevance in terms of eigenvalues of the graph Laplacian associated with the graph. The graph Laplacian is defined as $L = D - A$, in which A is the adjacency matrix and D a diagonal matrix with node connectivities as its terms (for the references see [71]). The *Salience* S of a network is defined as [72]

$$S = \langle T \rangle = \frac{1}{N} \sum_{k} T(k) \tag{10}$$

where S is a linear superposition of all Shortest Path Trees (SPTs). For a fixed reference node *r*, the collection of shortest paths to all other nodes defines the shortest-path tree (SPT) $T(r)$, which summarizes the most effective routes from the reference node *r* to the rest of the network. $T(r)$ is represented by NxN symmetric matrix with elements $t_{ij}(r) = 1$ if the link (i, j) is part of at least one of the shortest paths and $t_{ij}(r) = 0$ if it is not. According to these definitions, the element s_{ij} of the marix S quantifies the fraction of SPTs the link *(i,j)* partecipates in.

- An important class of topological parameters that deserve attention, is composed by measures of network resilience. This category is divided into *indirected* and *directed* measures. Indirect measures quantify the network vulnerability to attacks, like Degree Distribution and *Assortativity Coefficient*, which is a correlation coefficient between the degrees of all nodes on two opposite ends of a link. It is defined as

$$r = \frac{l^{-1} \sum_{(i,j)\in Ł} k_i K_j - \left[l^{-1} \sum_{(i,j)\in Ł} \frac{1}{2}\left(k_i + k_j\right)\right]^2}{l^{-1} \sum_{(i,j)\in Ł} \frac{1}{2}\left(k_i^2 + k_j^2\right) - \left[l^{-1} \sum_{(i,j)\in Ł} \frac{1}{2}\left(k_i + k_j\right)\right]^2} \tag{11}$$

Instead, the direct measures test the network before and after a presumed attack, such as a targeted removal of nodes or links.

2.4 COMPARISON BETWEEN GRAPHS

An important step of the graph theoretical analysis is the comparison between networks. For example, a comparison between graph generated by construction of connectivity pattern and Erdosh-Renyì random graphs [36] is very useful. In fact random graphs are often generated with the aim of obtaing topological parameters as a point of reference to judge the nonrandomness characteristic of the measures calculated from brain networks.

It is also frequent a comparison between groups of subjects in which topological parameters are compared between healthy controls and patients. In doing this, Bullmore and Bassett [27] recommended several important rules to be followed for an efficient comparison between brain graphs: firstly the networks must have the same number of nodes and links, because the topological parameters depend on the connection density and size of the graphs. Moreover it is recommended to use non-parametric tests for a statistical comparisons between group.

2.5 CLINICAL RESEARCH APPLICATIONS

To date, the graph theoretical analysis has not an effective application in clinical neuroscience, but it is interesting (also in a possible future clinical application) to investigate how brain graph can change - in parameters or in characteristics - when different diseases or conditions occur. In fact, many cognitive disorders have been characterized as dysconnectivity syndromes, as indicated by abnormal profiles of functional connectivity pattern. Application of graph analysis for cases of schizophrenia, Alzheimer's disease, epilepsy, multiple sclerosis, attention deficit hyperactivity disorder, and many others, were performed in the last years (for a deepening of these studies see [15] and [16]).

The architecture and organization of the human brain connectome, in addiction to diseases, also depend on different factors including age, gender and cognitive ability.

One of the most important aspects that must be considered during a graph theoretical analysis is the effect due to different *age* between subjects of study. Fair et al., in three different works, [32], [33], [34], described a dynamic reorganization of brain network structure over the course of development. They found, for example, some networks in children that became two disconnected networks in adults. They also demostrated an increasing in functional integration during development and also the comparable small-world topology observed in groups of subjects with different age, which means that the architecture of brain graphs is conserved over age.

Another important study performed using graph theoretical analysis was made by Archard et al. [37]. In this work they tested the hypothesis that resting state functional brain networks have performances affected by normal aging. They found that normal aging reduced the Global and Local Efficiency of parallel information processing.

Many others studies exist, in which analysis of influence of aging on the brain networks were performed, many of these are focalized on changes of module structures.

Together, these studies highlight the power and the efficacy of the graph theory in modeling brain networks.

2.6 FUTURE ISSUES

Brain graphs are apparently simple but powerful models of the brain's functional (and also structural) connectome. The reason why graph theory is an efficient tool for analysis of the complexity of brain structure and organization are its high degree of generalizability and interpretability. In fact, this kind of analysis is applicable to many scales and type of neuroimaging data and it is interpetable in relation to general principle of complex system organization.

The construction of a valid model passes through different steps, made of basic assumptions and different choices, from the selection of nodes and links, to the decision of what are the best topological parameters to be calculated.

Despite the application of graph theoretical analysis to the neurosciences is a field in continous expansion, it will be necessary in the near future to solve several issues. For example, it could be very interesting to be able to construct directed brain graphs, which means that improvements in techniques to capture directionality of connections are needed. Another important aspect that can be improved is the relationship between psycological and topological properties of brain networks, in order to have a better comprehension of the linking graph characteristics and cognitive performance. Besides, also a deeper analysis of the utility of graph measures as diagnostic markers of neurophysiatric syndromes should be done.

All these aspects, in addiction to the power and the elegance of graph theory, suggest that this approach will play an increasingly important role in the long process of comprehension of the dynamics underlying the human brain connectome.

3 NOCTURNAL FRONTAL LOBE EPILEPSY

Nocturnal Frontal Lobe Epilepsy (NFLE) is a peculiar form of focal epilepsy in which seizures, characterized by often bizarre motor behaviors or sustained dystonic posture, appear almost exclusively during sleep, [42], [43], [47], [48], [49].

In 1981 Lugaresi and Cirignotta [39] described five patients which presented episodes characterized by sprawls and dystonic-dyskinetic postures during sleep. The polygraphic recording had documented that the episodes were stereotyped and arose from stage 2 of non-rapid eye movement (NREM) sleep. The authors proposed three different hypotheses to explain the nature of the phenomena: a movement disorder not yet described; a particular type of pavor nocturnus; a peculiar epileptic syndrome with seizures originating from deep or mesial regions of frontal lobes. The last hypotesis was the most likely. In 1990, Tinuper et al. [40] described the semeiology of the crisis originated from mesio/orbital regions of the frontal lobe. These seizures are characterized by complex and bizarre motor behavior with bipedal and bimanual activity, weghing of the pelvis, torsion of the bust and sometimes rollators automatisms, and they were often accompanied by normal or aspecific EEG tracings. The analogies between frontal seizures and the episods observed by Lugaresi and Cirignotta, in addiction to the demonstration of the presence in several patients of epileptiform abnormalities by using depth electrodes, gave finally confirmation that the episods observed in 1981 were actually epileptic crisis which were originated from frontal lobe.

The epileptic syndrome was labelled under the term "nocturnal frontal lobe epilepsy" by Scheffer et al. in [42] and [44]. Although NFLE is considered mostly idiopathic, it has been demonstrated that in 25% of the cases is a positive familiarity for the epilepsy and in the 8% an autosomal dominant fashion can be described without clinical differences in comparion to sporadic cases, due to a mutations in the neuronal nicotinic acetylcholine receptor (nAChR) [44], [45].

The clinical spectrum of Nocturnal Frontal Lobe seizures comprises distinct paroxysmal sleep-related attacks of variable duration and mo-

tor pattern complexity. Based on these two parameters, four different semeiological patterns can be distinguished, [51]:

- Paraxysmal Arousals (PA), that are the shorter episodes (less than 20 sec) and consist in rude awakening from NREM sleep;
- Hyperkinetic Seizures (HS), that start from awakening from NREM sleep too, but they last longer (from 20 sec to 2 min) and have more complex motor activities than PA;
- Asymmetric Bilateral Tonic Seizures (ATS), which are characterized by a sudden assumption of a tonic/dystonic position of the four limbs;
- Epileptic Nocturnal Wandering (ENW), that are extended paroxysmal episodes (1 - 3 min), starting from NREM sleep and continue with agitated ambulation and dystonic movements.

In Figure 8 an example of video-images and scalp EEG recording of a paroxysmal arousal are displayed. This image is taken from [49]. In this study, all patients underwent a comprehensive presurgical evaluation, which included clinical history, interictal EEG, scalp video-EEG monitoring, high resolution MRI and invasive recording by stereo-EEG, if necessary. In particular, the video-EEG recordings were performed because more than 90% of seizures of the patients occurred during sleep. In three different cases, the MRI and video-EEG findings were considered adequate to consistently localize the epileptogenic zone and to define a surgical strategy.

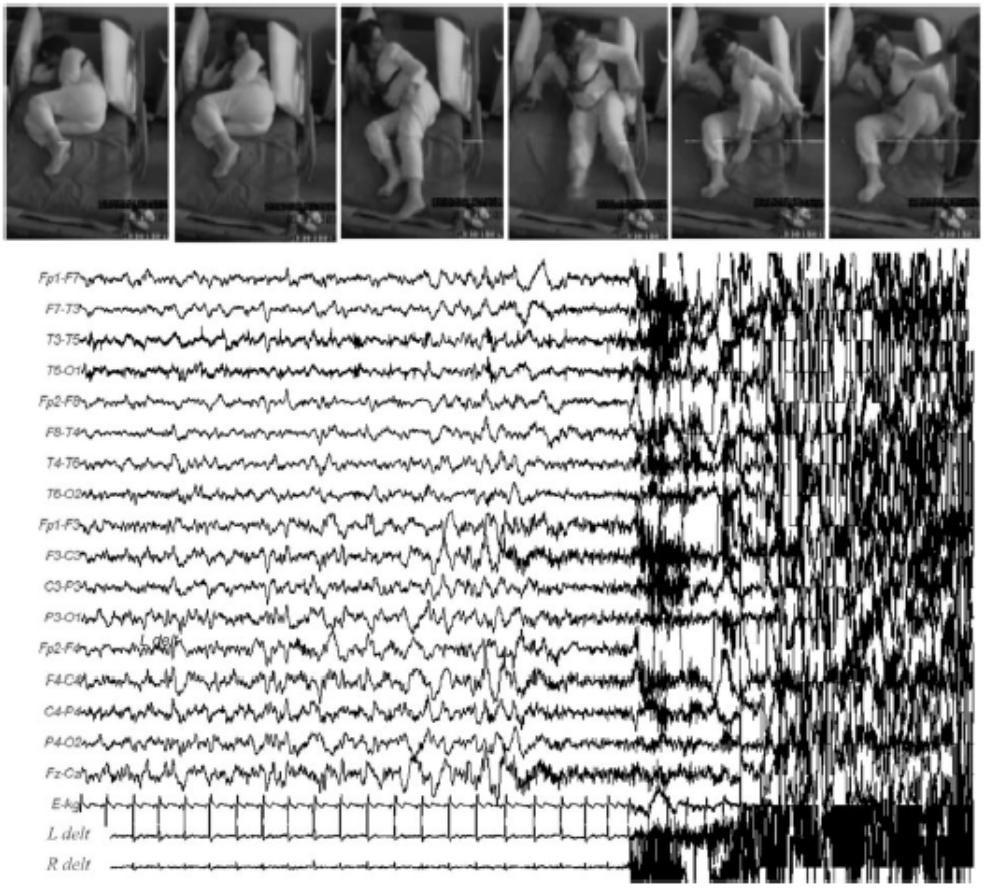

Figure 8: Example of a video-images and scalp EEG of a paroxysmal arousal. The first electromyographic modification corresponds to the second snapshot from the left.
The figure is taken from [49].

3.1 DIAGNOSIS

The problem of differential diagnosis between NFLE and parasomnias is an important clinical challenge. EEG and MR imaging often show no abnormalities. In fact, an epileptogenic lesion is documented in less than 20% and EEG is often normal [43].

The best method for the clinical and polysomnographic diagnosis of paroxysmal nocturnal events is the video EEG-polysomnography. This kind of investigation involves monitoring the patient during sleep through neurophysiological, cardio-respiratory, and video modalities.

It is proven that dystonic posturing and hyperkinetic automatism are specific for NFLE, and other motor patterns like sitting, standing or walking are not discriminant for the diagnosis instead [57].

From a therapeutic point of view, carbamazepine is the drug of first choice for the EFN. The response to low doses of this drug is even considered a diagnostic element ex adiuvantibus. In most patients is obtained a complete seizures control or a significant reduction of the episodes. In about a third of the cases, patients are resistant to treatment [58].

3.2 PATHOPHYSIOLOGY

Dystonic–dyskinetic features, observed during the seizures, suggest an involvement of subcortical structures like the basal ganglia (whose main components are the striatum - caudate nucleus and putamen nucleus - the pallidum nucleus, the sustantia nigra and the subthalamic nucleus). Instead, the characteristic motor beahaviors of NFLE patients are difficult to abscribe to a specific brain areas. Complex behaviors, as demonstrated by several surgical studies, [52], [53], [54], [55], have been demonstrated to be sustained by ictal discharges that may originate in the frontal lobes (including the insular structures and the anterior cingulate) and in the temporal lobe (including amygdala) and brainstem.

Various studies, in NFLE patients, have reported occurrence of sizures in the early stages of NREM sleep, especially the EEG discharge onset coincided with physiological sleep transient (K-complex, periodic arousals) [46], [47]; these evidences support the hypothesis that thalamocortical drive evoking physiological sleep transients and subcortical circuit, controlling the arousal mechanism, may trigger the epileptic foci in frontal mesial structures [47].

Besides, it is likely that the cortical discharges are not confined to the orbitofrontal or mesiofrontal regions but also act on other networks, involving for example the limbic system, to explain the primitive behaviors. In Figure 9, from [56], the limbic loop is shown. It participates in the production of sudden awakenings and complex motor behavior.

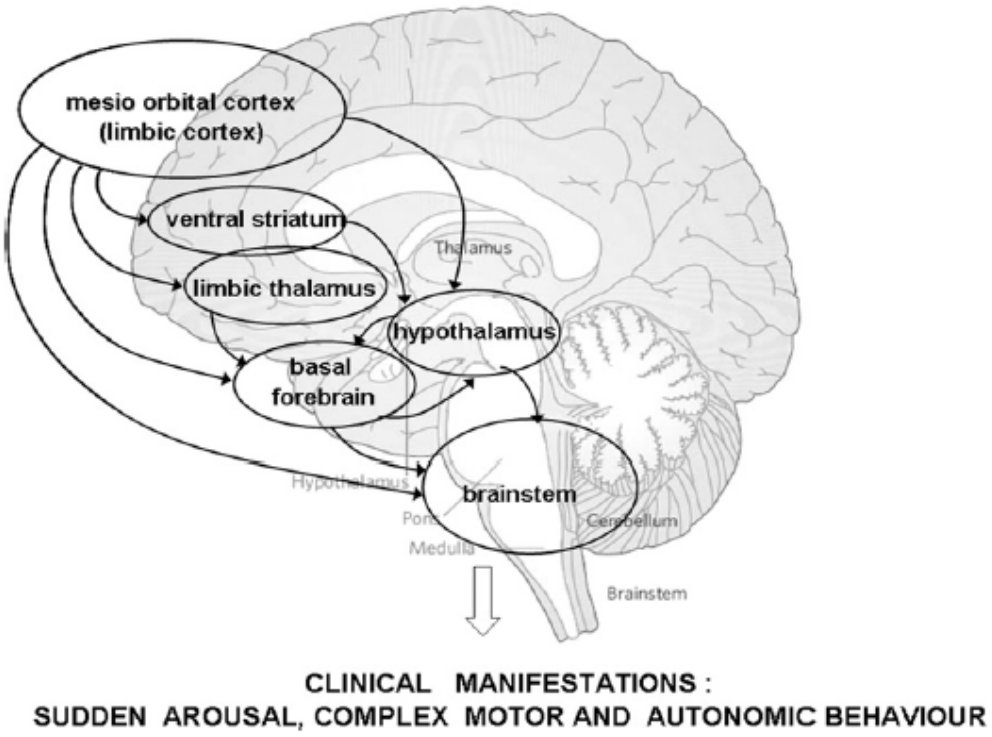

Figure 9: The limbic loops partecipating in the production of sudden awakenings and complex motor behaviors.
The image is taken from [56]

4 METHODS AND MATERIALS

4.1 PARTICIPANTS

Thirteen NFLE patients (6 males and 7 females), with a mean age of 38.3 years and standard deviation of 11.8 years (range between 18 and 55) participated in the study. The patients that underwent this study had been recruited by the Epilepsy and Sleep Center of IRCCS, Istituto delle Scienze Neurologiche di Bologna, Department of Biomedical and Neuromotor Sciences, University of Bologna, Italy. A total of thirteen healthy controls (6 males and 7 females), with a mean age of 38.5 years and standard deviation of 10.8 years (range between 19 and 53), were selected to match the patient group in age and gender. All the acquisition were performed between March 2012 and October 2014. This study was approved by the local Ethical Committee. General information of both groups are summarized in Table 1.

Table 1: List of patients and healthy controls, matched in gender and age.

Patients			Healthy Controls		
N	sex	age (yrs)	N	sex	age (yrs)
1	F	18	1	F	25
2	M	20	2	M	19
3	F	28	3	F	27
4	F	29	4	F	32
5	M	35	5	M	37
6	F	36	6	F	37
7	F	42	7	F	40
8	M	44	8	M	39
9	F	45	9	F	46
10	M	46	10	M	42
11	F	49	11	F	53
12	M	50	12	M	51
13	M	55	13	M	54

The clinical features of patients are various between the different subjects. The frequency of seizures was different at the onset of the disease and at the time before fMRI evaluation. In fact, at onset the seizures frequency ranged from 3/4 crises a year to several crises during a single night, instead in the last six months before the fMRI acquisition some patients showed no more symptoms and seizures frequency correspond at most to 2/3 crises during a night.

4.2 FMRI DATA ACQUISITION

The MRI scans were acquired using a MR scanner GE Medical System Signa HDx15, with the following characteristics:

- magnetic field strength: 1.5 T;
- gradient strength: 33 mT/m;
- receiver channels: 8 channels;
- slew rate: 276 ms;
- maximum rise time: 120 T/m s;
- coil: 8-channel brain phased array coil GE (1.5 T HD 8 Channel High Res Head Array for the GE HDx MR System).

For each subject two runs of resting-state were collected, one following the other one, during the same scan section. The subjects did not exit the MR scanner between the two scans. During each scan, gradient echo - echo planar imaging (GE-EPI) sequences were acquired over a period of 4 min 30 s. The partecipants were instructed to rest with their eyes closed and to stay awake during the acquisition process.
In Table 2 the parameters of rs-fMRI acquisition are shown.

Table 2: Parameters of resting-state fMRI acquisition process

TR	3000 ms
TE	40 ms
flip angle	90 °
slices per volume	34
number of volumes	90
FOV	24 cm (nv 128)
voxel dimension	1.875 x 1.875 x 4 mm

For each acquisition, the first five volumes acquired, called dummy volumes, were rejected, beacause an imaging steady-state has not yet been reached.

4.3 DATA PREPROCESSING

Data preprocessing was previously performed by the functional MR Unit, paying specific attenction to the removal of noise and in particular physiological noise. In this study the entire procedure for completeness is reported.

Data preprocessing was carried out using FSL (the FMRIB Software Library, version 5.0.6), [64] . This software is a comprehensive library of analysis tools for functional, structural and diffusion MRI brain imaging data.

The FSL tool MELODIC (Multivariate Exploratory Linear Optimized Decomposition into Indipendent Components, version 3.14) was used to perform a single-session ICA on each run of each subject [66]. Here the procedure is briefly reported: firstly a high pass filtering with cut off of 100 *s* was applied, the motion correction with MCFLIRT (an intra-modal motion correction tool designed for use on fMRI time series and based on optimization and registration techniques used in FLIRT, a fully automated robust and accurate tool for linear inter- and inter-modal brain image registration) was performed and also slice timing correction (acquired in an inteleaved way) was accomplished. Subsequently, a Gaussian smoothing with a FWHM of 6 mm was performed and a maximum automatic dimensionality estimation was achieved. Finally, a threshold of 0.99 was applied to IC maps.

In Figures 10, 11, 12, 13, 14, the parameters listed above are shown in the MELODIC toolbox windows.

After using MELODIC, a linear registration of EPI images to 3D space was performed for each run of each subject, using the Boundary-Based Registration (BBR) method [67]. In Figure 15 the EPI image of one patient (N=12) is displayed.

Subsequently, a visual inspection of the components was performed, following the criteria reported in [65].

Finally the noise components were regressed out, with fsl function *fsl_regfilt*.

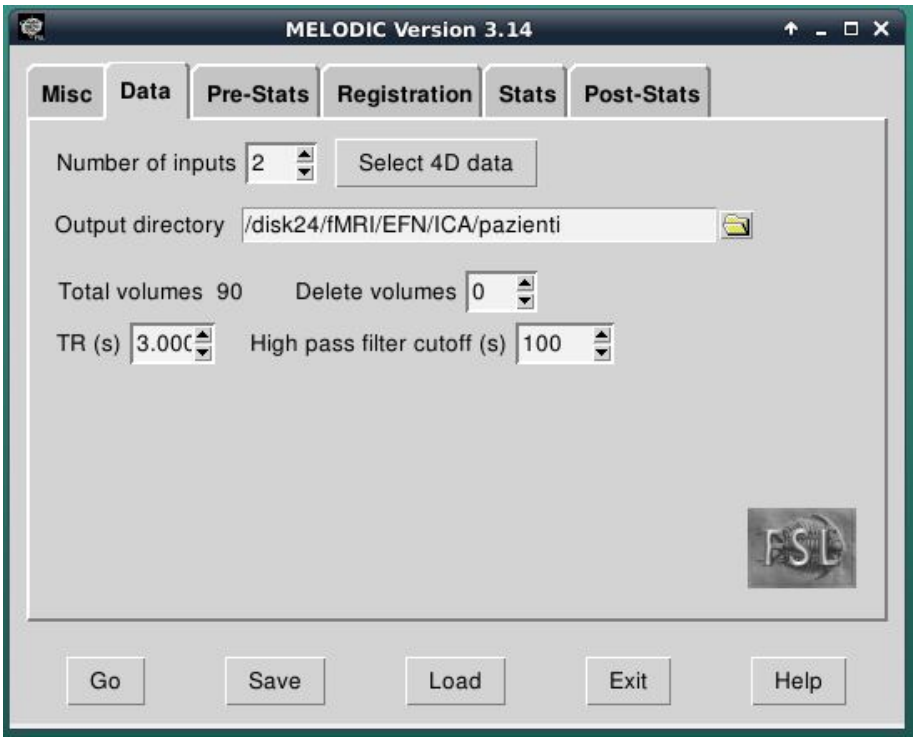

Figure 10: Melodic parameters - Data.

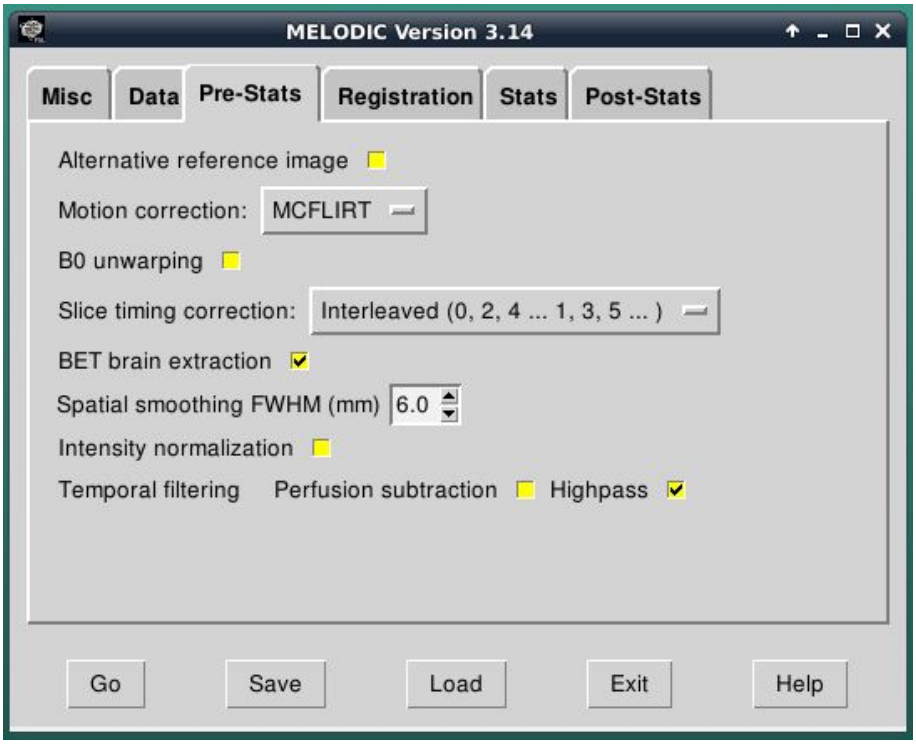

Figure 11: Melodic parameters - Pre-Stats.

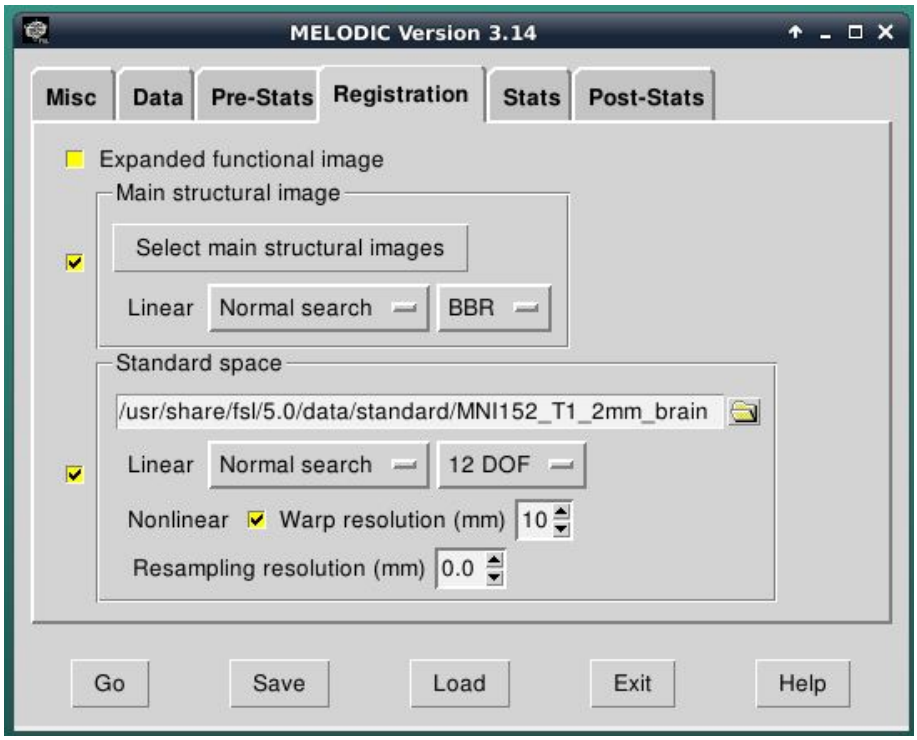

Figure 12: Melodic parameters - Registration.

Figure 13: Melodic parameters - Stats.

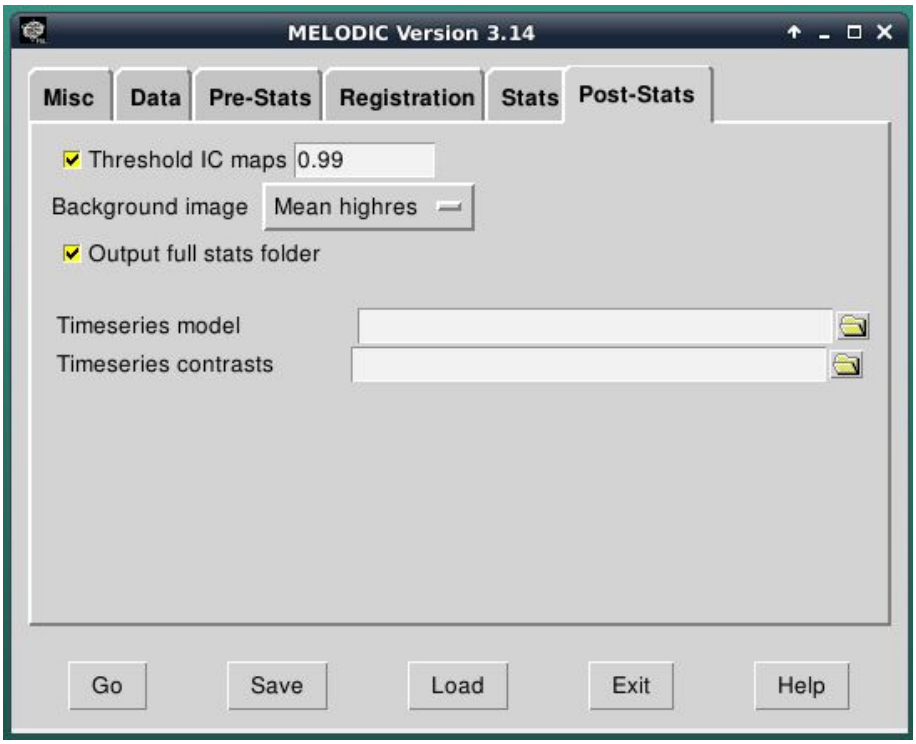

Figure 14: Melodic parameters - Post-Stats.

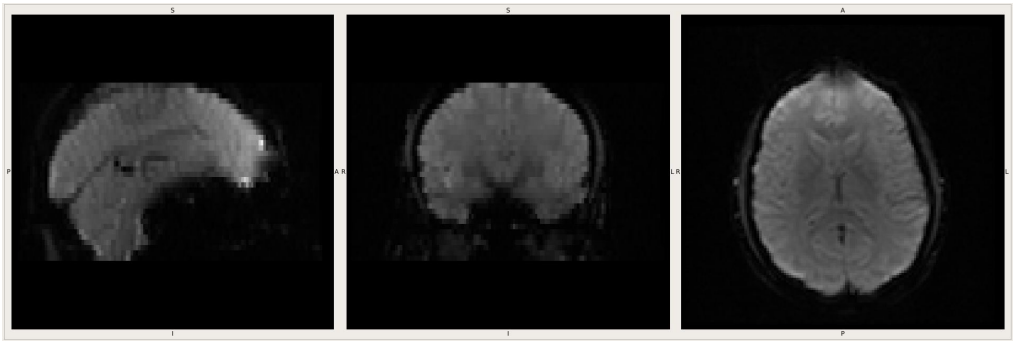

Figure 15: EPI of the 12th patient.

4.4 DATA ANALYSIS

The pre-processing procedure has had the aim of prepare fMRI data for the following statistical analysis. I have dealt with this analysis in the first person.

We dealt with several steps, from the modalities of choice of nodes of future networks to graph analysis performed by using Matlab software.

4.4.1 Nodes decision method

Firstly, we chose a way to segment 3D brain image in different region of interest (ROIs). This step is usually carried out using an anatomical atlas. To date, many atlases exist but there is not an atlas better than the others. Nevertheless, the Automated Anatomical Labeling (AAL) is the most used in functional brain studies, [59], [60], and the second most commonly used is the Harvard-Oxford probabilistic atlas, [61]. However, these methods, and in general any methods using atlases, are flawed and limited by a priori knowledge. The best thing to do is to use a method with the fewest prior assumptions (the only method that completely avoid any *a priori* assumption is the voxel-wise method, in which any voxel corresponds to a node).

We chose a different modality to obtain the ROIs in our study. We resorted to a specific software, called Freesurfer [62], that works with complex segmentation algorithms. The main advantages in using this software are that the segmentation is subject-specific and we can avoid the critical step of registration to a standard space. Freesurfer is an open source software suite for processing and analyzing brain MRI images. We performed it for each subject and this allowed us to obtain regions subject-specific. We then obtained all the ROIs that Freesurfer was able to segment, and we chose 85 regions between these covering the entire cortex and deep grey matter. For the result of segmentation, see Figure 20.

In Tables 3, 4 and 5 subcortical and cortical ROIs are listed. All the regions, *i.e.* the future nodes, are associated with a number which will make the recognition easier.

Table 3: List of subcortical ROIs, left and right side

N	ROI
1	Brainstem
2	Left Accumbens area
3	Left Amygdala
4	Left Caudate
5	Left Cerebellum Cortex
6	Left Hippocampus
7	Left Pallidum
8	Left Putamen
9	Left Thalamus
10	Left VentralDC
11	Right Accumbens area
12	Right Amygdala
13	Right Caudate
14	Right Cerebellum Cortex
15	Right Hippocampus
16	Right Pallidum
17	Right Putamen
18	Right Thalamus
19	Right Ventral DC

Table 4: List of cortical ROIs on the left side

N	ROI
20	Left Caudal Anterior Cingulate
21	Left Caudal Middle Frontal
22	Left Cuneus
23	Left Entorhinal
24	Left Frontal Pole
25	Left Fusiform
26	Left Inferior Parietal
27	Left Inferior Temporal
28	Left Insula
29	Left Isthmus Cingulate
30	Left Lateral Occipital
31	Left Lateral Orbito Frontal
32	Left Lingual
33	Left Medial Orbito Frontal
34	Left Middle Temporal
35	Left Paracentral
36	Left Parahippocampal
37	Left Pars Opercularis
38	Left Pars Orbitalis
39	Left Pars Triangularis
40	Left Pericalcarine
41	Left Postcentral
42	Left Posterior Cingulate
43	Left Precentral
44	Left Precuneus
45	Left Rostral Anterior Cingulate
46	Left Rostral Middle Frontal
47	Left Superior Frontal
48	Left Superior Parietal
49	Left Superior Temporal
50	Left Supramarginal
51	Left Temporal Pole
52	Left Transverse Temporal

Table 5: List of cortical ROIs on the right side

N	ROI
53	Right Caudal Anterior Cingulate
54	Right Caudal Middle Frontal
55	Right Cuneus
56	Right Entorhinal
57	Right Frontal Pole
58	Right Fusiform
59	Right Inferior Parietal
60	Right Inferior Temporal
61	Right Insula
62	Right Isthmus Cingulate
63	Right Lateral Occipital
64	Right Lateral Orbito Frontal
65	Right Lingual
66	Right Medial Orbito Frontal
67	Right Middle Temporal
68	Right Paracentral
69	Right Parahippocampal
70	Right Pars Opercularis
71	Right Pars Orbitalis
72	Right Pars Triangularis
73	Right Pericalcarine
74	Right Postcentral
75	Right Posterior Cingulate
76	Right Precentral
77	Right Precuneus
78	Right Rostral Anterior Cingulate
79	Right Rostral Middle Frontal
80	Right Superior Frontal
81	Right Superior Parietal
82	Right Superior Temporal
83	Right Supramarginal
84	Right Temporal Pole
85	Right Transverse Temporal

4.4.2 Temporal series

For each ROI, the respective temporal series was obtained by averaging the time series across all voxels inside that specific region, using the fsl function *fslmerge*.

An interesting and important issue arises before importing time series in Matlab: we had two temporal series for each region for all the patients and the healthy controls, because two runs per subject were acquired initially. This is the standard protocol for rs-fMRI acquisition optimised at the functional MR Unit at the S.Orsola-Malpighi polyclinic. This method reduce the problems related to incorrect acquisitions (*e.g.* if one run was damaged by head motion or by some other artifacts, it is however possible to use the other for studies) but primarily this process allows to improve the Signal to Noise Ratio (SNR).

Unlike the fMRI analysis, in which the two runs are tipically averaged at different possible levels, a procedure to handle with two scans does not exist in fMRI graph based analysis. Hence, we decided to average these two acquisitions for each ROI. The problem was to decide at which level of the entire process of data analysis we should have had average the two temporal series. We decide that the averaging process would have been done before binarization of correlation matrices, because after that, the information inside the temporal series would have been lost. Therefore, we decided to average the time series in their signal form, as the first process subsequent to their importation in Matlab. It could be interesting in the future to develop other processing methods to handle with the two runs.

4.4.3 Graph theoretical data analysis in binary graphs

The graph theory data analysis consisted in generating a network for every subject and calculating the topological parameters for each of these. After rs-fMRI data have been collected from the subjects and mean time series of each region of interest have been extracted from the set of images, the Pearson Correlation analysis was performed between all possible pairs of ROIs. The correlations were represented in the form of a correlation matrices, which were binarized at given thresholds to yield different adjacency matrices. Therefore the functional networks were defined, since each ROI was represented by a node and each functional connection was represented by a link. In Figure 16 the whole process of generating functional network is shown, following the scheme of Wang et al. in [68], with our own data.

In the next subparagraphs the entire process will be explained in more detail.

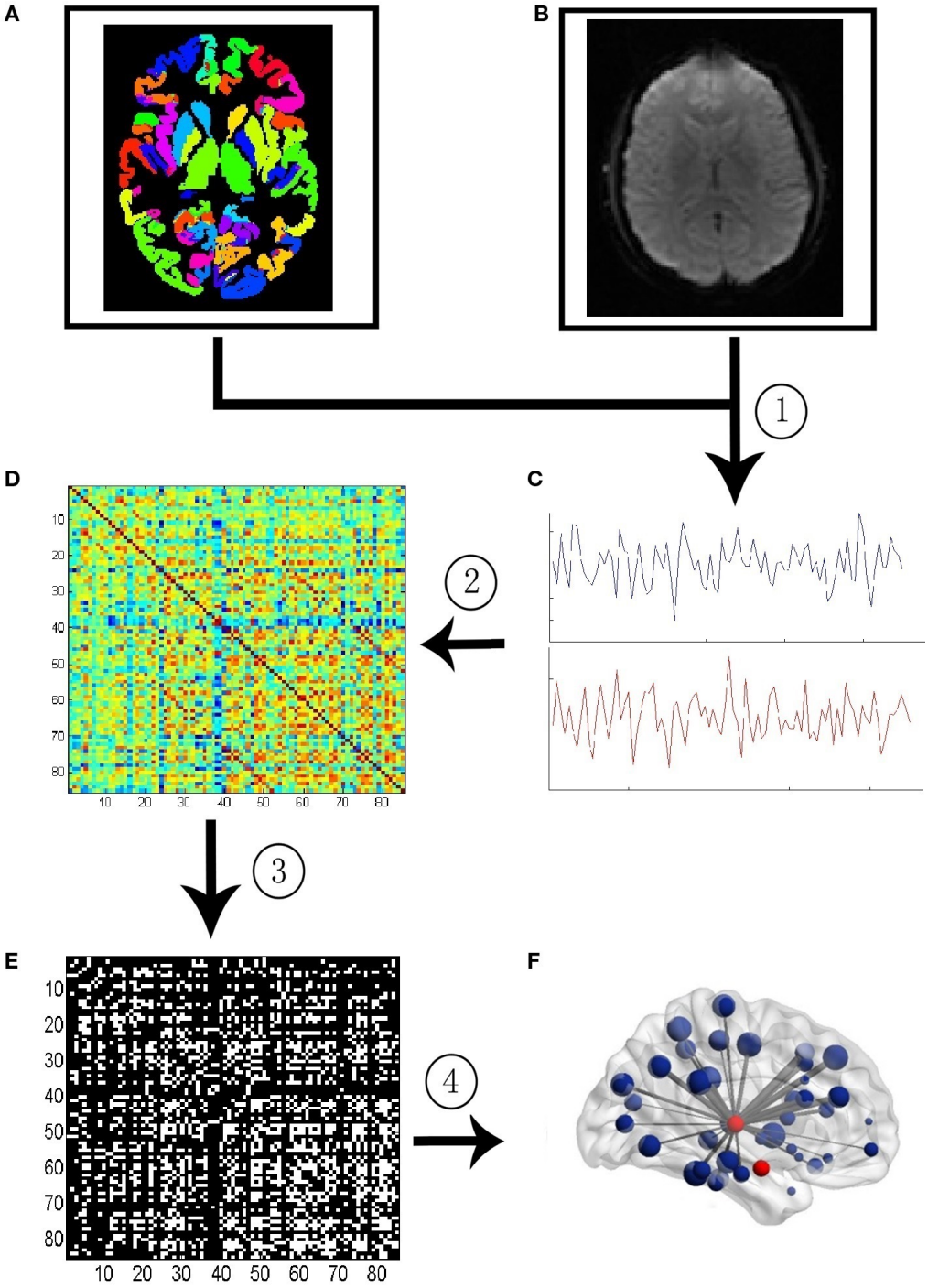

Figure 16: Process of generating functional network: **(1)** Extraction of the time series (C) from rs-fMRI data (B) within each anatomical region. ROIs are obtained according to the Freesurfer results (A); **(2)** Calculation of the functional connectivity correlation matrix (D) between any pairs of nodes; **(3)** Application of the threshold to the correlation matrix to generate the binary connectivity matrix; **(4)** Visualization of the association matrix as a graph (F).
The structure of the image was taken from [68].

Definition of Correlation Matrices

Once the temporal series have been imported in Matlab and the average of the two runs has been performed, the first step was to decide which correlation metrics must be used to generate the correlation matrices. There were different possibilities of choice. As reported in the study made by Xia Liang et al. [63] , which investigated the influences of different correlation metrics on the topological properties of functional brain networks obtained starting from rs-fMRI, the Pearson Correlation showed the most valid and reliable results for resting-state brain network studies, whereas partial correlation should be treated with caution.

Based on these results, we chose the Pearson Correlation to obtain the correlation matrices. In Matlab environment, this corresponds to use *corr* function between every couples of ROIs for each subject. An example of the resulted matrix is shown below in Figure 17

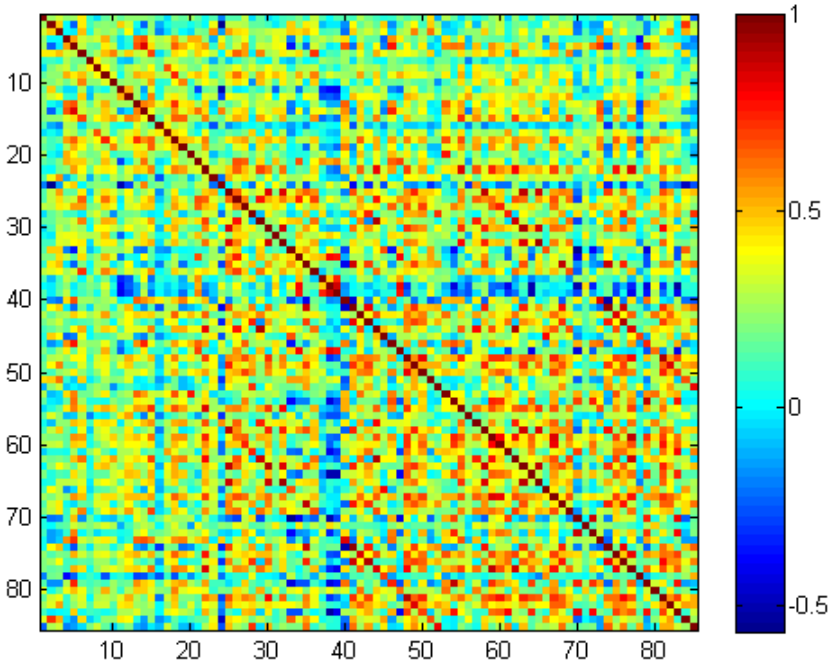

Figure 17: Correlation matrix of a healthy control (N=10). The colorbar shows the range of the values, between -1 and 1.

To evaluate the correlation coefficients values, the histograms of these distributions and the histograms of p values distributions were plotted.

We also plotted these distributions with a magnification on x axes and y axes separately, with the aim of obtaining the plots of p values distributions with better details.

To understand if there were any obvious differences between the correlation coefficients of the patients and the correlation coefficients of the healthy controls, we performed a preliminary statistic test for each of these between the two groups.

First of all, we performed the normality test, namely one-sample Kolmogorov-Smirnov test, to figure out if the samples were normally distribuited or not. The normality test rejected the null hypotesis that the samples had Gaussian distributions, so we chose a non-parametric test, namely the Mann-Whitney test (see section 5.2).

Finally, to be sure that the information extracted from the temporal series were not due to chance, we performed a phase shuffling of data. We shifted a number (n) of values from the start to the end in each temporal series of each subject, since n was a random number between 1 and 90 (number of values in each time series that correspond to the number of the acquired volumes). In this way we wanted to understand if the data - and the information carried by them - were due to fortuity or not (see section 5.2).

Thresholding and Adjacency Matrices

Before any consideration on which threshold we chose, we have neglected all the values of the correlation matrices between -1 and 0, as reported in [74], because, to date, there is not a physiological interpretation for the negative functional connection between two regions of the brain. Maybe, the future network methods may be able to quantify the role of the negative weights in the global network organization.

As Bullmore and Bassett affirm, [70], the best choice to implement process of a threshold to the adjacency matrices is to investigate the topological properties as a function of changing connection density value.

The connection density (δ), or density link, is defined as

$$0 \leqslant \delta \leqslant 1 = \frac{\varepsilon_\tau}{\frac{N(N-1)}{2}} \tag{12}$$

where ε_τ is the number of links generated by that value of threshold τ, N is the number of nodes and $\frac{N(N-1)}{2}$ is the maximum number of links that could exist in a network with N nodes.

In order to calculate network properties as function of the threshold, we started with choosing one hundred different values of "density link" between 0 and 1, with step of 0.01. For every δ value we force all the adjacency matrices to have the same number of links.

At each step, we knew δ value and the total number of links, so we calculated the number of connections (ε_τ) for a specific threshold τ, for each network for every value of δ. ε_τ correspond at each step to the number n of link with greater significance.

Deepening the methodological process, we sorted in descending order, for every δ, the r values of the n links, knowing that the n-th of these values (where the n-th value is equal to ε_τ) coincides with the r value relative to the threshold value for that particular δ.

So, we had 100 different values of *density link* for 26 different correlation matrices (13 healthy controls and 13 patients).

In Figure 18 the same connection matrix with different number of links is shown. That means that for each matrix was used a different threshold (and different δ).

Obviously, the number of the connections in the matrices (white pixels) are twice the number of the links, because if a connection between the node i and the node j exists, then there is a connection in both i,j and j,i positions. It follows that the connection matrices are symmetric.

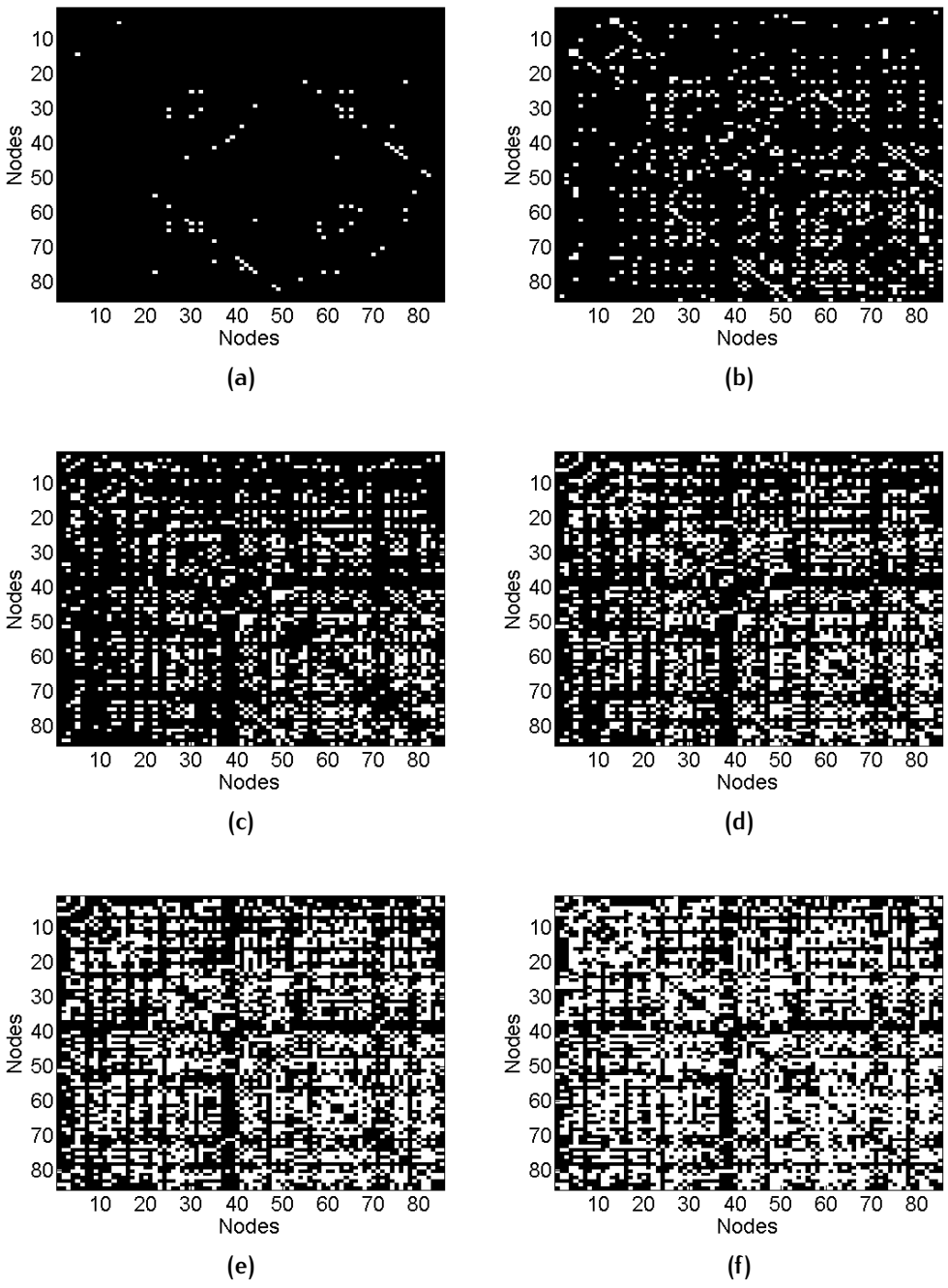

Figure 18: Adjacency matrices resulting from the application of six different thresholds to the correlation matrix of a healthy control (N=10): (a) $\tau = 0.01$, (b) $\tau = 0.1$, (c) $\tau = 0.2$, (d) $\tau = 0.3$, (e) $\tau = 0.4$, (f) $\tau = 0.5$. Where the colour of the pixel is white that means there is a connection.

Topological parameters and group analysis

The calculation of the topological parameters of the networks was performed using Matlab functions contained in BGL [73], and BCT [74], software libraries.

The parameters that we chose to calculate can be divided into two main groups: those related to the entire network and those related to a specific node.

For the first group, we calculated the number of the connected components, the dimension of the giant connected component and the Global Efficiency, all three as function of threshold values, for every network. The Matlab functions that we used are *components.m* and *efficiency_bin.m* respectively. We performed also the Mann-Whitney test to analyze differences between the connected components of the healthy controls and the patients, for each value of the threshold. We performed the same Mann-Whitney test also for Global Efficiency (see 5.3).

The second group of parameters, those related to a specific node, is composed by Clustering Coefficient, Node Degree, Local Efficiency and Betweenness Centrality.

The respective functions in Matlab are *clustering_coefficient.m*, *degrees_und.m*, *efficiency_bin.m* and *betweenness_bin.m*. For each of these parameters the Mann-Whitney test was carried out with the aim of investigate about the possible significant differences between the healthy controls and the patients for all values of the thresholds (see section 5.3).

4.4.4 Graph theoretical data analysis in weighted graphs

Until this moment, we have analyzed the unweighted graphs, in which the information carried by the links is limited to the connection existence. If the links of the graphs had a weight for each connection, the information would extend to the strenght of the connection itself.

We resumed the correlation matrices of networks and we considered only values between 0.2 and 1. Starting from this matrices, we generated weigthed networks, in order to study two more topological parameters, namely Spectral Centrality and Salient Centrality.

The two functions used in Matlab are *spectral_centrality_scott.m* and *salient_centrality.m*. For the reference, see respectively [71] and [72].

5 RESULTS

5.1 FREESURFER SEGMENTATION

The Freesurfer segmentation performed on the 3D image of one healthy control (Figure 19) is shown in Figure 20, where the 85 ROIs that we chose as nodes are represented in false colors.

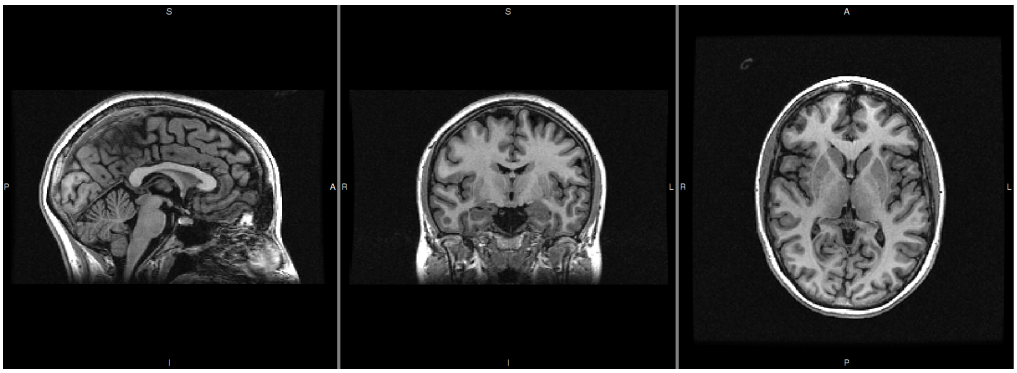

Figure 19: Morphological 3D image of one healthy control. From left to right sagittal, coronal and axial views are shown.

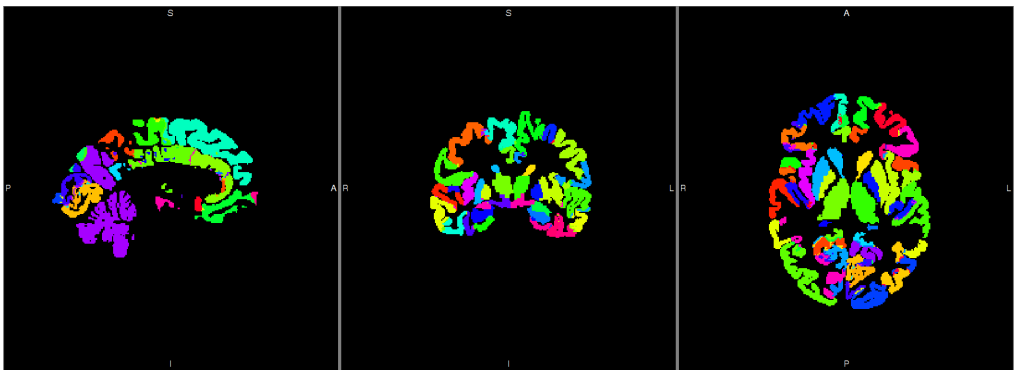

Figure 20: Result of Freesurfer segmentation performed on 3D image of one healthy control. The 85 ROIs are represented with false colours. From left to right sagittal, coronal and axial views are shown.

5.2 CORRELATION ANALYSIS

Pearson correlation was used to measure the association between every couple of nodes.

Figures 21 and 22 show the distribution of correlation coefficients of 13 healthy controls and 13 patients. We can note that values in the histograms go from - 0.5 to 1, and these bin distributions are centered around 0.5.

We were also interested in the significance of these correlations, so we analyzed and plotted the distributions of the p values of the correlations seen before. The distribution of p values of the correlation coefficients of one healthy control is shown in Figure 23 and the same distribution for one patient is shown in Figure 24. In order to better visualize the distributions, we zoomed in all the plots of the p values distributions along both axes separately. In Figures 25 and 26 the plots of all subjects with y values between 0 and 100 are shown, in Figures 27 and 28 the same distributions are displayed but with a zoom on x axis, in particular with x values that go from 0 to 0.1. In this way we can observe in a better detail the range of p values that are lower than 0.05, that correspond to correlations that are significant.

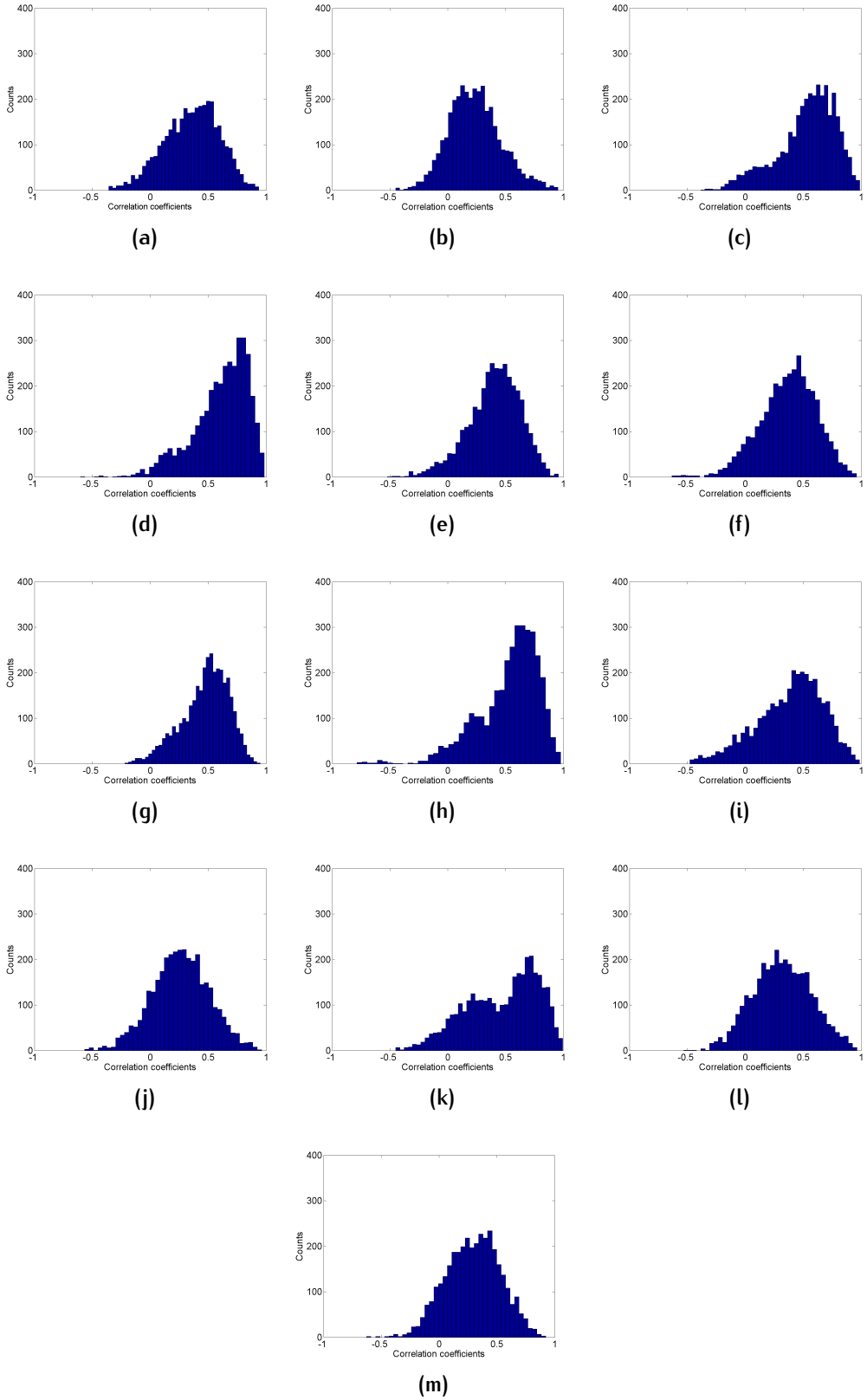

Figure 21: Histograms of correlation coefficients distributions in healthy controls.

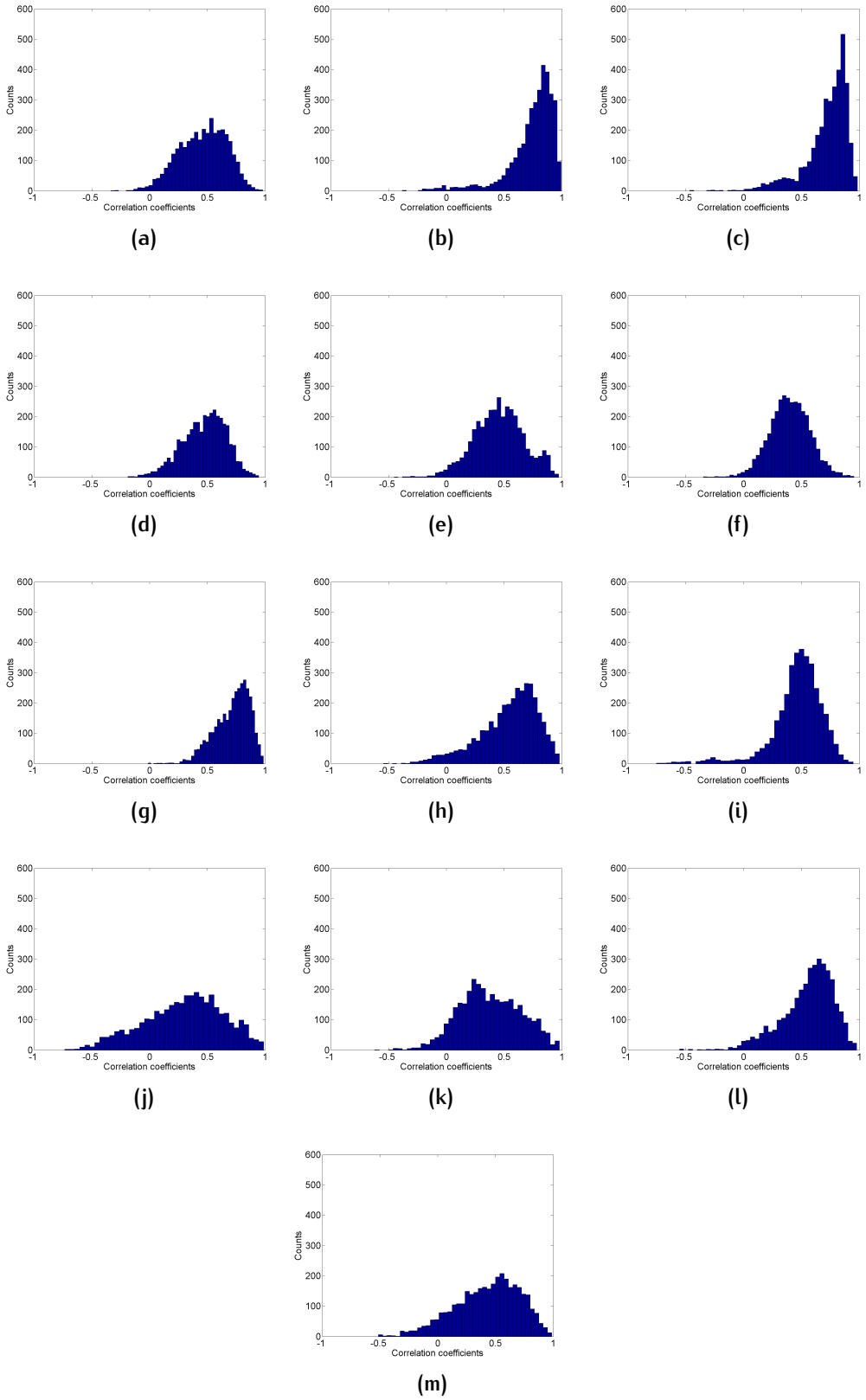

Figure 22: Histograms of correlation coefficients distributions in patients.

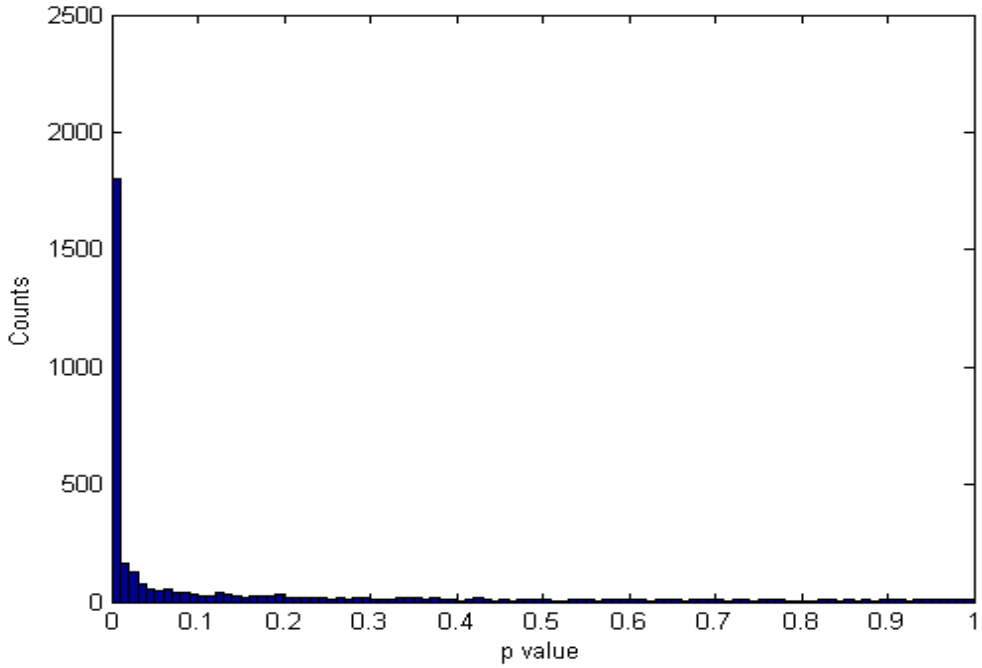

Figure 23: Histogram of p values distribution in one healthy control.

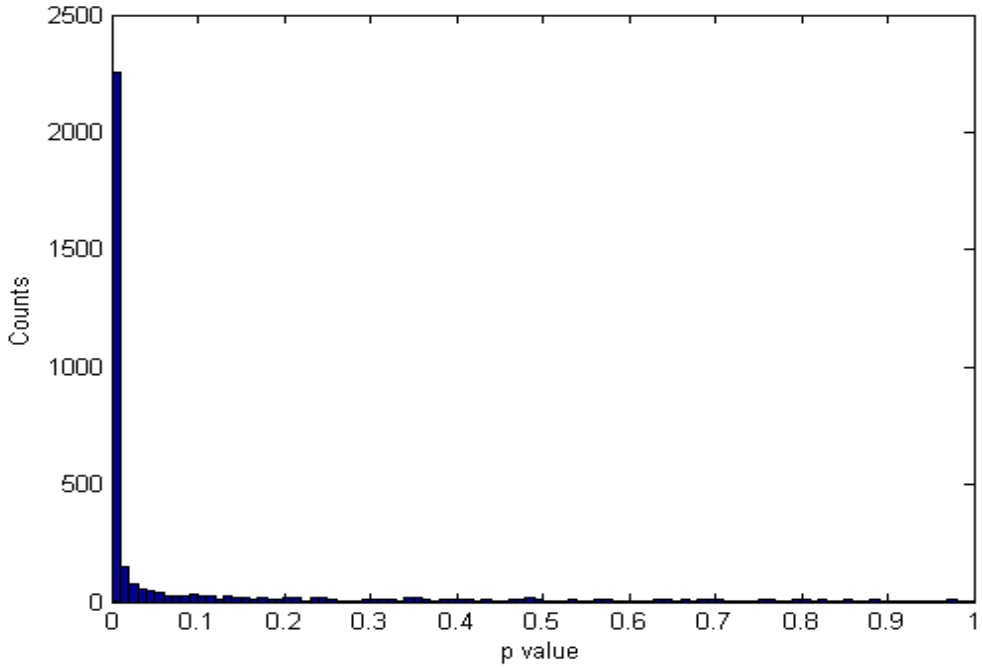

Figure 24: Histogram of p values distribution in one patient.

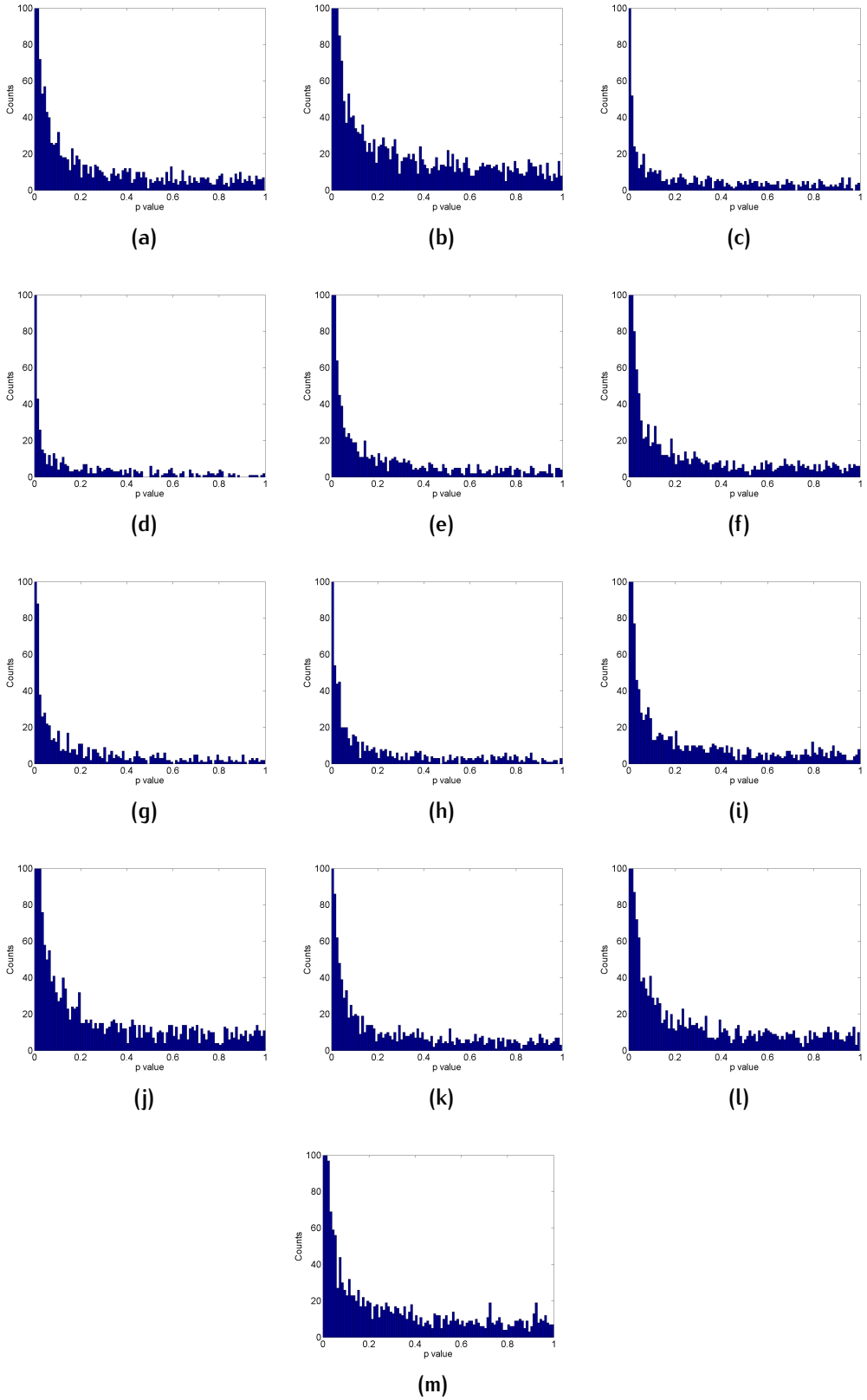

Figure 25: Histograms of p values distributions in healthy controls, with a zoom on y axes.

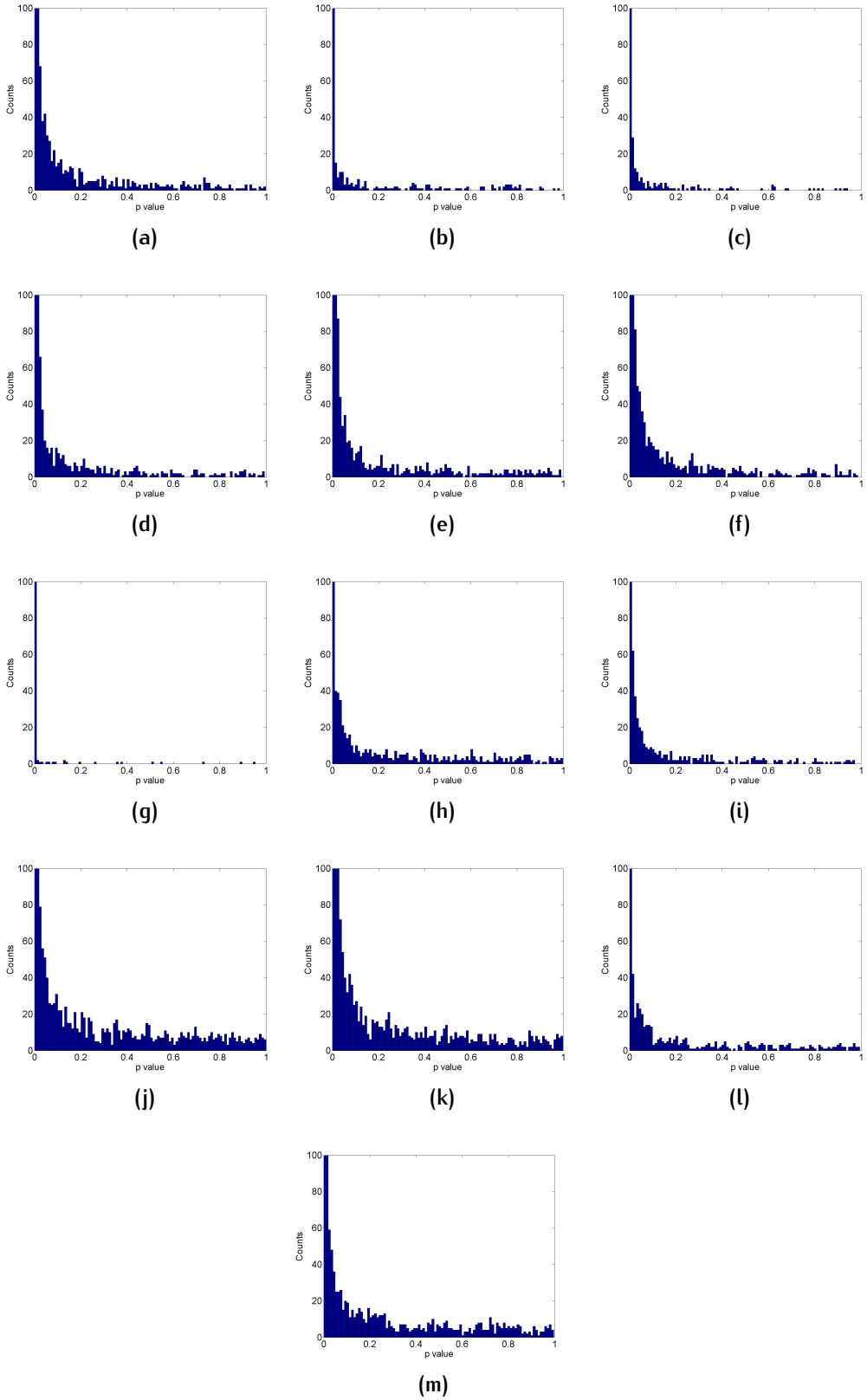

Figure 26: Histograms of p values distributions in patients, with a zoom on y axes.

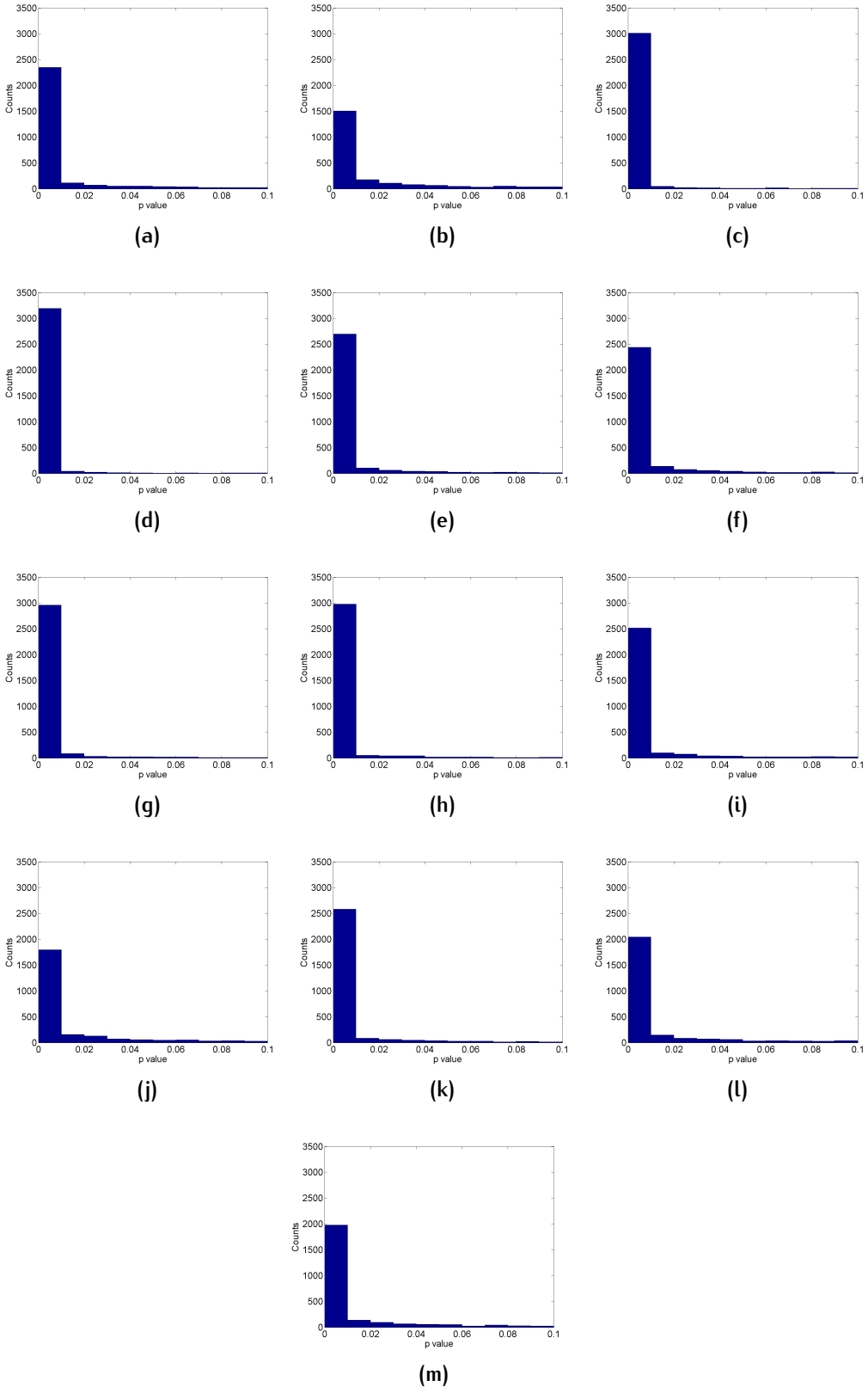

Figure 27: Histograms of p values distributions in healthy controls, with a zoom on x axes.

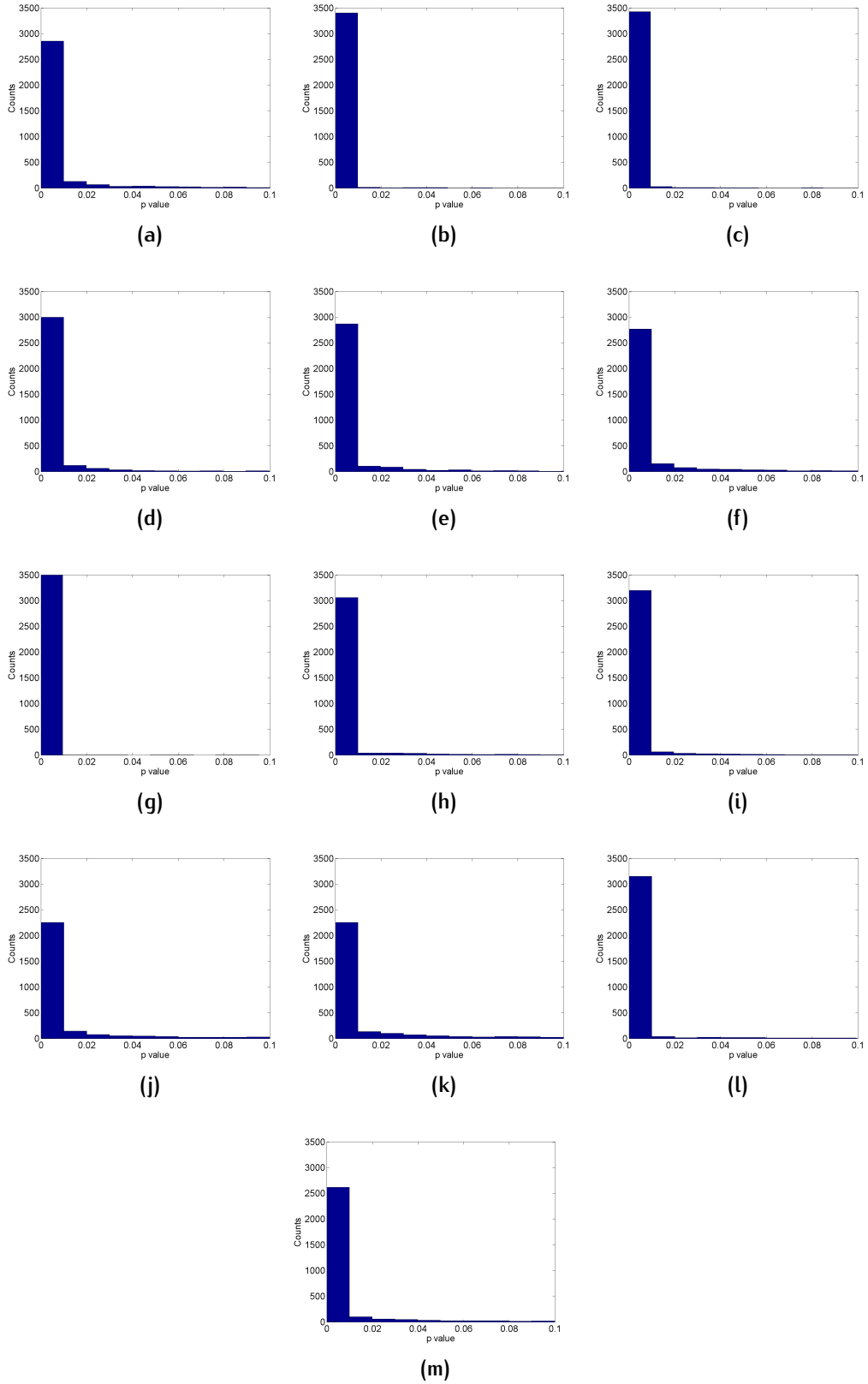

Figure 28: Histograms of p values distributions in patients, with a zoom on x axes.

The results of the Mann-Whitney test performed for each correlation coefficient between the two groups are shown in Figure 29. The colours represent the p values of the statistic test, from 0 to 1. If the value of p is less than 0.05, the difference between the correlation coefficients is statistically significant, instead if p is greater than 0.05, the difference is not significant, since 0.05 has been chosen as the discriminant level for the test. We did not performed any correction for multiple comparisons beacause it was only an explorative analysis.

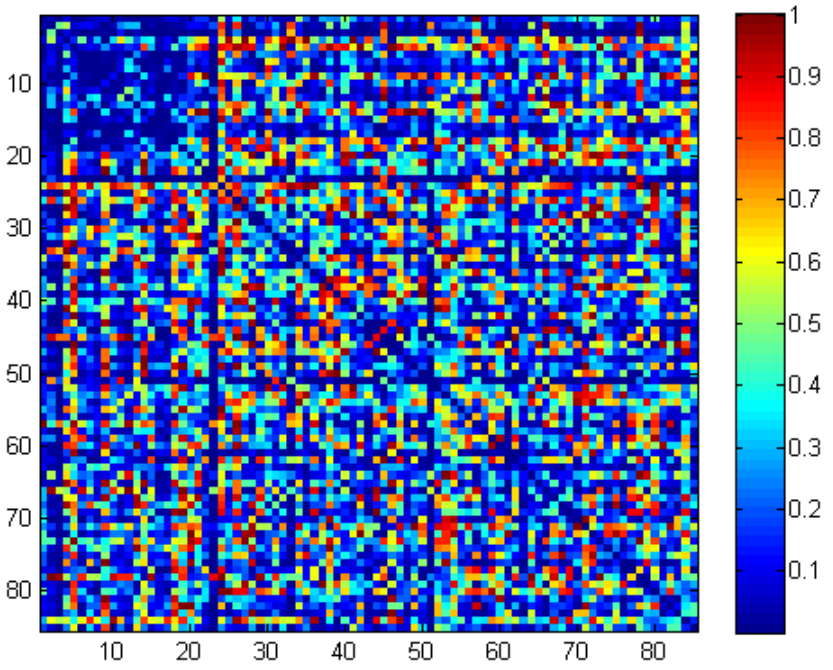

Figure 29: Matrix of p values of Mann-Whitney test for correlation coefficients.

In Figures 30 and 31 the distributions of correlation coefficients of healthy controls and patients are shown after shifting the first n values from the start to the end of the temporal series. As we expected, after data shuffling, correlation coefficients distributions are centered around zero and they have a tipical Gaussian shape. We plotted also the distributions of p values of shuffled data, and the results are displayed in Figures 32 and 33. We noticed that the number of p values that are less than 0.05 are substantially less than p values in the same range before shuffling of data.

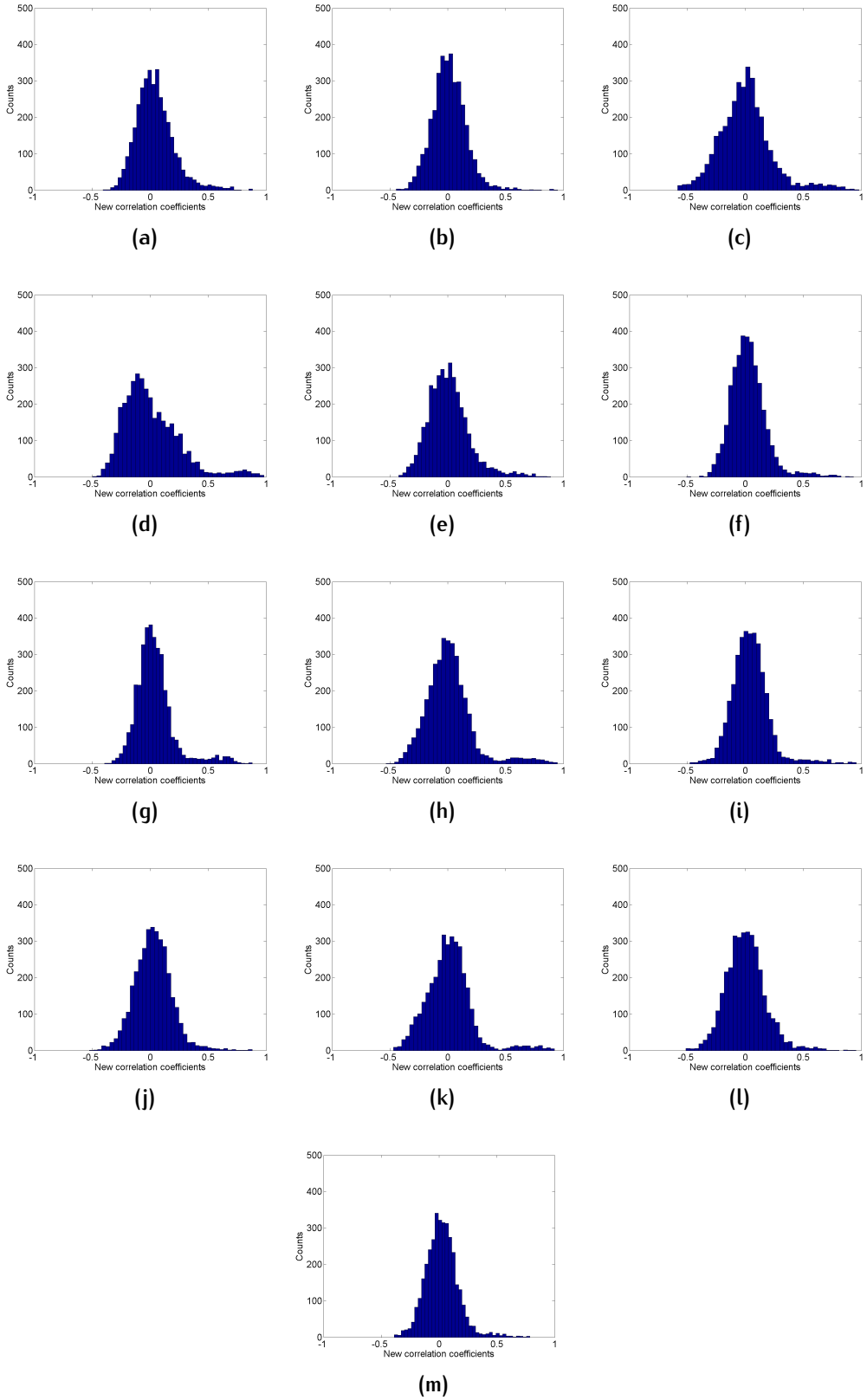

Figure 30: Histograms of correlation coefficients distributions in healthy controls after phase shuffling

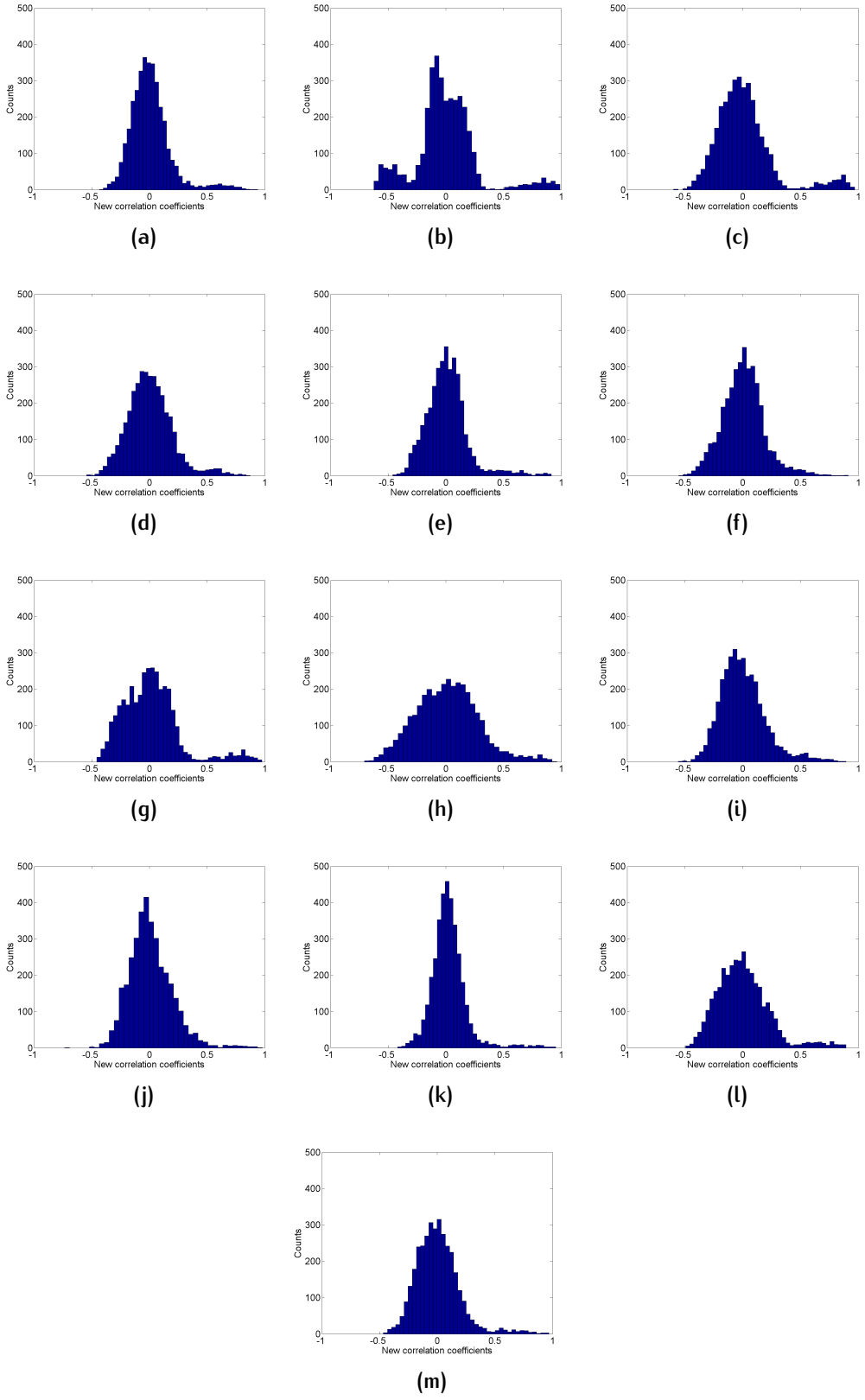

Figure 31: Histograms of correlation coefficients distributions in patients after phase shuffling

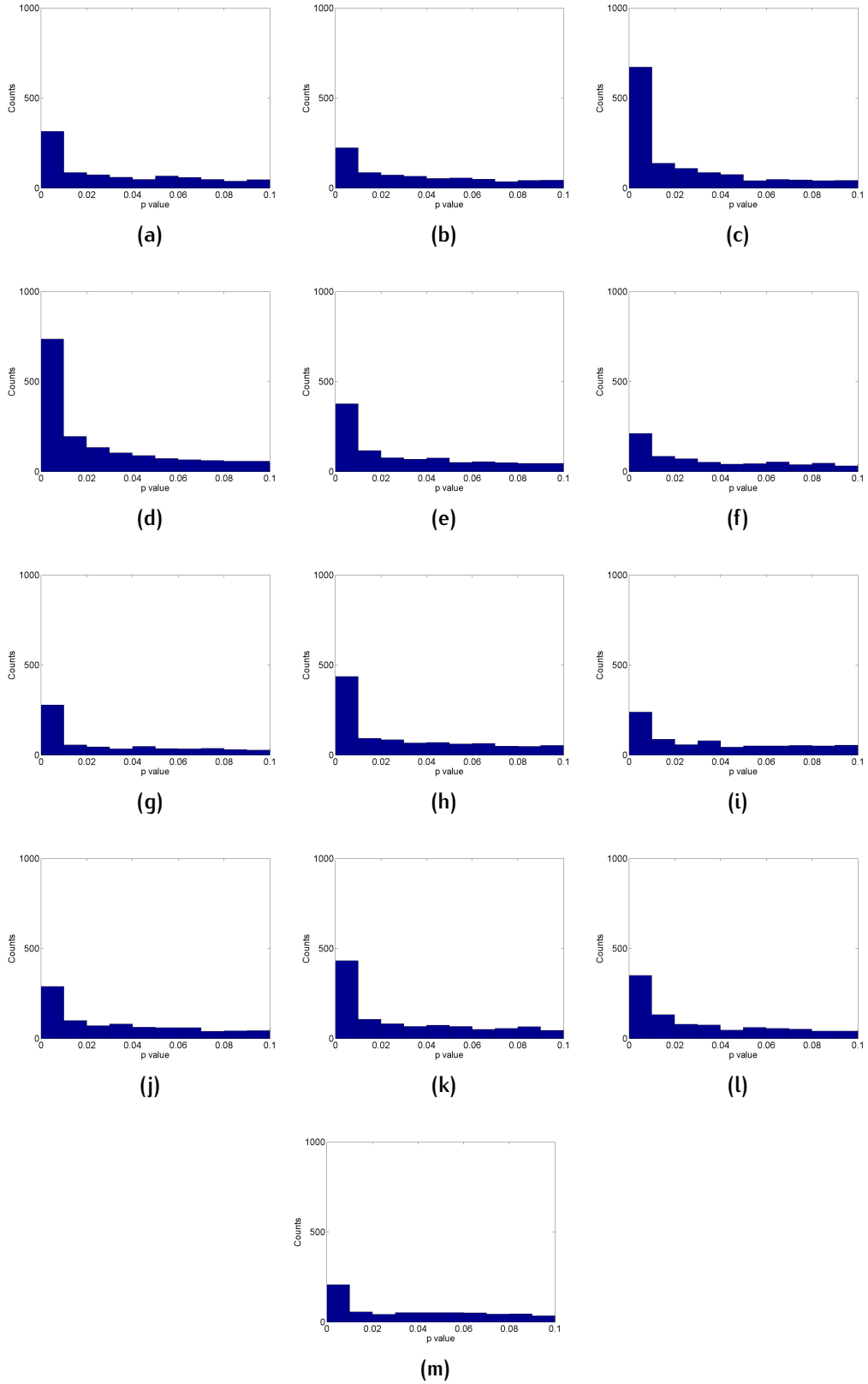

Figure 32: Histograms of p values distributions in healthy controls after phase shuffling of temporal series, with a zoom on x axes.

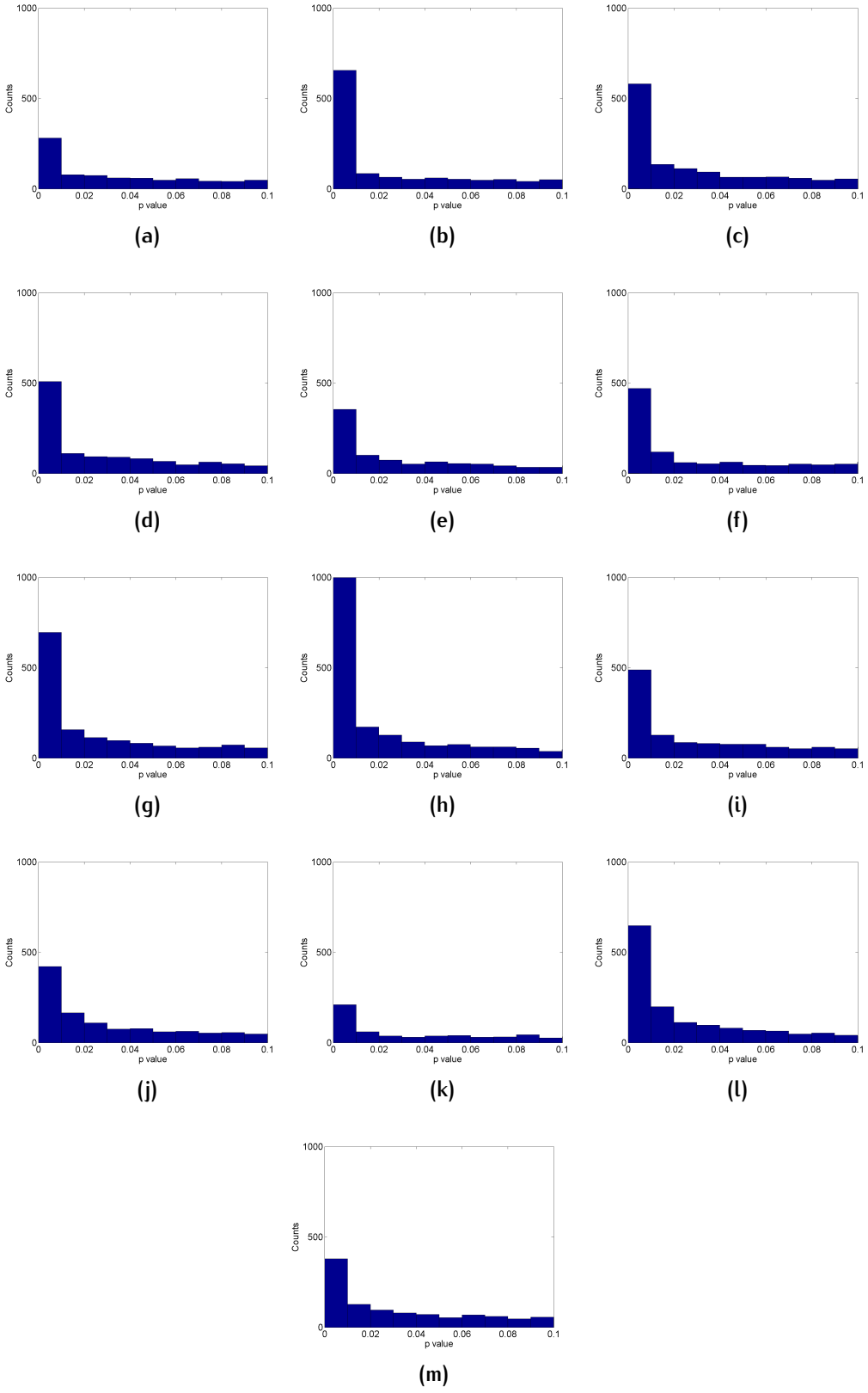

Figure 33: Histograms of p values distributions in patients after phase shuffling of temporal series, with a zoom on x axes.

5.3 TOPOLOGICAL PARAMETERS AND GROUP ANALYSIS

Topological parameters are divided into two main groups: those related to the entire network and those related to a specific node.

For the first group, we calculated the number of the connected components, the dimension of the giant connected component and the Global Efficiency for different thresholds for every networks. In Figures 34 and 35 we noticed that the number of the connected components, both in healthy controls and in patients, decreases with the increasing of the threshold value. The connected components averaged across all healthy controls and all patients are shown in Figure 36, and we noticed a very similar tendency for the two groups of subjects. We did also the Mann-Whitney test (also called Wilcoxon test) to analyze differences between the connected components of healthy controls and patients, for each value of the threshold. The result showed that there were not statistically significant differences between the two groups of values.

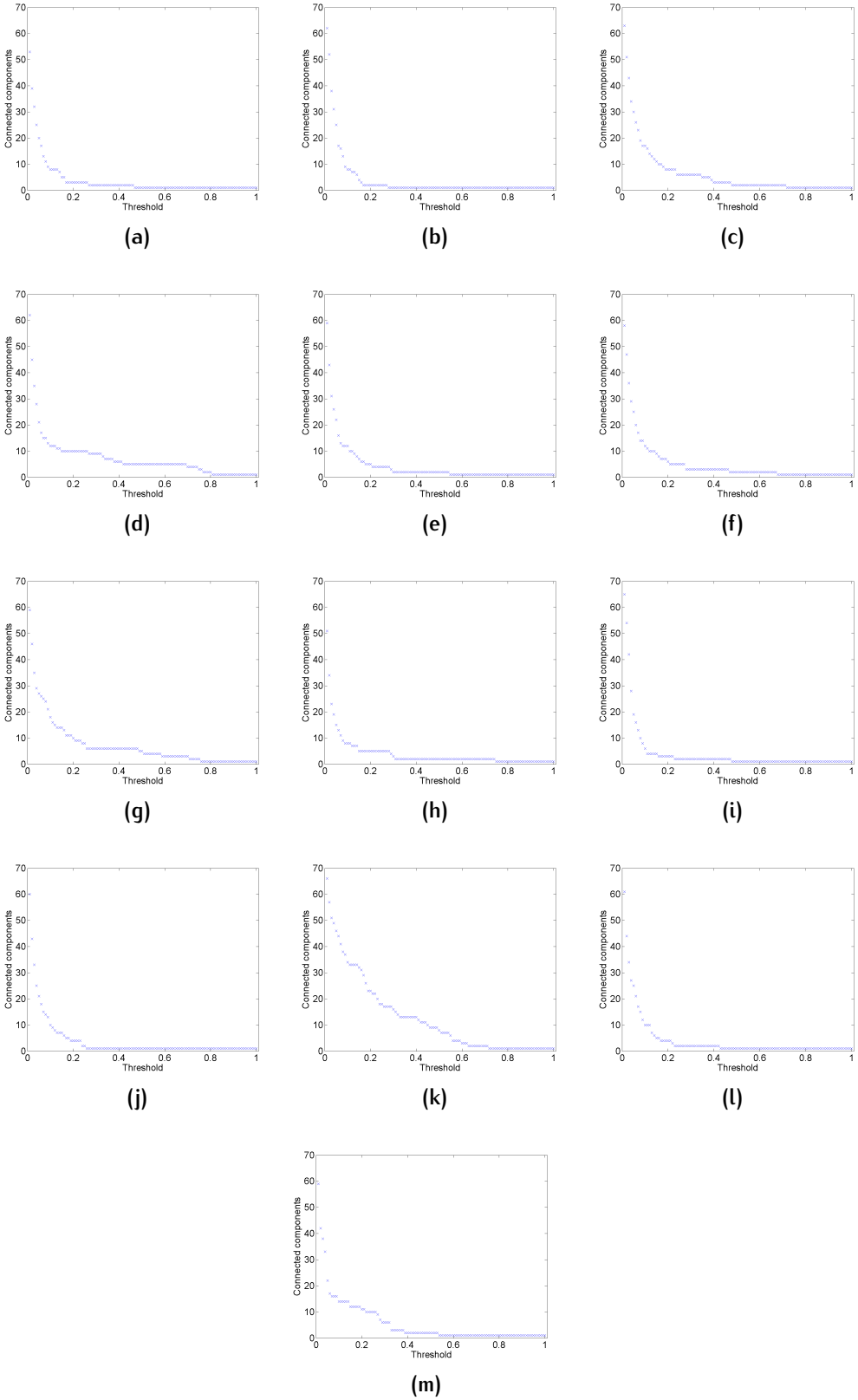

Figure 34: Connected components as function of threshold in healthy controls

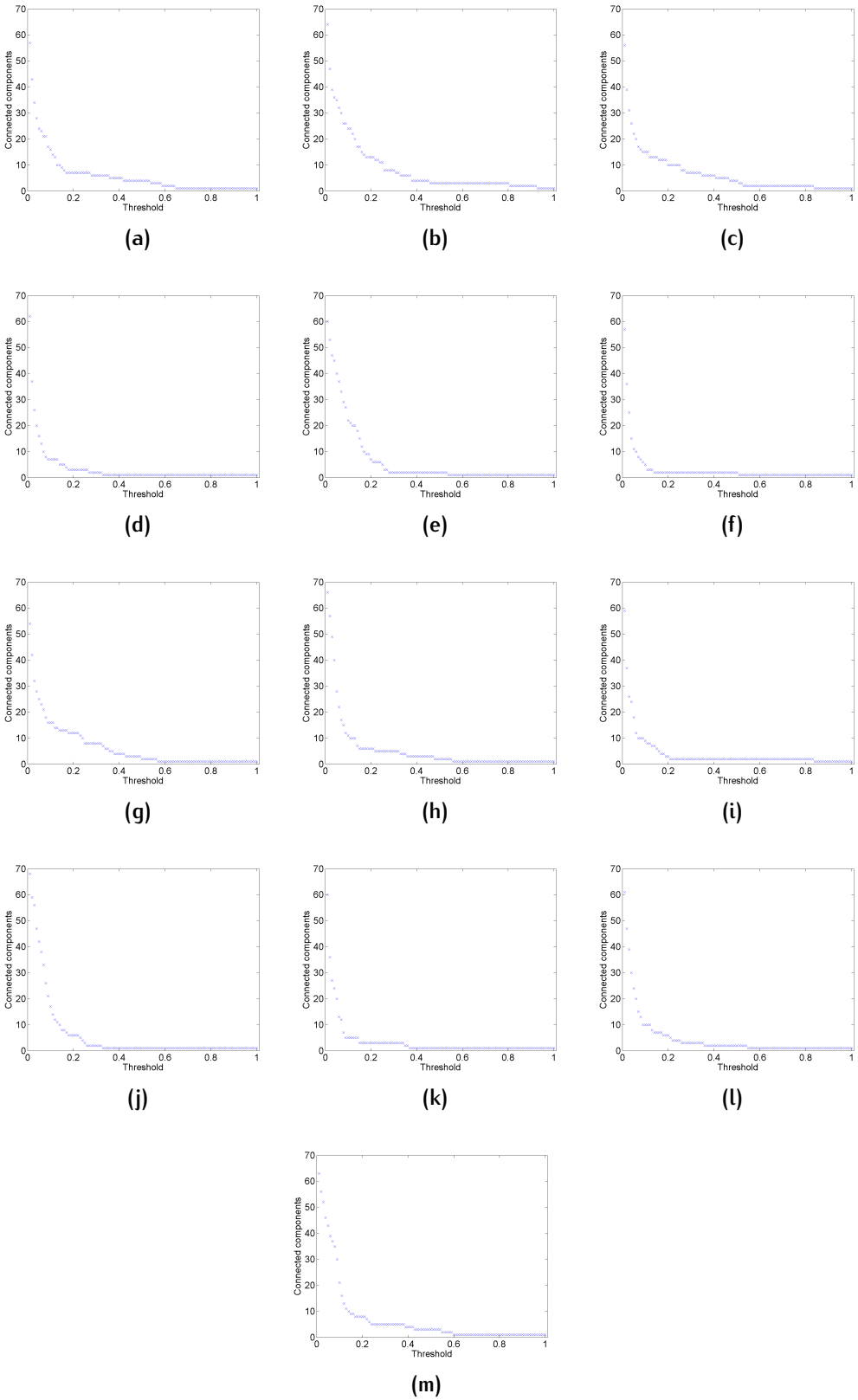

Figure 35: Connected components as function of threshold in patients

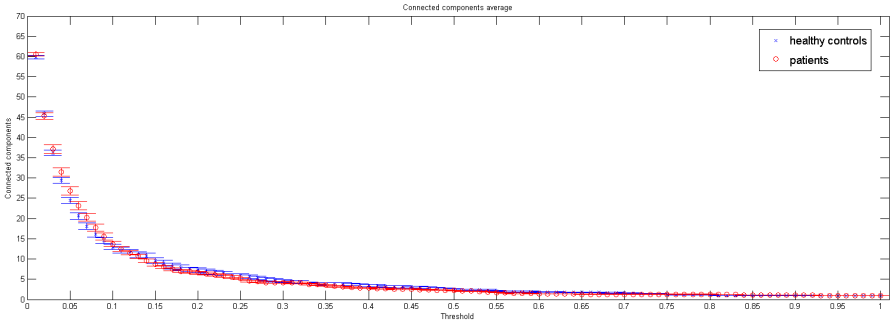

Figure 36: Connected components as function of threshold in healthy controls (blue) and patients (red), with bar errors. The result of the Mann-Whitney test showed that there were not statistically significant differences between the two groups.

In Figures 37 and 38 the dimensions of giant connected components for different thresholds for each subject are shown. We noticed that for a threshold value equal to 0.1, which means that there is 10% of maximum number of links, the giant connected component in almost every subject contains already 50-60 nodes, so it is already well defined.

The Global Efficiency was calculated for every threshold point, averaged across all patients and all healthy controls. The results are shown in Figure 39. Once more, the Global Efficiency is similar for the two groups and the Mann-Whitney test revealed that there weren't statistically significant differences.

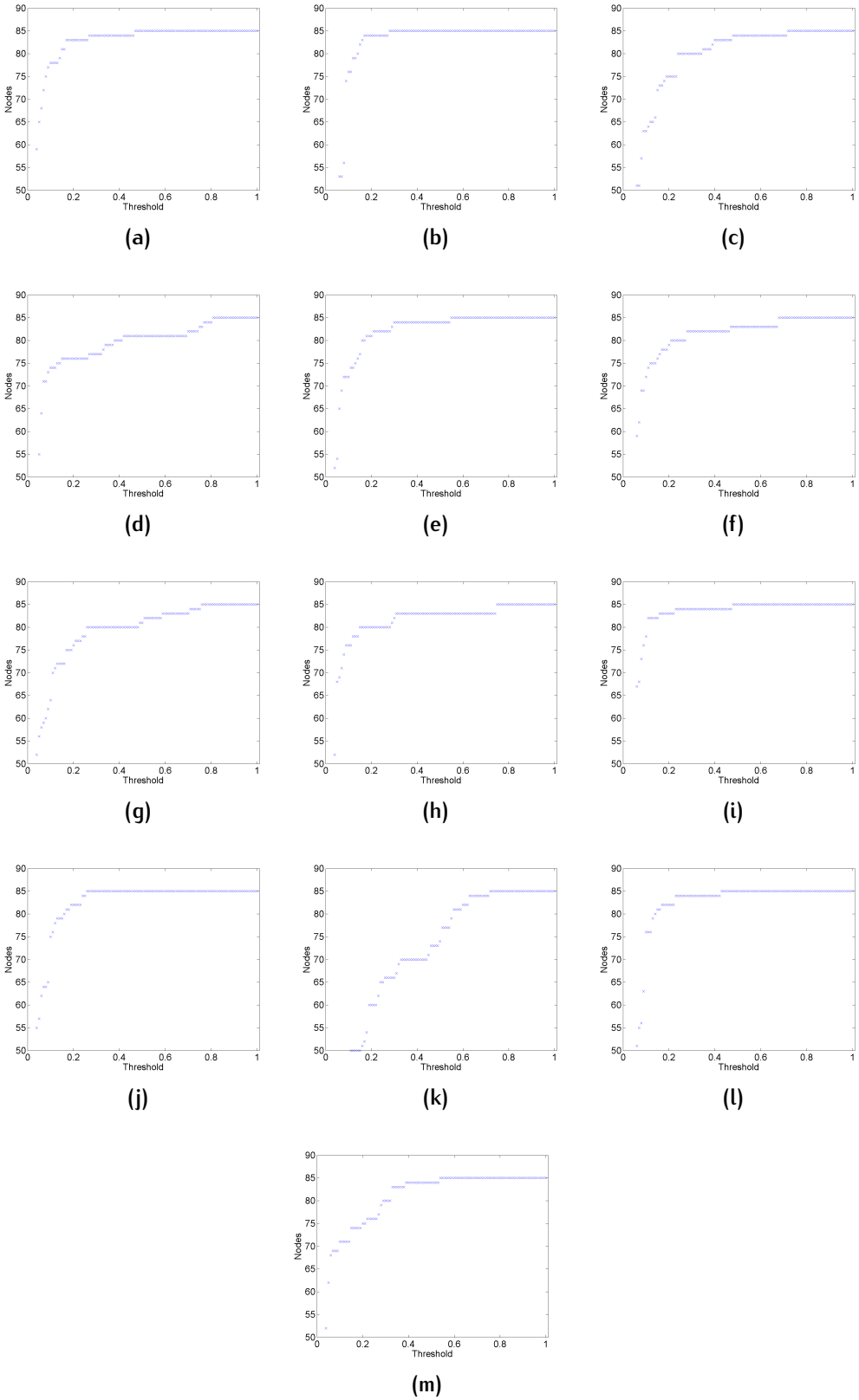

Figure 37: Dimension of giant connected component in healthy controls as function of threshold

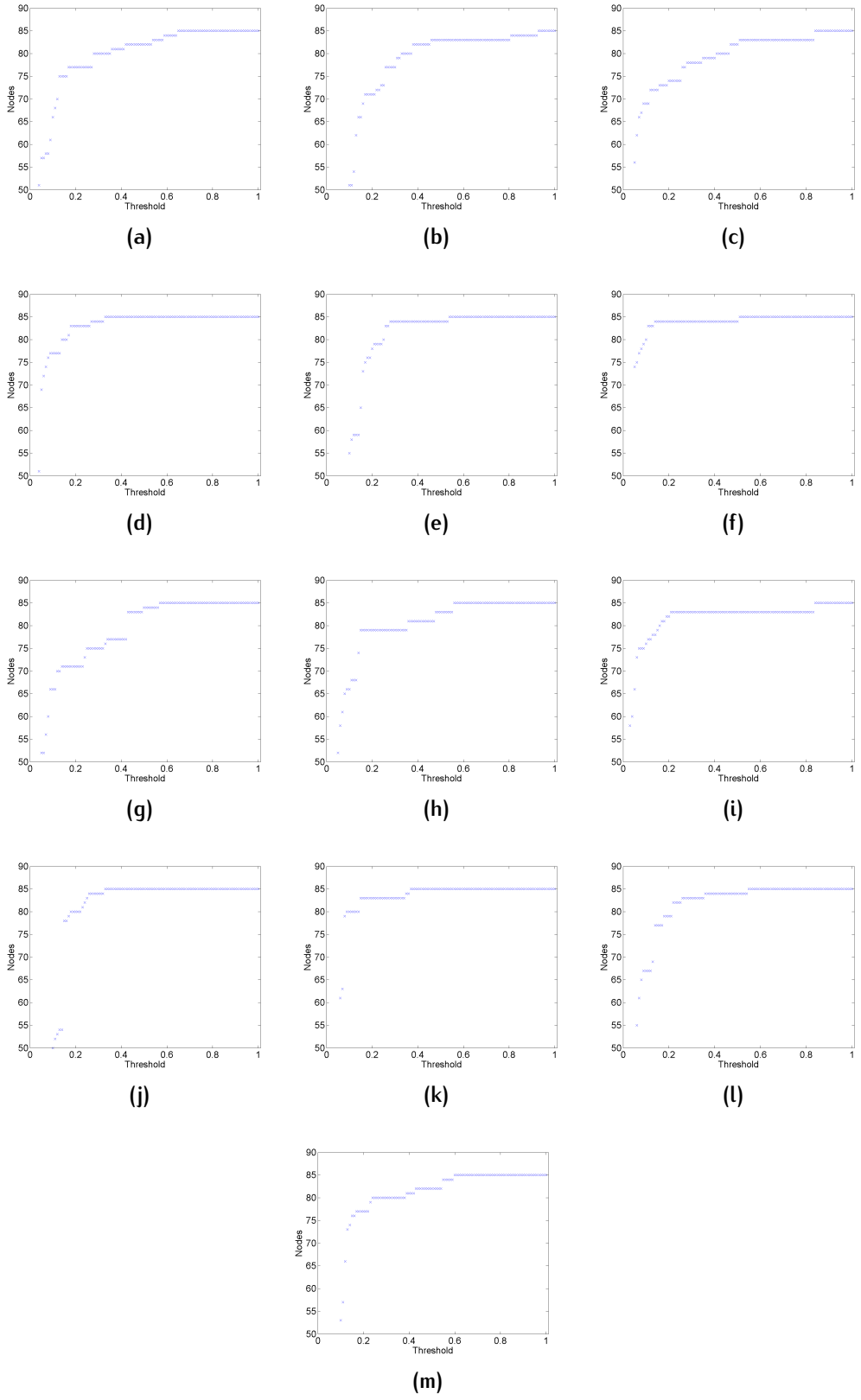

Figure 38: Dimension of giant connected component in patients as function of threshold

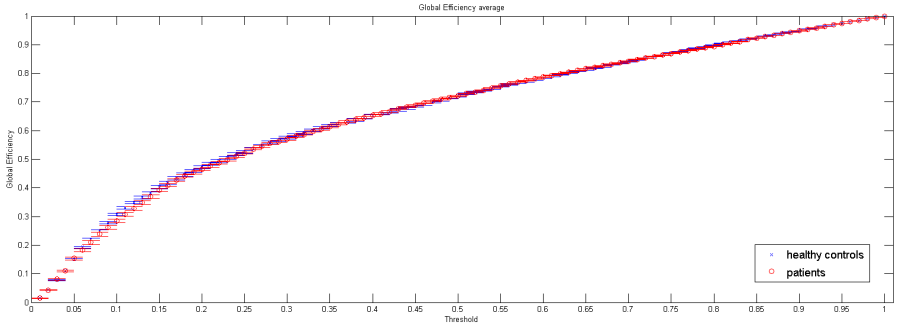

Figure 39: Global Efficiency in patients (red) and healthy controls (blue) as function of threshold. The result of the Mann-Whitney test showed that there weren't statistically significant differences between the two groups of values

The second group of parameters, those related to specific node, is composed by Clustering Coefficient, Node Degree, Local Efficiency and Betweenness Centrality. For each of these parameters the Mann-Whitney test was performed with the aim to investigate about possible significant differences between healthy controls and patients along all values of threshold. The results are shown below: the Clustering Coefficient in Figure 40, the Node Degree in Figure 45, the Local Efficiency in Figure 52, the Betweenness Centrality in Figure 57.

All of these results were corrected for multiple comparisons, using False Discovery Rate. Any difference after correction did not survive. For this reason, we considered a more strict criterion to test significance ($p < 0.01$), without performing multiple comparison correction. The four specific node measures showed some significant differences at this new level of significance, which are displayed in figures 41, 46, 53, 58, near the images with $p < 0.05$.

We consider more robust the differences that we found within a density link range approximatively between 0.2 and 0.6. This range includes the Small-Worldness topology range [37], but it is slightly wider because we did not evaluete the Small-Worldness of our data.

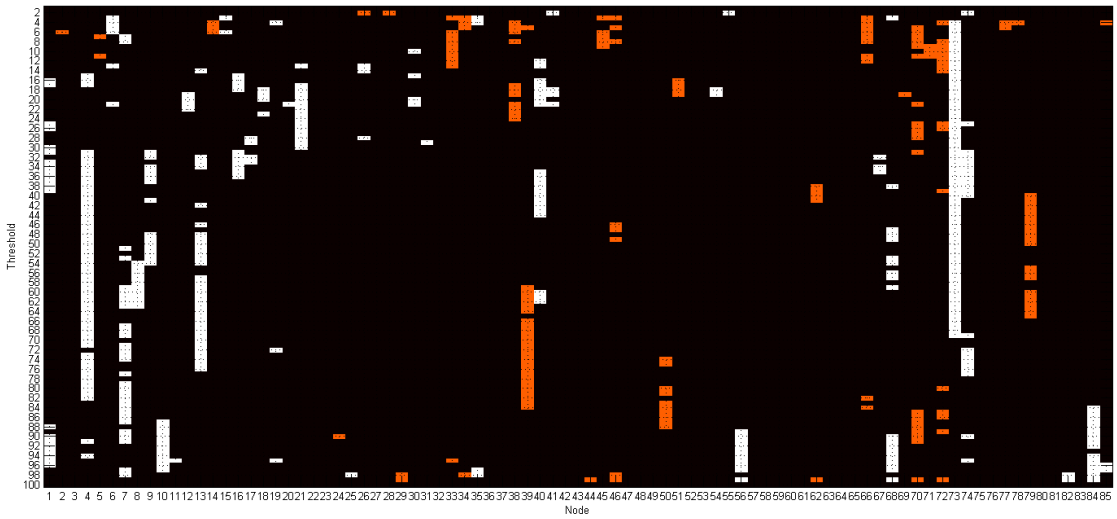

Figure 40: Statistically significant differences in Clustering Coefficient between patients and healthy controls. Along x axis the index for the nodes is reported, from 1 to 85, and along y the density link is reported as a percentage. Color white means that there is a significant difference ($p < 0.05$), with a higher value for the patients and color red means that there is a significant difference ($p < 0.05$), with a lower value for the patients.

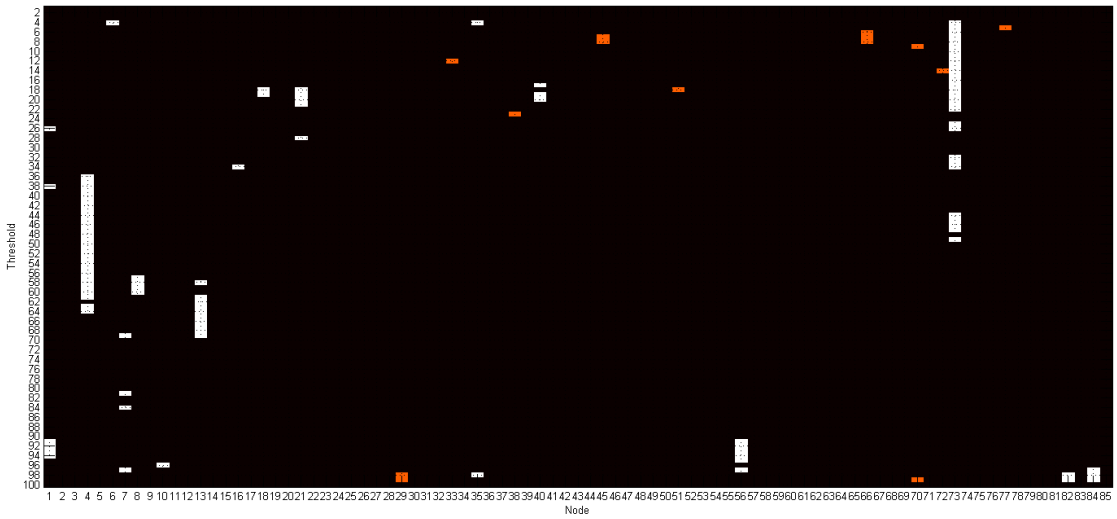

Figure 41: Statistically significant differences in Clustering Coefficient between patients and healthy controls. Along x axis the index for the nodes is reported, from 1 to 85, and along y the density link is reported as a percentage. Color white means that there is a significant difference ($p < 0.01$), with a higher value for the patients and color red means that there is a significant difference ($p < 0.01$), with a lower value for the patients. The main values that survived are in nodes 4 (left caudate), 13 (right caudate) and 73 (right pericalcarine).

In all the nodes 4 (left caudate), 13 (right caudate) and 73 (right pericalcarine), the value of Node Degree of the patients is higher than the value of Node Degree of healthy controls.

Figures 60 and 55 show the ROIs obtained by segmentation of Freesurfer in which some significance differences have been identified for Clustering Coefficient.

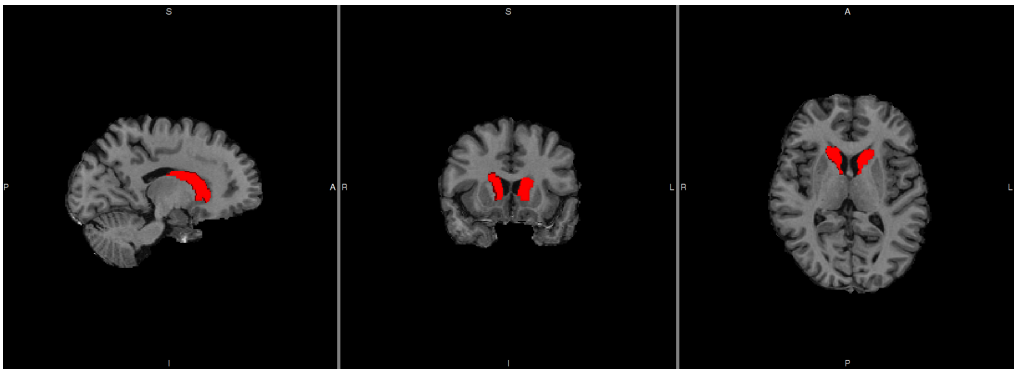

Figure 42: Result of Freesurfer segmentation of left and right caudate performed on 3D image of one patient (N = 11). The ROIs are represented in red. From left to right sagittal, coronal and axial views are shown.

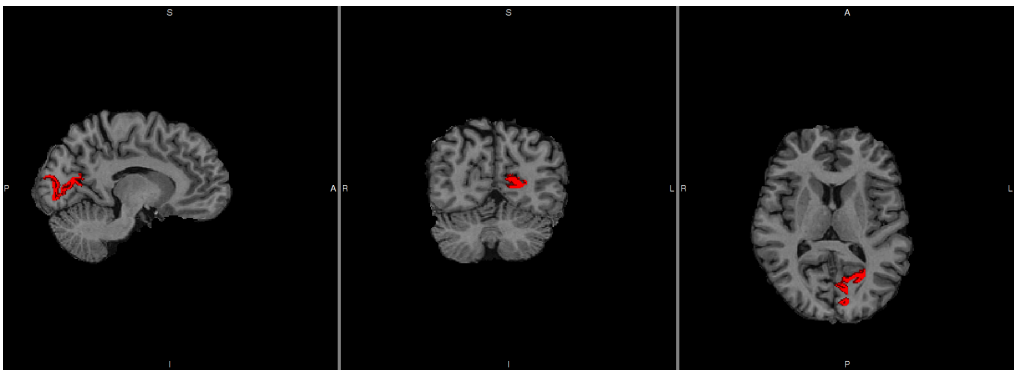

Figure 43: Result of Freesurfer segmentation of left pericalcarine performed on 3D image of one patient (N = 11). The ROI is represented in red. From left to right sagittal, coronal and axial views are shown.

In Figure 44 the 85 ROIs are visualized with the BrainNet Viewer (Xia et al. [75]). The regions in which we found a significant difference for the Clustering Coefficient value, within a density link range between 0.2 and 0.6, are represented in green (if the value is higher for the patients than the healthy controls, like left caudate and right pericalcarine) and in red (if the value is lower for the patients than the healthy controls). The regions in which we did not found any significant difference within that range are represented in blue.

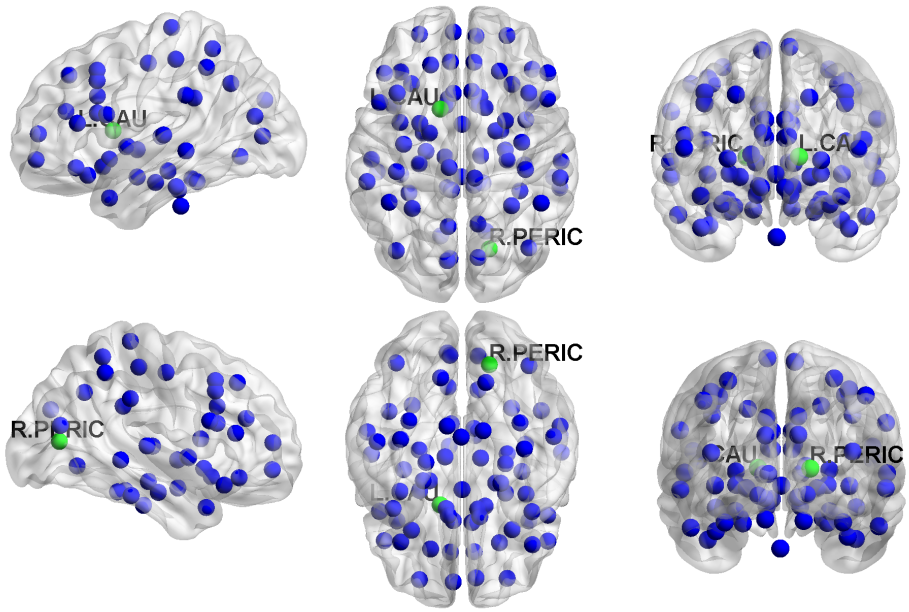

Figure 44: The 85 ROIs are visualized with the BrainNet Viewer. Color blue means that there is not a significant difference, color green means that there is a significant difference ($p < 0.05$), with a higher value for the patients and color red means that there is a significant difference ($p < 0.05$), with a lower value for the patients. **L.CAU** stands for left caudate and **R.PERIC** stands for right pericalcarine.

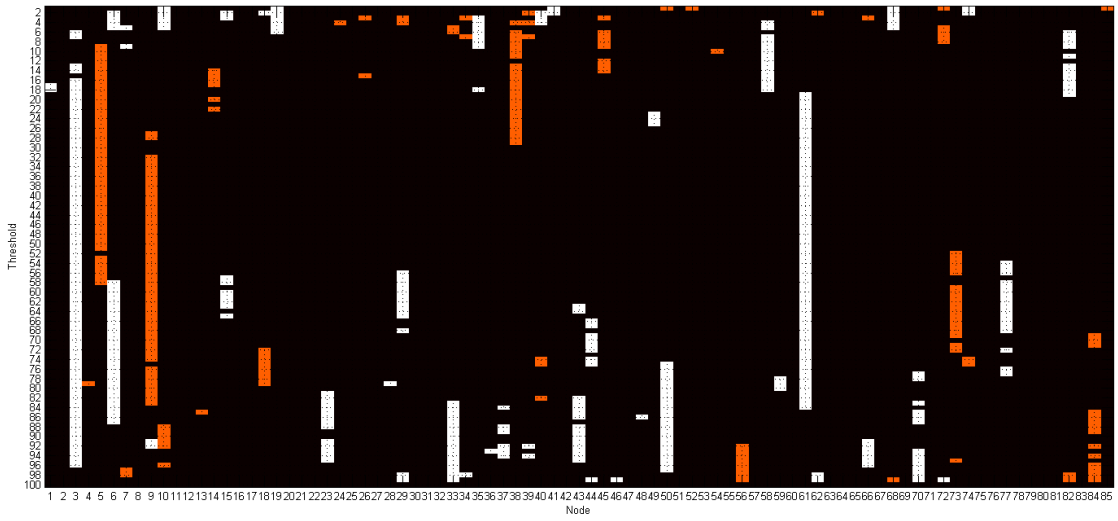

Figure 45: Statistically significant differences in Node Degree between patients and healthy controls. Along x axis the index for the nodes is reported, from 1 to 85, and along y the density link is reported as a percentage. Color white means that there is a significant difference ($p < 0.05$), with a higher value for the patients and color red means that there is a significant difference ($p < 0.05$), with a lower value for the patients.

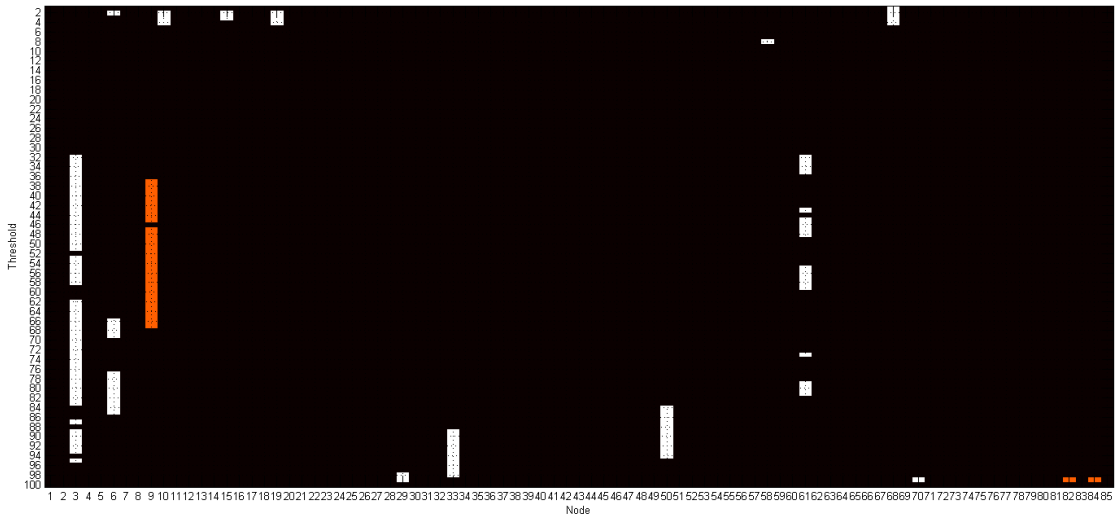

Figure 46: Statistically significant differences in Node Degree between patients and healthy controls. Along x axis the index for the nodes is reported, from 1 to 85, and along y the density link is reported as a percentage. Color white means that there is a significant difference ($p < 0.01$), with a higher value for the patients and color red means that there is a significant difference ($p < 0.01$), with a lower value for the patients. The main values that survived are in nodes 3 (left amygdala), 6 (left hippocampus), 9 (left thalamus), 61 (right insula).

In the nodes 3 (left amygdala), 6 (left hippocampus) and 61 (right insula), the value of Node Degree of the patients is higher than the value of Node Degree of healthy controls. Instead, in the nodes 9 (left thalamus), the values of Node Degree of the patients is lower than the value of Node Degree of healthy controls.

Figures 59, 48, 49 and 50 show the ROIs obtained by segmentation of Freesurfer in which some significance differences have been identified for Node Degree.

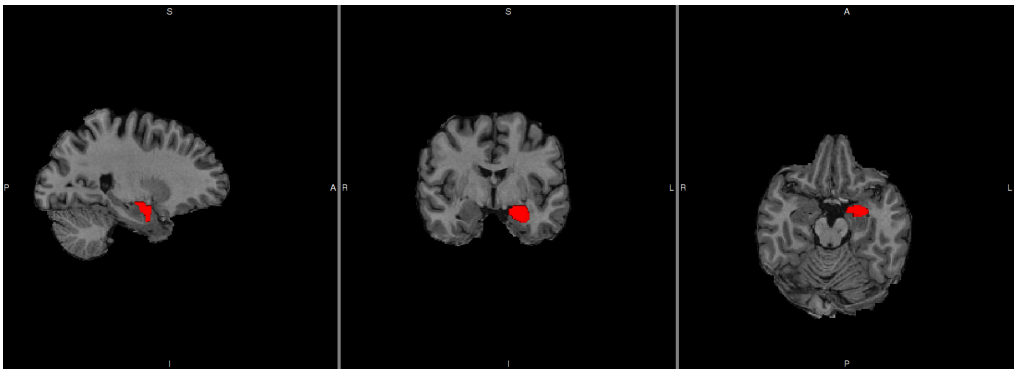

Figure 47: Result of Freesurfer segmentation of left amygdala performed on 3D image of one patient (N = 11). The ROI is represented in red. From left to right sagittal, coronal and axial views are shown.

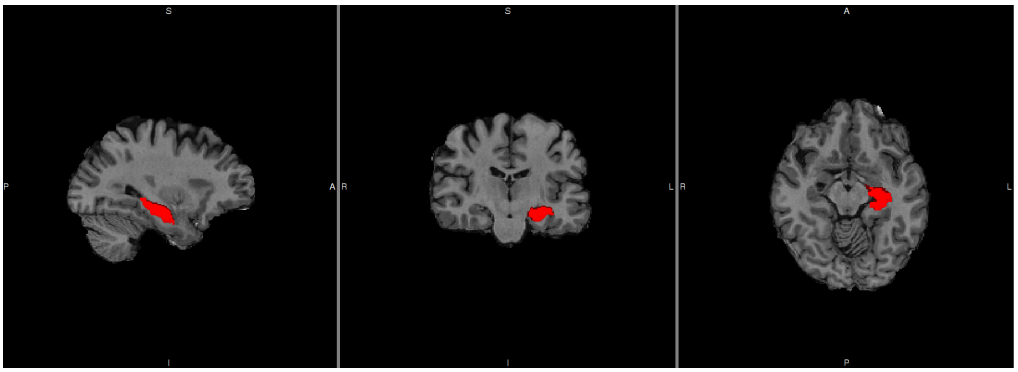

Figure 48: Result of Freesurfer segmentation of left hippocampus performed on 3D image of one patient (N = 11). The ROI is represented in red. From left to right sagittal, coronal and axial views are shown.

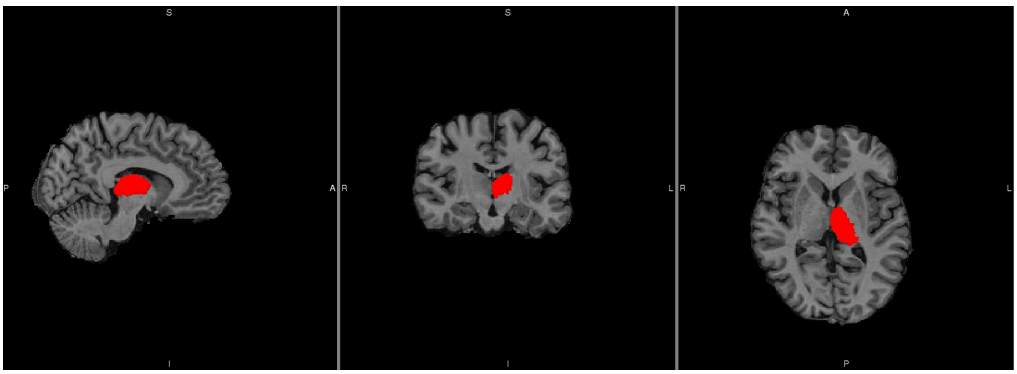

Figure 49: Result of Freesurfer segmentation of left thalamus performed on 3D image of one patient (N = 11). The ROI is represented in red. From left to right sagittal, coronal and axial views are shown.

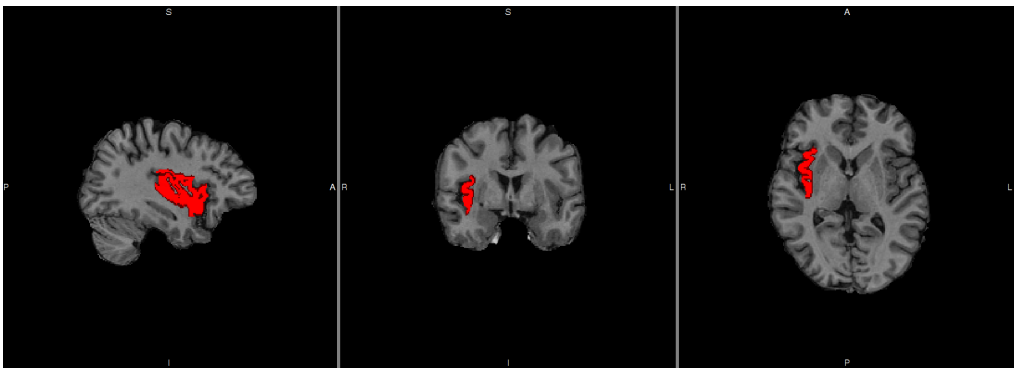

Figure 50: Result of Freesurfer segmentation of right insula performed on 3D image of one patient (N = 11). The ROI is represented in red. From left to right sagittal, coronal and axial views are shown.

In Figure 51 the 85 ROIs are visualized with the BrainNet Viewer (Xia et al. [75]). The regions in which we found a significant difference for the Node Degree value, within a density link range between 0.2 and 0.6, are represented in green (if the value is higher for the patients than the healthy controls, like left amygdala and right insula) and in red (if the value is lower for the patients than the healthy controls, like left thalamus). The regions in which we did not found any significant difference within that range are represented in blue.

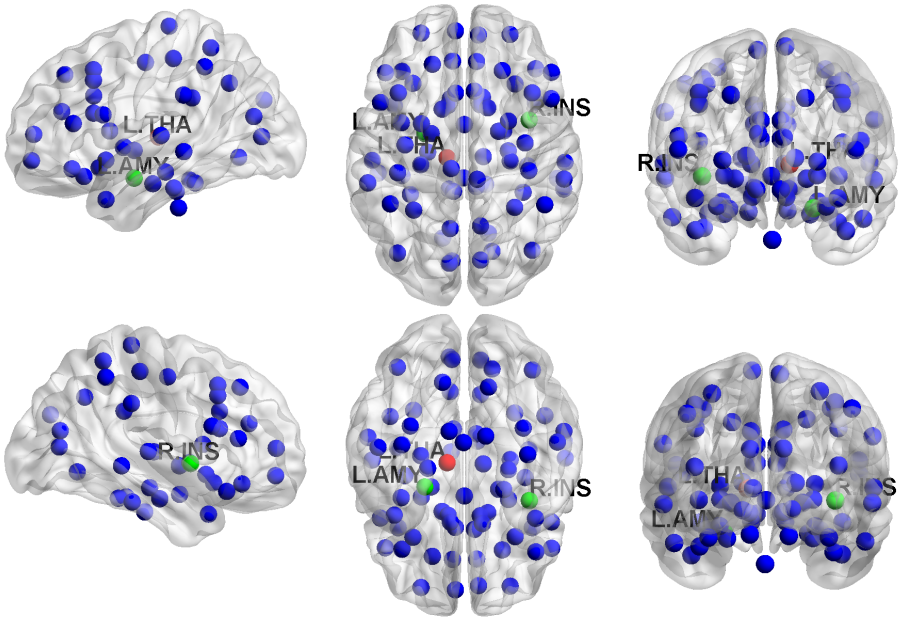

Figure 51: The 85 ROIs are visualized with the BrainNet Viewer. Color blue means that there is not a significant difference, color green means that there is a significant difference ($p < 0.05$), with a higher value for the patients and color red means that there is a significant difference ($p < 0.05$), with a lower value for the patients. **L.AMY** stands for left amygdala, **R.INS** stands for right insula and **L.THA** stands for left thalamus.

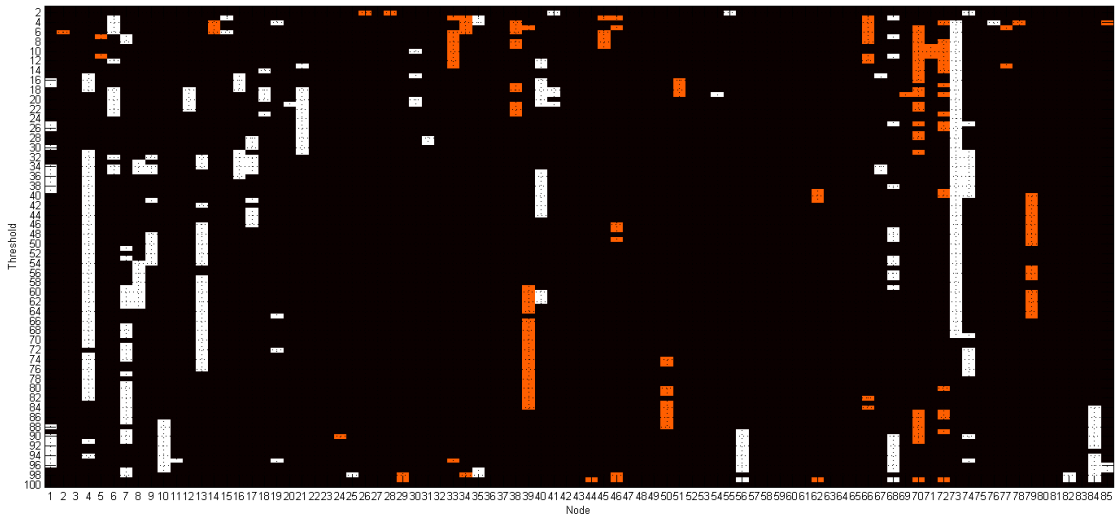

Figure 52: Statistically significant differences in Local Efficiency between patients and healthy controls. Along x axis the index for the nodes is reported, from 1 to 85, and along y the density link is reported as a percentage. Color white means that there is a significant difference ($p < 0.05$), with a higher value for the patients and color red means that there is a significant difference ($p < 0.05$), with a lower value for the patients.

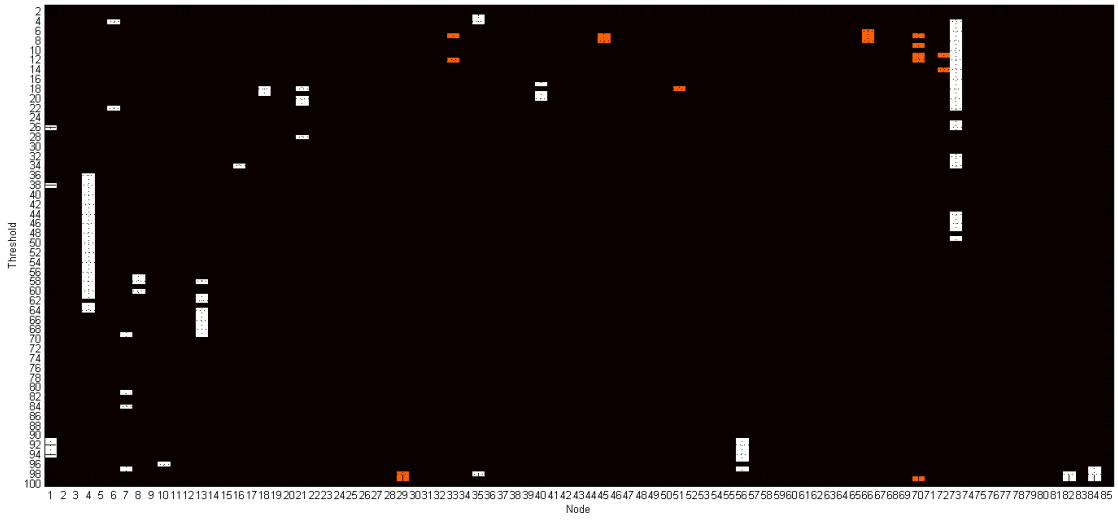

Figure 53: Statistically significant differences in Local Efficiency between patients and healthy controls. Along x axis the index for the nodes is reported, from 1 to 85, and along y the density link is reported as a percentage. Color white means that there is a significant difference ($p < 0.01$), with a higher value for the patients and color red means that there is a significant difference ($p < 0.01$), with a lower value for the patients. The main values that survived are in nodes 4 (left caudate), 13 (right caudate) and 73 (right pericalcarine).

In all of these nodes, in which the difference is significance, the value of Local Efficiency of the patients is higher than the value of Local Efficiency of healthy controls.

Figures 54 and 55 show the ROIs obtained by segmentation of Freesurfer in which some significance differences have been identified for Local Efficiency.

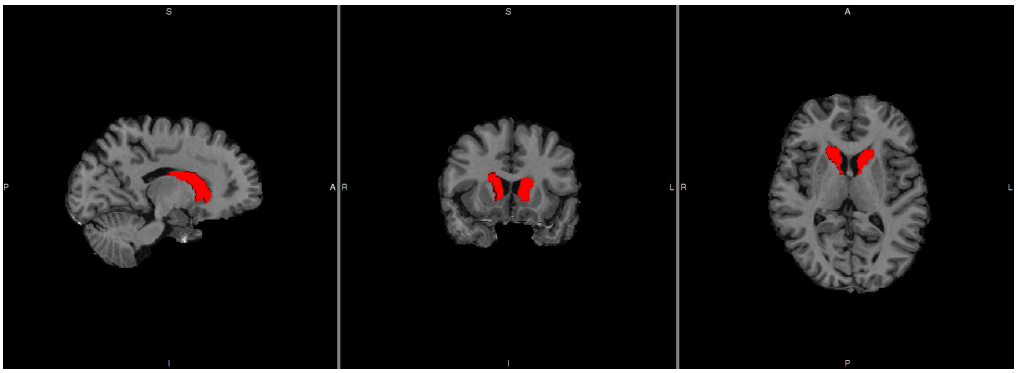

Figure 54: Result of Freesurfer segmentation of left and right caudate performed on 3D image of one patient (N = 11). The ROIs are represented in red. From left to right sagittal, coronal and axial views are shown.

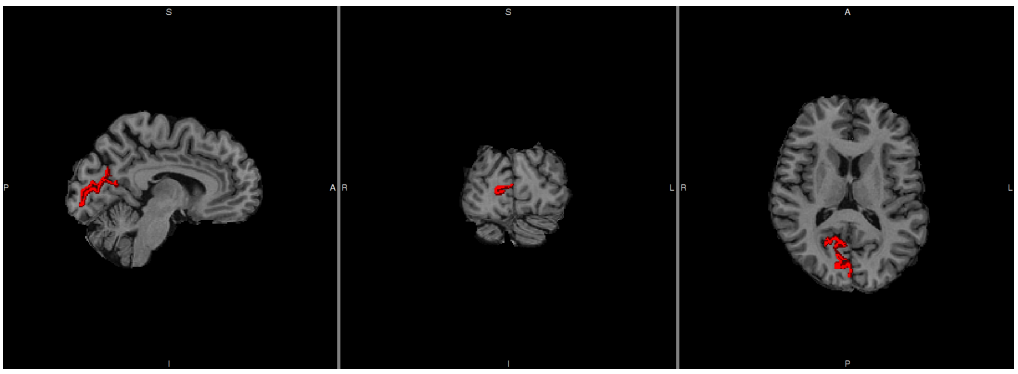

Figure 55: Result of Freesurfer segmentation of right pericalcarine performed on 3D image of one patient (N = 11). The ROI is represented in red. From left to right sagittal, coronal and axial views are shown.

In Figure 56 the 85 ROIs are visualized with the BrainNet Viewer (Xia et al. [75]). The regions in which we found a significant difference for the Local Efficiency value, within a density link range between 0.2 and 0.6, are represented in green (if the value is higher for the patients than the healthy controls, like left caudate and right pericalcarine) and in red (if the value is lower for the patients than the healthy controls). The regions in which we did not found any significant difference within that range are represented in blue.

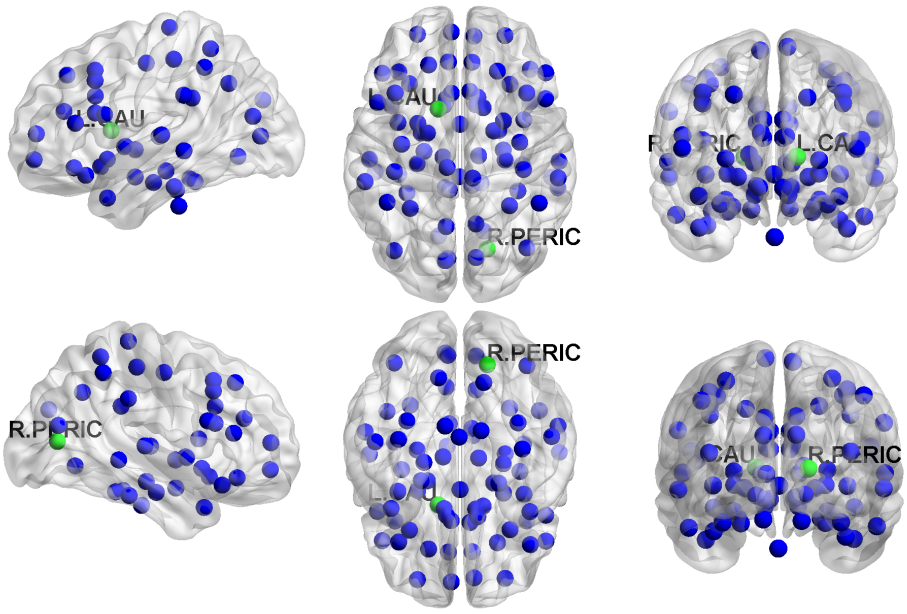

Figure 56: The 85 ROIs are visualized with the BrainNet Viewer. Color blue means that there is not a significant difference, color green means that there is a significant difference ($p < 0.05$), with a higher value for the patients and color red means that there is a significant difference ($p < 0.05$), with a lower value for the patients. **L.CAU** stands for left caudate and **R.PERIC** stands for right pericalcarine.

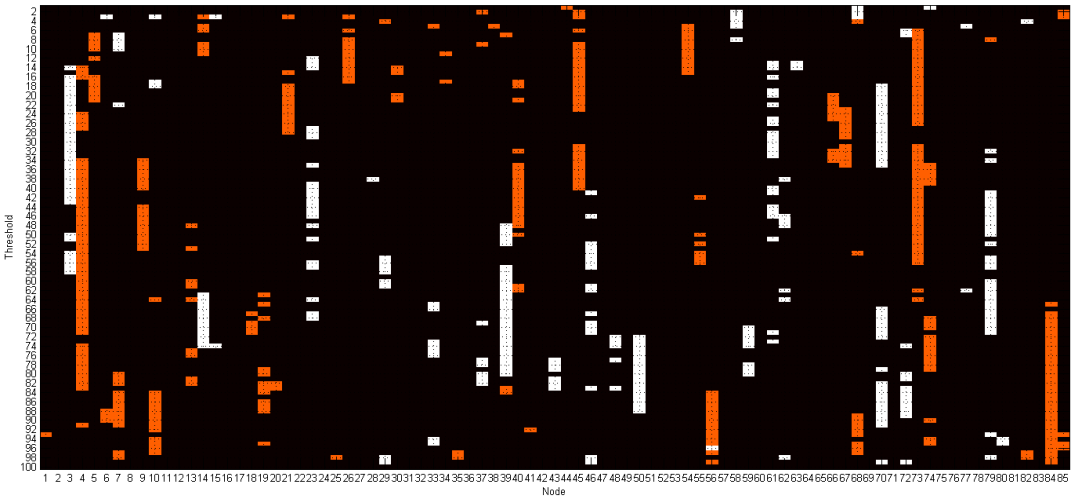

Figure 57: Statistically significant differenct in Betweenness Centrality between patients and healthy controls. Along x axis the index for the nodes is reported, from 1 to 85, and along y the density link is reported as a percentage. Color white means that there is a significant difference ($p < 0.05$), with a higher value for the patients and color red means that there is a significant difference ($p < 0.05$), with a lower value for the patients.

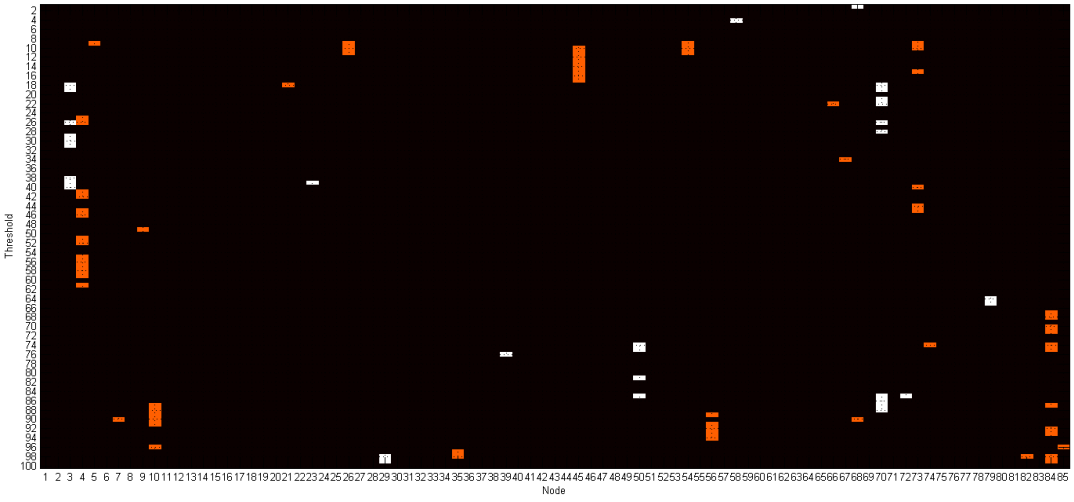

Figure 58: Statistically significant differences in Betweenness Centrality between patients and healthy controls. Along x axis the index for the nodes is reported, from 1 to 85, and along y the density link is reported as a percentage. Color white means that there is a significant difference ($p < 0.01$), with a higher value for the patients and color red means that there is a significant difference ($p < 0.01$), with a lower value for the patients. The main values that survived are in nodes 3 (left amygdala) and 4 (left caudate), the nodes 45 (left rostral anterior cingulate) and 54 (right caudal middle frontal) survived also to a more stringent significance level ($p < 0.001$).

In node 3 (left amygdala) the value of Betweenness Centrality of the patients is higher than the value of Betweenness Centrality of healthy controls. Instead, in node 4 (left caudate), 45 (left rostral anterior cingulate) and 54 (right caudal middle frontal) the value of Betweenness Centrality of the patients is lower than the value of Betweenness Centrality of healthy controls.

Figures 59, 60, 61 and 62 show the ROIs obtained by segmentation of Freesurfer in which some significance differences have been identified for Betweenness Centrality.

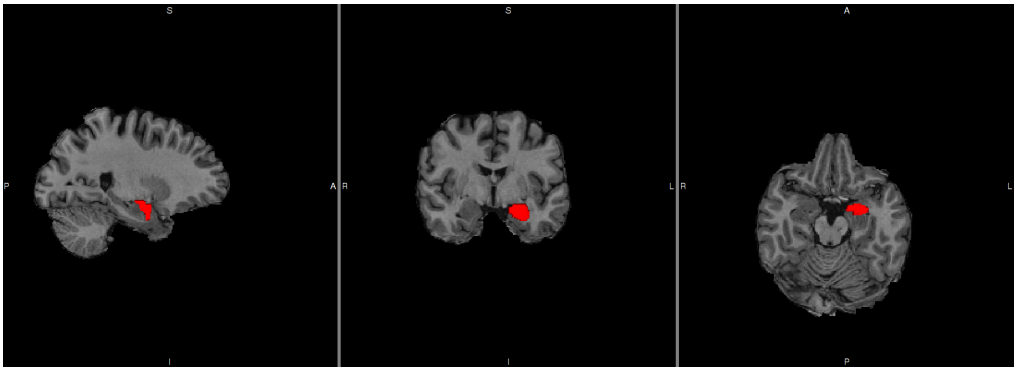

Figure 59: Result of Freesurfer segmentation of left amygdala performed on 3D image of one patient (N = 11). The ROI is represented in red. From left to right sagittal, coronal and axial views are shown.

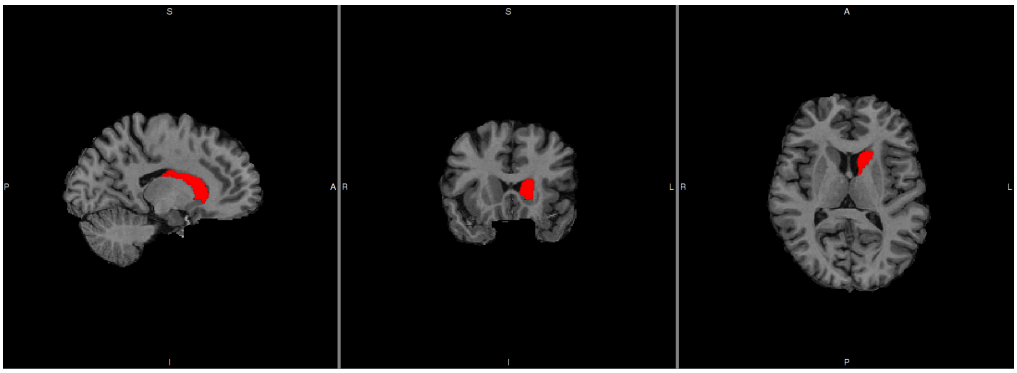

Figure 60: Result of Freesurfer segmentation of left caudate performed on 3D image of one patient (N = 11). The ROI is represented in red. From left to right sagittal, coronal and axial views are shown.

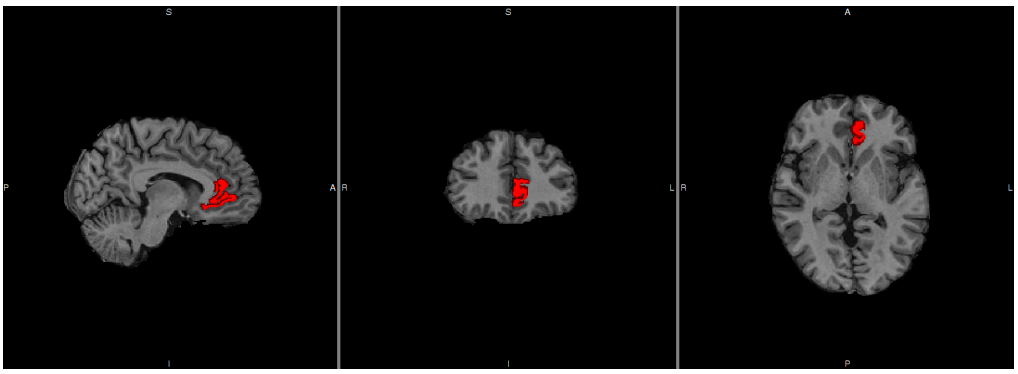

Figure 61: Result of Freesurfer segmentation of left rostral anterior cingulate performed on 3D image of one patient (N = 11). The ROI is represented in red. From left to right sagittal, coronal and axial views are shown.

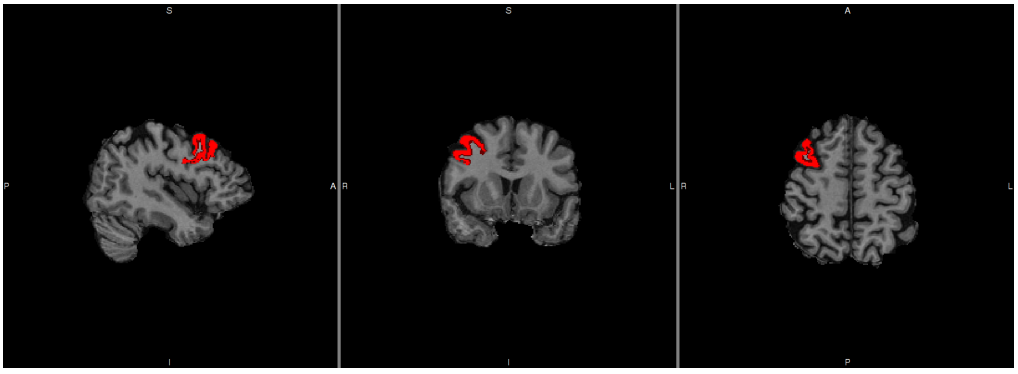

Figure 62: Result of Freesurfer segmentation of right caudal middle frontal performed on 3D image of one patient (N = 11). The ROI is represented in red. From left to right sagittal, coronal and axial views are shown.

In Figure 63 the 85 ROIs are visualized with the BrainNet Viewer (Xia et al. [75]). The regions in which we found a significant difference for the Betweenness Centrality value, within a density link range between 0.2 and 0.6, are represented in green (if the value is higher for the patients than the healthy controls, like left amygdala) and in red (if the value is lower for the patients than the healthy controls, lik left caudate). The regions in which we did not found any significant difference within that range are represented in blue.

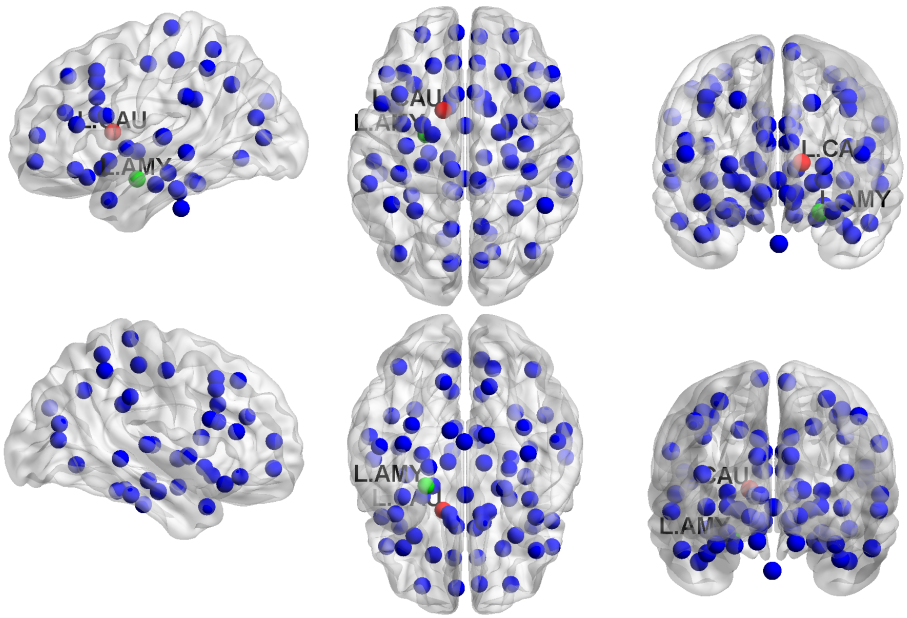

Figure 63: The 85 ROIs are visualized with the BrainNet Viewer. Color blue means that there is not a significant difference, color green means that there is a significant difference ($p < 0.05$), with a higher value for the patients and color red means that there is a significant difference ($p < 0.05$), with a lower value for the patients. **L.AMY** stands for left amygdala and **L.CAU** stands for left caudate.

We were also interested in calculating two topological parameters like Spectral Centrality and Salient Centrality. These two measures, however, are more suitable for weighted graphs. So we went back to correlation matrices, we considered only weights from 0.2 to 1, and from those we calculated these two new parameters. The results of Mann-Whitney test for patients and healthy controls are displayed in Figures 64 and 66. Also in this case we performed correction for multiple comparisons, with False Discovery Rate, but nothing survived. So we changed level of significance from 0.05 to 0.01. These two results are showned in Figures 65 and 67.

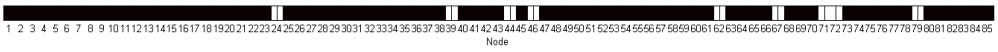

Figure 64: Significant differences for Spectral Centrality in weighted graphs. Color white means that there is a significant difference ($p < 0.05$), with a higher value for the patients and color red means that there is a significant difference ($p < 0.05$), with a lower value for the patients.

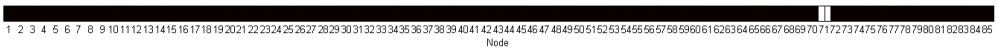

Figure 65: Significant differences for Spectral Centrality in weighted graphs. Color white means that there is a significant difference ($p < 0.01$), with a higher value for the patients and color red means that there is a significant difference ($p < 0.01$), with a lower value for the patients. The value that survived is in node 71 (right pars orbitalis).

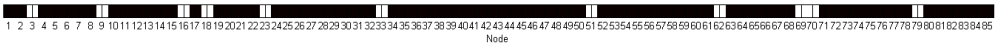

Figure 66: Significant differences for Salient Centrality in weighted graphs. Color white means that there is a significant difference ($p < 0.05$), with a higher value for the patients and color red means that there is a significant difference ($p < 0.05$), with a lower value for the patients.

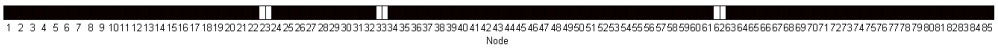

Figure 67: Significant differences for Salient Centrality in weighted graphs. Color white means that there is a significant difference ($p < 0.01$), with a higher value for the patients and color red means that there is a significant difference ($p < 0.01$), with a lower value for the patients. The values that survived are in nodes 23 (left entorhinal), 33 (left medial orbito frontal) and 62 (right isthmus cingulate).

In the node 71 (right pars orbitalis) the value of Spectral Centrality of the patients is higher than the value of Spectral Centrality of healthy controls.

In all the nodes 23 (left entorhinal), 33 (left medial orbito frontal) and 62 (right isthmus cingulate), the value of Salient Centrality of the patients is higher than the value of Salient Centrality of healthy controls.

Figures 68, 69, 70 and 71 show the ROIs obtained by segmentation of Freesurfer in which some significance differences have been identified for Spectral Centrality and Salient Centrality.

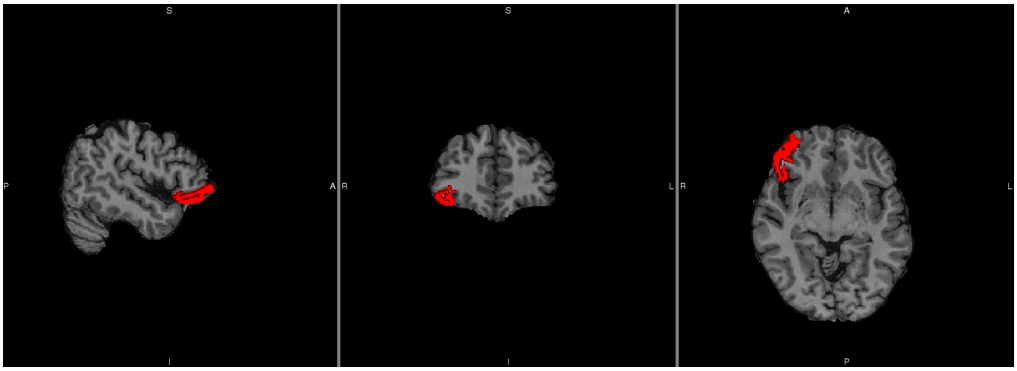

Figure 68: Result of Freesurfer segmentation of right pars orbitalis performed on 3D image of one patient (N = 11). The ROI is represented in red. From left to right sagittal, coronal and axial views are shown.

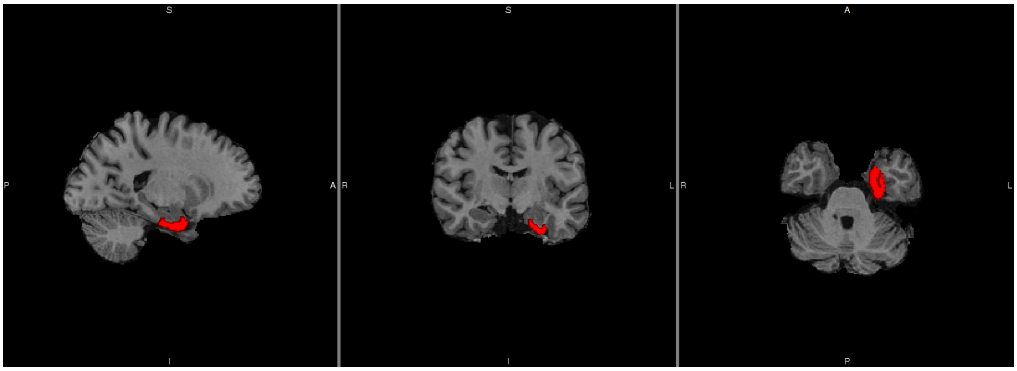

Figure 69: Result of Freesurfer segmentation of left frontal pole performed on 3D image of one patient (N = 11). The ROI is represented in red. From left to right sagittal, coronal and axial views are shown.

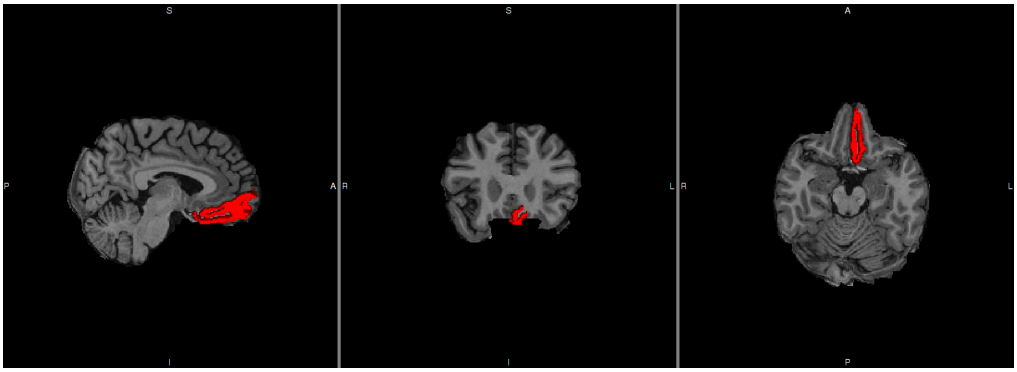

Figure 70: Result of Freesurfer segmentation of left medial orbito frontal performed on 3D image of one patient (N = 11). The ROI is represented in red. From left to right sagittal, coronal and axial views are shown.

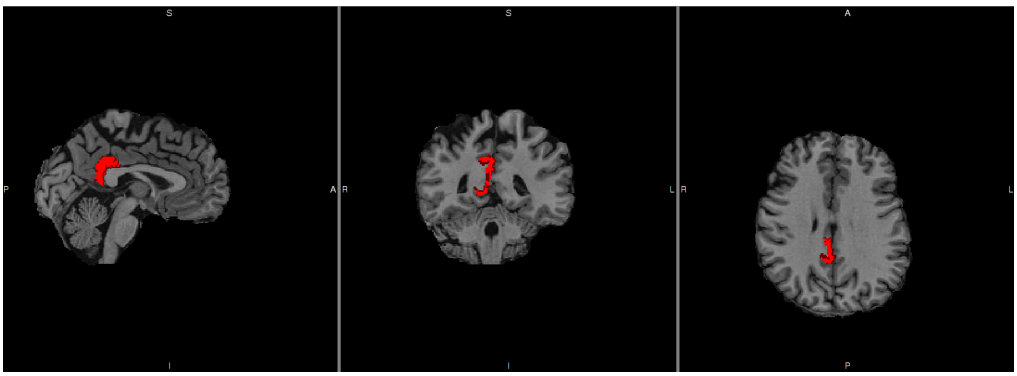

Figure 71: Result of Freesurfer segmentation of right isthmus cingulate performed on 3D image of one patient (N = 11). The ROI is represented in red. From left to right sagittal, coronal and axial views are shown.

6 DISCUSSION

This study investigated the global organization properties of functional brain networks using graph theoretical analysis on rs-fMRI data, which were recorded in nocturnal frontal lobe epilepsy patients and in healthy controls.

To date, this study is the only one that provides a graph theoretical analysis on rs-fMRI data acquired from NFLE patients (and healthy controls).

There are only four other studies performed with different neuroimaging techniques based on a comparison between NFLE patients and healthy controls. In the study performed by Ferini Strambi et al. [76], they utilized magnetization transfer imaging (MTI) and diffusion-weighted imaging (DWI) in patients with NFLE to assess in vivo whether subtle brain changes able to modify the relative proportions of free and bound water and water diffusivity were present in patients with NFLE. The study involved 29 patients with NFLE and two control groups, one consisted of 17 healthy controls and the other one consisted of 9 patients with idiopathic generalized epilepsy (IGE) without sleep disorders. The results showed that patients with NFLE have lower peak heights of the whole brain magnetization transfer ratio (MTR) and mean diffusivity (MD) histograms than those from healthy controls and patients with IGE. These findings have suggested mild but widespread changes in the brain of NFLE patients. Therefore they found that in patients with NFLE the extent of the truly normal brain tissue was reduced. They did not find any difference in MTR and MD metrics between frontal and nonfrontal brain regions. These results suggested that subclinical abnormalities were not confined to a single anatomic location.

In other studies in NFLE patients single photon emission computed tomography (SPECT) or the positron emission tomography (PET) were used.

Fedi et al. [77] put their attention to the unresolved issue of how altered function of the neuronal nicotinic acatylcholine (nACh) receptor causes frontal lobe seizures. Their hypothesis was that the mutation of nACh caused changes in excitability of a network of cortical and subcor-

tical neurons preferentially affecting the mesial prefrontal area, which is the site of seizure origin. They also hypothesized that dopaminergic system was a key part of the network. To test this hypothesis, they examined the effect of a mutation associated with NFLE on dopamine receptor binding measured with PET. The study involved 12 affected subjects with the same mutation of a subunit of the nACh receptor and 19 healthy controls. The reduction in the D1 receptor (the dopamine receptor) binding in the striatum, detected in the right and left putamen was postulated secondary to elevated extracellular dopamine levels. The authors concluded that the increase in striatal dopamine results in reduced inhibition of excitatory thalamocortical projections to the frontal lobe and then contributes to paroxysmal motor events genesis.

In another study made by Picard et al. [78], the metabolic consequences of the molecular defect of the receptors nAChRs were explored in NFLE patients compare to healthy controls. The study involved 8 NFLE patients and 7 age-matched healthy controls with the aim to assess nAChR distribution using PET with a tracer of nicotinic acetylcholine receptor. The images showed a difference in the pattern of the nAChR density in the brains of the patients compared to the healthy controls in the mesencephalon, the pons and the cerebellum. Furthermore, the volume of distribution values revealed an increase in the NFLE patients in the same regions seen before when compared to control subjects. Statistical paramteric mapping (SPM) confirmed the increase in nAChR density in the epithalamus, ventral mesencephalon and cerebellum of patients, associated with a decrease in nAChR density in the right prefrontal cortex, right caudatus and right rolandic area. An additional [^{18}F]-fluorodeoxyglucose (FDG) PET experiment revealed a hypometabolism in the neighbouring area of the right orbitofrontal cortex. They finally concluded that the nAChR density decrease in the prefrontal cortex was consistent with a focal epilepsy involving the frontal lobe and hypothesized that the nAChR density increase in mesencephalon was correlated to the brainstem ascending cholinergic system involved in the arousal mechanism.

The fourth study of Heymann et al. [79] focused on NFLE investigated seizure localization and intrafamilial variation combining video-EEG monitoring and functional neuroimaging. The ictal EEG localization resulted inaccurate in the localization of sizures in several cases. The study involved 4 NFLE patients. Three of these performed interictal PET studies, using FDG, and two performed both interictal and ictal SPECT. The PET analysis showed that one patient had a consistent left fronto-polar onset that was corroborated by congruent focal hypometabolism on interictal PET and focal hyperperfusion on ictal SPECT. A second case studied with ictal SPECT showed a right

parasagittal, midfrontal focus. They concluded that NFLE causes frontal lobe foci that are unilateral and in variable locations in different individuals.

To date, a complete pathophysiological interpretation of the nocturnal frontal lobe epilepsy is not defined. Nevertheless, some hypothesis have been proposed, since the first description of NFLE was done. Tinuper at al. [56] formulated a tentative hypothesis designed to unify the clinical, anatomo-physiological, and genetic aspects underlying this disease. They proposed that NFLE was due to a disorder in the thalamocortical circuit involved in the arousal mechanism and they also suggested that the primitive behavior observed in the disease, like screaming, grasping, implorations, imprecations and compulsive wandering, were due to other cortical networks involving the limbic system (for a detailed explanation of the areas involved in NFLE see section 3.2).

Another important study in which the possible areas involved in the fronto-limbic seizures and in parasomnias were investigated, is the one made by Tassinari et al. [80]. In this study they considered only the motor expression of events related to epileptic seizures and parasomnias, in order to establish if these two disorders can be the expression of tha same central pattern generator (CPG). They analized seizures only of a proven epileptic nature, recorded by intensive video-polygraphic monitoring of patients. For each recorded seizure they focused their attention on movements involving the limbs, the trunk and particularly the face. On the basis of video and polygraphic analysis of movements in NFLE patients they finally suggested that in some seizures, the consequent behaviors were the expression of inborn motor patterns, related to CPG, mainly located outside the cerebral cortex in the mesodiencephalic-pontine regions and the spinal cord.

Regarding this study, we calculated different parameters from the constructed brain graphs (see section 5.3), with the aim to characterizing the functional networks of NFLE patients and healthy controls.

In our study in NFLE patients we did not found any alteration of the global topology in the brain networks that we constructed. The same result was obtained in the study of Wang et al. in [82] although focused on a set of temporal lobe epileptic patients. We compared our results with fMRI studies that investigated different forms of epilepsy respect to NFLE because, to date, there are no works in literature that examined NFLE patients. The Connected Components and Global Efficiency, in our study, did not show differences between the two groups of subjects, unlike the study made by Liao et al. [84], in which they found differences in several parameters, such as the degree of connectivity or the absolute clustering coefficient (defined as the average between all

the Clustering Coefficient of the nodes), between healthy controls and patients affected by mesial temporal lobe epilepsy (mTLE).

The local measures that we calculated, Clustering Coefficient, Node Degree, Local Efficiency and Betweenness Centrality, showed several differences into the deep grey matter, the limbic system and the frontal regions.

The Clustering Coefficient resulted to be different for the regions of left caudate and right pericalcarine. The Node Degree resulted to be different for the regions of left amygdala, left thalamus and right insula. The Betweenness Centrality is different for left amygdala and left caudate. The Local Efficiency measure showed differences for the regions of left caudate and right pericalcarine.

For the Clustering Coefficient, which is a measure of the degree to which nodes in a graph tend to cluster together, the presence of caudate could be explained remembering its localization in the brain: the caduate is part of basal ganglia, which are thought be one of the components involved in the dystonic–dyskinetic features during the epileptic seizures of NFLE patients. We found that this measure was higher for the patients than the healthy controls, and this could be reflect that caudate is more connected to its close regions (the higher the clustering coefficient of a node, the bigger is the number of that node's neighbors that are also neighbors of each other). Indeed, a region that shows an increase of Clustering Coefficient, increases its ability for specialized processing [74] and this happens when a group of regions are densely interconnected. Regarding the Clustering Coefficient value of right pericalcarine, to date, we can not give a definitive physiopathological interpretation on the basis of known findings of the disease.

For the Node Degree, a measure that underlines the importance of a node in the network (if a node shows an high value of Node Degree means that it is interacting with many other nodes in the graph [74]), the regions that resulted significantly different between patients and healthy controls are left amygdala, left thalamus and right insula. The amygdala is a region that is part of the temporal lobe, which is one of the two areas (the other is the frontal lobe) involved in the generation of the ictal discharges, that are the main causes of complex behaviors during seizures. For this region, the Node Degree is higher for the patients, and it could be explained as a greater functional participation in the creation of these particular motor attitudes.

Also the presence of the region of right insula could be explained focusing on its localization in the brain. In fact this region is part of the frontal lobe, which is the other structure (with the temporal lobe) involved in the generation of the aforementioned ictal discharges. Also for this area the Node Degree is higher in the patients than the healthy

controls, and we could hypothesized that if the number of connections of a particular region increases, this could represents a greater involvement of the brain structure in the mechanism of generation of the complex behaviors typical of the NFLE.

Regarding the region of left thalamus, the mean value of Node Degree of the healthy controls is higher than the mean value of the patients. This result could be explained analyzing the connection pattern of the region of interest: maybe, in the NFLE patients, we observed a decrease of number of connections of the thalamic structure, but the remained associations might be the strongest ones. We could not know if this hypothesis is true or not, because we generated unweighted brain graphs, but it could be an interesting future integration of this work.

For the Local Efficiency, which is a measure of integration that represents the efficiency of a given node in communicating with the rest of the brain [83], the implication of left caudate could be explained in a similar way: the higher values obtained in patients groups could represent the fact that the regions involved in the process of generation of epileptic seizures might be more efficient in the flowing of the information to other parts of the brain, and that could cause an overload of information which determines those particular dystonic–dyskinetic features. The measure of the Local Efficiency assumes even greater importance if we recall the Small Worldness definition (see section 2.3) in fact, if a network has a Small World topology means that it has an increase of Clustering Coefficient and a decrease of Characteristic Path Lenght [74], which is inversely related to the Local Efficiency. Therefore, since we obtained an increase of Local Efficiency measure in the patients, we can only suppose that this group of subjects has a stronger Small World topology than healthy controls. Regarding the Local Efficiency value of right pericalcarine, we made the same consideration as for Clustering Coefficient.

In the case of Betweenness Centrality, which represents a measure of the node importance inside the network (nodes with high Betweenness Centrality are located on highly traveled paths), the main important differences appear for the left amygdala and the left caudate. The first one shows an increase of the value of the Betweenness Centrality for the patients than the healthy controls, and this could mean that in NFLE patients the amygdala becomes an important region through which passes most of the flow of the information. Instead, for the left caudate, the value of the Betweenness Centrality is lower in the patients than the healthy controls: it means that there is a decrease in the number of total paths that pass through the caudate.

Finally, we found also statistically significant differences in several regions, across the four topological measures node-specific that we cal-

culated, only for a small range of thresholds. During the entire study we focused on statistical differences that we observed into a range of thresholds between 0.2 and 0.6 (or 20% of link and 60% of links), based on several studies that reported their range selection (and their relative modalities of selection [37],[38]). In this case we found these differences outside the prefixed range, and we report them for completeness. For the Clustering Coefficient we found the right caudate (the value of patients is higher than healty controls, such as left caudate), and this region was found with the same characteristic also for the Local Efficiency outside our preselected range. For the measure of Node Degree we found differences in left hippocampus (the value of patients is higher than healthy controls), instead for Betweenness Centrality the statistically significant differences was found for left rostral anterior cingulate and for right caudal middle frontal. These two regions show higher values for healthy controls than patients and the respective differences was found in a very little range of density value, but they have a very high significance. All these last mentioned regions are involved in the aforementioned processes related to the generation of primitive behaviors typical of NFLE.

We also performed an exploratory analysis on two relatively new graph measures, Spectral Centrality and Salient Centrality, that have not been applied yet in brain networks. In both cases we performed the analysis on weighted graphs. For the Spectral Centrality we found statistically significant differences in right pars orbitalis and for Salient Centrality in left entorhinal, left medial orbito frontal and right isthmus cingulate. In all of these regions, the respective values are higher for patients than healthy controls.

7 CONCLUSIONS AND FUTURE DIRECTIONS

In conclusion, in this study we investigated using graph theoretical analysis the global and the local topological organization in the whole brain functional networks constructed starting from rs-fMRI data of thirteen NFLE patients and thirteen healthy controls.

Whole brain network organization showed no alterations in NFLE patients compared to healthy controls. Indeed, the number of Connected Components and the Global Efficiency, as we saw in section 5.3, did not show any differences between the group of NFLE patients and the group of healthy controls.

In NFLE patients an altered topology was observed in limbic system and basal ganglia. Regarding node-specific measures of centrality, the Node Degree was higher in amygdala and insula in patients while it was lower in thalamus; Betweenness Centrality was higher in amygdala and lower in caudate in patients compared to healthy controls. As for measures of integration/segregation, the Clustering Coefficient and Local Efficiency were higher in caudate and pericalcarine in patients.

These results showed local alterations in brain structures which are hypothesized to be involved in the pathophysiology of the NFLE. In fact the typical dystonic–dyskinetic features and primitive and complex behaviors, observed during the seizures, suggest an involvement of subcortical structures like the basal ganglia and limbic system.

As far as our analysis is concerned, possible future deepening and development could be suggested by the results obtained so far. First of all it could be interesting to investigate the predominant involvement of the left side of the brain. It could be related to the lateralization of seizures, that it was impossible to clearly define with scalp EEG in some patients. So, it could be suggestive to further investigate in this direction to find out if there is a sort of correspondence between the data and the obtained side differences of parameters. In the next future, it could be interesting to flip only a part of the initial EPI images (those with a predominant lateralization) applying the entire protocl study analysis to explore the same connectivity parameters. Regarding to the topological parameters, there is a huge number of measures that could

be calculated in order to better characterize the brain graphs. One of these is the Small-Worldness, a parameter that represents the high capacity of the network to integrate and segregate, which is one of the most important feature of the (fully connected) graphs. Another fascinating application of the graph-based analysis on rs-fMRI data could be the construction of a single network focused on specific brain regions, using the voxel-wise technique to define nodes. Combining these multilevels modalities of fMRI data analysis based on graph approach an advance in the characterization of brain networks connectivity related to epileptogenesis will be achieved.

BIBLIOGRAPHY

[1] P. Jezzard, P.M. Matthews and S.M. Smith. *Functional MRI: An Introduction to Methods*. Oxford University Press, (2001)

[2] J.P. Hornak. *The basics of MRI*. Copyright 1996-2010, www.cis.rit.edu/htbooks/mri/inside.htm, Interactive Learning Software, Henietta, NY.

[3] P.T. Callaghan. *Principles of nuclear magnetic resonance microscopy*. Clarendon Press, Oxford (1991)

[4] D.A. Gusnard and M.E. Raichle. *Searching for a baseline: functional imaging and the resting human brain*. Nat. Rev. Neurosci. (2001); 2(10):685-94

[5] J.J. Harris, C. Reynell and D. Attwell. *The physiology of developmental changes in BOLD functional imaging signals*. Developmental Cognitive Neuroscience (2011) 1(3):199-216

[6] R. Bammer, S. Skare, R. Newbould, C. Liu, V. Thijs, S. Ropele, D. B. Clayton, G. Krueger, M.l E. Moseley and G. H. Glover. *Foundations of Advanced Magnetic Resonance Imaging*. NeuroRx. (2005) 2(2): 167–196.

[7] S. Ogawa, T.M. Lee, A.R. Kay and D.W. Tank. *Brain magnetic resonance imaging with contrast dependent on blood oxygenation*. Proc. Natl. Acad. Sci. U.S.A. (1990) Dec; 87(24): 9868-9872

[8] B. Biswal, F.Z. Yetkin, V.M. Haughton and J.S. Hyde. *Functional connectivity in the motor cortex of resting human brain using echo-planar MRI*. Magnetic Resonance in Medicine (1995) 34 (4), 537-541

[9] M.D. Fox, M.E. Raichle. *Spontaneus fluctuations in brain activity observed with functional magnetic resonance imaging*. Nature Reviews Neuroscience (2007) 8 (9), 700-711

[10] J. S. Damoiseaux, S. A. R. B. Rombouts, F. Barkhof, P. Scheltens, C. J. Stam, S. M. Smith and C. F. Beckmann. *Consistent resting-state networks across healthy subjects*. Proc. Natl. Acad. Sci. U.S.A. (2006) 103 (37), 13.848-13.853

[11] M.P. Van Den Heuvel and H.E. Hulshoff Pol. *Exploring the brain network: A review on resting-state fMRI functional connectivity*. European Neuropsychopharmacology (2010) 20, 519-534

[12] M.P. Van Den Heuvel, R. Mandl and H.E. Hulshoff Pol. *Normalized Cut Group Clustering of Resting-State fMRI Data*. PLoS ONE 3(4), (2001)

[13] B.B. Biswal, J. VanKylen and J.S. Hyde. *Simultaneous assessment of flow and BOLD signals in resting-state functional connectivity maps*. Nmr in Biomedicine (1997) 10(4-5):165-170.

[14] K. Friston *Causal Modelling and Brain Connectivity in Functional Magnetic Resonance Imaging*. Plos Biology (2009) 7(2):220-225.

[15] M.H. Lee, C.D. Smyser and J.S. Shimony. *Resting state fMRI: A review of methods and clinical applications*. AJNR An J Neuroradiol. (2013) 34(10): 1866-1872

[16] M.D. Fox and M. Greicius. *Clinical applications of resting state functional connectivity*. Front Syst Neurosci (2010) 4:19.

[17] D. Zhang, J.M. Johnston, M.D. Fox et al. *Preoperative sensorimotor mapping in brain tumor patients using spontaneous fluctuations in neuronal activity imaged with functional magnetic resonance imaging: initial experience*. Neurosurgery (2009) 65:226–36

[18] H. Liu, R.L. Buckner, T. Talukdar et al. *Task-free presurgical mapping using functional magnetic resonance imaging intrinsic activity*. J Neurosurg (2009) 111:746–54

[19] K. Supekar, V. Menon, D. Rubin et al. *Network analysis of intrinsic functional brain connectivity in Alzheimer's disease*. PLoS Comput Biol (2008) 4:e1000100

[20] E. Bullmore and O. Sporns. *Complex brain networks: graph theoretical analysis of structural and functional systems*. Nat. Rev. Neurosci. (2009); 10(3): 186-98

[21] M.E. Raichle, A.M. MacLeod, A.Z. Snyder, W.J. Powers, D.A. Gusnard and G.L. Shulman. *A default mode of brain function*. Proc. Natil. Acad. Sci. U.S.A. (2001); 98(2):676-82

[22] M. DIng, Y. Chen, S.L. Bressler. *Granger causality: basic theory and application to neuroscience. In Handbook of Time Series Analysis*. (2006): 451-474

[23] W. Liao, D. Mantini, Z. Zhang, Z. Pan, J. Ding, Q. Gong, Y. Yang and H. Chen. *Evaluating the effective connectivity of resting state networks using consitional Granger causality*. Biol Cybern (2010) 102: 57-69

[24] A. Roebroeck, E. Formisano and R. Goebel. *Mapping directed influence over the brain using Granger causality and fMRI*. Neuroimage (2005) 25(1):230-42

[25] Q. Jiao, G. Lu, Z. Zhang, Y. Zhong, Z. Wang, Y. Guo, K. Li, M. Ding and Y. Liu. *Granger Causal Influence Predicts BOLD Activity Levels in the Default Mode Network*. Human Brain Mapping (2011) 32:154-161

[26] O. Sporns, G. Tononi and R. Kotter. *The human connectome: a structural description of the human brain*. PLoS Comput. Biol. (2005) 1:e42

[27] E.T. Bullmore and D.S. Bassett. *Brain Graphs: Graphical Models of the Human Brain Connectome*. Annu. Rev. Clin. Psychol. (2011) 7:113–40

[28] J. Wang, L. Wang, Y. Zang, H. Yang, H. Tang, Q. Gong, Z. Chen, C. Zhu and Y. He. *Parcellation-dependent small-world brain functional networks: a resting-state fMRI study* Human Brain Mapping (2009) 30:1511-1523

[29] R. Salvador, J. Suckling, M.R. Coleman, J.D. Pickard, D. Menon and E.T. Bullmore. *Neurophysiological architecture of functional magnetic resonance images of human brain*. Cerebral Cortex (2005) 15:1332-1342

[30] G. Tononi, O. Sporns and G.M. Edelman. *A measure for brain complexity: Relating functional segregation and integration in the nervous system*. Proc. Natl. Acad. Sci. USA Vol. 91, pp. 5033-5037, (1994) Neurobiology

[31] M. Girvan and M.E.J. Newman. *Community structure in social and biological networks*. Proc. Natl. Acad. Sci. U.S.A. (2002) 99, 7821–7826.

[32] D.A. Fair, A.L. Cohen, N.U. Dosenbach, J.A. Church, F.M. Miezin, D.M. Barch, M.E. Raichle, S.E. Petersen and B.L. Schlaggar. *The maturing architecture of the brain's default network.* Proc. Natl. Acad. Sci. U.S.A. (2008) 105, 4028–4032.

[33] D.A. Fair, A.L. Cohen, J.D. Power, N.U. Dosenbach, J.A. Church, F.M. Miezin, B.L. Schlaggar, and S.E. Petersen. *Functional brain networks develop from a "local to distributed" organization*. (2009) PLoS Comput. Biol. 5, e1000381. doi:10.1371/journal.pcbi.1000381.

[34] D.A. Fair, N.U. Dosenbach, J.A. Church, A.L. Cohen, S. Brahmbhatt, F.M. Miezin, D.M. Barch, M.E. Raichle, S.E. Petersen and SB.L. Schlaggar. *Development of distinct control networks through segregation and integration*. (2007) Proc. Natl. Acad. Sci. U.S.A. 104, 13507–13512.

[35] G.A. James, S.P. Tripathi, J.C. Ojemann, R.E. Gross and D.L. Drane. *Diminished default mode network recruitment of the hippocampus and parahippocampus in temporal lobe epilepsy*. J Neurosurg (2013) 119:288-300

[36] P. Erdos and A. Renyi. *On random graphs:I*. (1959) Publ. Math. 6:290–97

[37] S. Archard and E.T. Bullmore. *Efficiency and cost of economical brain functional networks*. (2007) PLoS COmput Biol 3(2):e17. doic:10.1371/journal.pcbi.0030017

[38] E. Tagliazucchi, F. von Wegner, A. Morzelewski, V. Brodbeck, S. Borisov, K. Jahnke and H. Laufs. *Large-scale brain functional modularity is reflected in slow electroelectroencephalographic rhythms across the human non-rapid eye movement sleep cycle*. NeuroImage 70 (2013) 327–339

[39] E. Lugaresi and F. Cirignotta. *Hypnogenic paroxysmal dystonia: epileptic seizure or a new syndrome?* Sleep (1981) 4(2):129-138

[40] P. Tinuper, A. Cerullo, F. Cirignotta, P. Cortelli, E. Lugaresi and P. Montagna. *Nocturnal paroxysmal dystonia with short lasting attacks: three cases with evidence for an epileptic frontal lobe origin of seizures*. Epilepsia (1990) 31:549-556

[41] F. Bisulli , L. Vignatelli, F. Provini, C. Leta, E. Lugaresi and P. Tinuper. *Parasomnias and nocturnal frontal lobe epilepsy (NFLE): Lights and shadows – Controversial points in the differential diagnosis*. Sleep Medicine, 12 (2011) S27–S32.

[42] I.E. Scheffer, K.P. Bhatia, I. Lopes-Cendes, D.R. Fish, C.D. Marsden, F. Andermann, E. Andermann, R. Desbiens, F. Cendes, J.I. Manson, et al. *Autosomal dominant frontal epilepsy misdiagnosed as sleep disorder.* Lancet (1994) Feb 26;343(8896):515-7.

[43] F. Provini, G. Plazzi, P. Tinuper, S. Vandi, E. Lugaresi, P. Montagna. *Nocturnal frontal lobe epilepsy. A clinical and polygraphic overview of 100 consecutive cases*. Brain (1999) 122:1017-31

[44] I.E. Scheffer, K.P. Bhatia, I. Lopes-Cendes, D.R. Fish, C.D. Marsden, F. Andermann, E. Andermann, R. Desbiens, D. Keene, F. Cendes, J.I. Manson, J. Contantinou, A. McIntosh, S.F. Berkovic. *Autosomal dominant nocturnal frontal lobe epilepsy: a distinctive clinical disorder.* Brain 118 (1995) pp. 61-73

[45] C. Marini and R. Guerrini. *The role of the nicotinic acetylcholine receptors in sleep-related epilepsy*. Biochem Pharmacol (2007) 74(8):1308-14

[46] P. Montagna, E. Sforza, P. Tinuper, F. Cirignotta and E. Lugaresi. *Paroxysmal arousals during sleep*. Neurology (1990) 40:1063-1066

[47] P. Tinuper and E. Lugaresi. *The concept of paraxysmal nocturnal dystonia*. in C.W. Bazil B.A. Malow M.R. Sammaritano (Eds.) Sleep and epilepsy: the clinical spectrum. Elseviers Science, Amsterdam; (2002) 277-282

[48] F. Provini, G. Plazzi, P. Montagna and E. Lugaresi. *The wide clinical spectrum of nocturnal frontal lobe epilepsy*. Sleep Med Rev (2000) 4:375-386

[49] L. Nobili, S. Francione, R. Mai, F. Cardinale, L. castagna, et al. *Surgical treatment of drug-resistant nocturnal frontal lobe epilepsy*. Brain (2007) 130:561-573

[50] *ASDA American Academy of Sleep Medicine. The international classification of sleep disorders: diagnostic and coding manual*. 2nd ed. Westchester (ILL): ASD Association, American Academy of Sleep Medicine; (2005).

[51] G. Plazzi, P. Tinuper, P. Montagna, F. Provini and E. Lugaresi. *Epileptic Nocturnal Wandering*. Sleep (1995) 18(9):749-756.

[52] L. Nobili, I. Sartori, M. Terzaghi, S. Francione, R. Mai, L. Tassi, et al. *Relationship of epileptic discharges to arousal instability and periodic leg movements in a case of nocturnal frontal lobe epilepsy: a stereo-EEG study*. Sleep (2006) 29:701–4.

[53] P. Revlyn Ryvlin, L. Minotti, G. Demarquay, E. Hirsch, A. Arzimanoglou, D. Hoffman, et al. *Nocturnal hypermotor seizures, suggesting frontal lobe epilepsy, can originate in the insula*. Epilepsia (2006) 47:755–65

[54] S. Rheims, P. Ryvlin, C. Scherer, L. Minotti, D. Hoffmann, M. Guenot, et al. *Analysis of clinical patterns and underlying epileptogenic zones of hypermotor seizures*. Epilepsia (2008) 49:2030–40.

[55] L. Vaugier, S. Aubert, A. McGonigal, A. Trébuchon, M. Guye, M. Gavaret, et al. *Neural networks underlying hyperkinetic seizures of "temporal lobe" origin*. Epilepsy Res (2009) 86:200–8.

[56] P. Tinuper, F. Bisulli, F. Provini, P. Montagna and E. Lugaresi. *Nocturnal Frontal Lobe Epilepsy: New pathophysiological interpretations*. Sleep Medicine 12 (2011) S39–S42

[57] C.P. Derry, A.S. Harvey, M.C. Walker, J.S. Duncan and S.F. Berkovic. *NREM arousal parasomnias and their distinction from nocturnal frontal lobe epilepsy: a video EEG analysis*. Sleep (2009) 32: 1637–44.

[58] H. Kurahashiand and S. Hirose. *Autosomal Dominant Nocturnal Frontal Lobe Epilepsy*. Gene Reviews [Internet], Last Update: February 2015

[59] Matthew L. Stanley, Malaak N. Moussa, Brielle M. Paolini, Robert G. Lyday, Jonathan H. Burdette and Paul J. Laurienti. *Defining nodes in complex brain networks*. (2013).

[60] N. Tzourio-Mazoyer, B. Landeau, D. Papathanassiou, F. Crivello, O. Etard, N, Delcroix, Bernard Mazoyer and M. Joliot. *Automated Anatomical Labeling of activations in SPM using a Macroscopic Anatomical Parcellation of the MNI MRI single-subject brain*. NeuroImage (2002) 15(1):273-289

[61] Rahul S. Desikan, Florent Se´gonne, Bruce Fischl, Brian T. Quinn, Bradford C. Dickerson, Deborah Blacker, Randy L. Buckner, Anders M. Dale, R. Paul Maguire, Bradley T. Hyman, Marilyn S. Albert and Ronald J. Killianya. *An automated labeling system for subdividing the human cerebral cortex on MRI scans into gyral based regions of interest*. NeuroImage 31 (2006) 968 – 980

[62] *www.freesurfer.net/fswiki*

[63] Xia Liang et al. *Effects of Different Correlation Metrics and Preprocessing Factors on Small-World Brain Functional Networks: A Resting-State Functional MRI Study*. (2012).

[64] M. Jenkinson, C. F. Beckmann, T. E.J. Behrens, M. W. Woolrich, S. M. Smith. *FSL*. NeuroImage 62 (2011) 782-790.

[65] Robert E. Kelly Jr., George S. Alexopoulos, Zhishun Wang, Faith M. Gunning, Christopher F. Murphy, Sarah Shizuko Morimoto, Dora Kanellopoulos, Zhiru Jia, Kelvin O. Lim, Matthew J. Hoptman. *Visual inspection of independent components: Defining a procedure for artifact removal from fMRI data*. Journal of Neuroscience Methods 189 (2010) 233-245

[66] Christian F. Beckmann, Stephen M. Smith. *Probabilistic Indipendent Component Analysis for Functioanl Magnetic Resonance Imaging*. IEEE transaction on medical imaging, vol.23, no.2, (2004)

[67] D.N. Greve and B. Fischl. *Accurate and robust brain image aligment using bounday-based registration*. NeuroImage 48 (2009) 63-72

[68] Jinhui Wang, Xinian Zuo, Yong He. *Graph-based network analysis of resting-state functional MRI*. Frontiers in Systems Neuroscience, vol. 4, art. 16, (2010)

[69] Mikail Rubinov and Olaf Sporns. *Complex network measures of brain connectivity: Uses and interpretations*. NeuroImage 52 (2010) 1059–1069

[70] Edward T. Bullmore and Danielle S. Bassett. *Brain Graphs: Graphical Models of the Human Brain Connectome*. Annual Review of Clinical Psychology, (2011) 7:113–4

[71] Scott D. Pauls and D. Remondini. *Measures of centrality based on the spectrum of the Laplacian*. Physical Review E 85, 066127 (2012)

[72] D. Grady, C. Thiemann and D. Brockmann. *Robust classification of salient links in complex networks*. Nature Communication (2012) 3:864. doi: 10.1038/ncomms1847

[73] D. Gleich. *Matlab BGL v2.1*. (2007).

[74] M. Rubinov and O. Sporns. *Complex network measures of brain connectivity: Uses and interpretations*. NeuroImage 52 (2010) 1059–1069.

[75] M. Xia, J. Wang and Y. He. *BrainNet Viewer: a Network Visualization Tool for Human Brain Connectomics*. PLoS ONE (2013) 8:e68910.

[76] L. Ferini Strambi, M. Bozzali, M. Cercignani, A. Oldani, M. Zucconi and M. Filippi. *Magnetization transfer and diffusion-weighted imaging in nocturnal frontal lobe epilepsy*. Neurology (2000) 54(12):2331-3

[77] M. Fedi, S.F. Berkovic, I.E. Scheffer, G. O'Keefe, C. Marini, R. Mulligan, S. Gong, H. Tochon-Danguy and D.C. Reutens. *Reduced striatal D1 receptor binding in autosomal dominant frontal lobe epilepsy*. Neurology (2008) 71(11):795-8

[78] F. Picard, D. Bruel, D. Servent, W. Saba, C. Fruchart-Gaillard, M.-A. Schollhorn-Peyronneau, D. Roumenov, E. Brodtkorb, S. Zuberi, A. Gambardella, B. Steinborn, A. Hufnagel, H. Valette and M. Bottlaender. *Alteration of the in vivo nicotinic receptor density in ADNFLE patients: a PET study*. Brain (2006) 129:2047–2060

[79] M. Heymann, I.E. Scheffer, Y. Chinvarun, S.U. Berlangieri and S.F. Berkovic. *Autosomal dominant nocturnal frontal lobe epilepsy: demonstration of focal onset and intrafamilial variation*. Neurology (1997) 49(4):969-75

[80] C.A. Tassinari, G. Rubboli, E. Gardella, G. Cantalupo, G. Calandra-Buonaura, M. Vedovello, M. Alessandria, G. Gandini, S. Cinotti, N. Zamponi and S. Meletti. *Central pattern generators for a common semiology in fronto-limbic seizures and in parasomnias. A neuroethologic approach*. Neurol Sci (2005) 26:s225–s232

[81] Z. Haneef and S. Chiang. *Clinical correlates of graph theory findings in temporal lobe epilepsy*. Seizure (2014) 23:809–818

[82] J. Wang, S. Qiu, Y. Xu, Z. Liu, X. Wena, X. Huc, R. Zhang, M. Li, W. Wang and R. Huang. *Graph theoretical analysis reveals disrupted topological properties of whole brain functional networks in temporal lobe epilepsy*. Clinical Neurophysiology 125 (2014) 1744–1756

[83] S. Chiang and Z. Haneef. *Graph theory findings in the pathophysiology of temporal lobe epilepsy*. Clin Neurophysiol. (2014) 125(7): 1295-1305

[84] W. Liao, Z. Zhang, Z. Pan, D. Mantini, J. Ding, X. Duan, C. Luo, G. Lu and H. Chen. *Altered Functional Connectivity and Small-World in Mesial Temporal Lobe Epilepsy*. PLoS ONE 5(1): e8525. doi:10.1371/journal.pone.0008525

ACKNOWLEDGEMENTS

First of all, I would like to thank Dott.ssa Claudia Testa for giving me the opportunity to perform my master thesis at the functional MR Unit at the S.Orsola-Malpighi polyclinic, DIBINEM, and for her valuable and constructive suggestions during the development of this work. I would like to express my gratitude also to Dott.ssa Stefania Evangelisti, for following me in each step of this study with expertise, enthusiasm and personality. I am sincerely grateful to both for their patience and availability that have shown throughout these months in which we have worked closely.

I would like to thank Prof. Gastone Castellani and Prof. Daniel Remondini for the advices for this thesis.

I would also like to thank Prof. Raffaele Lodi, and all persons that work at the U.O. RM funzionale, for making me feel from the outset an integral and functional part of the group. In particular, I thank Prof.ssa Caterina Tonon, Dott. Stefano Zanigni and Dott.ssa Ludovica Gramegna for helping me with the revision of the clinical part of the study. I was very impressed by the dedication and the competence demonstrated by every member of the department in their respective fields of study. This aspect has been very inspiring for me.

Thanks also to all the other persons that help me, directly and indirectly, to the drafting of this thesis.
A great hug and a special thanks go to all my family, who have always believed in me, demonstrating their closeness and their support in any circumstance.
Thanks to those six guys that have always been present for me: without you I would have been probably a better person but I don't think it would be worth it, thanks to exist.
Thanks to all those people that help me even just with a joke or a thought.
Finally, thanks to a special person that, with his willpower, his determination and his innate ability to motivate me, has contributed to the achievement of a result which, until quite recently, it seemed only a distant goal.